Molecular Characterization of Quality Control Factors at the Protein Entry Gate of Mitochondria

Dissertation

zur

Erlangung der Doktorgrades (Dr. rer. nat.)

der

Mathematisch-Naturwissenschaftlichen Fakultät

an der

Rheinischen Friedrich-Wilhelms-Universität Bonn

vorgelegt von

Arushi Gupta

aus Neu-Delhi

Bonn, 2023

Angefertigt mit Genehmigung der Mathematisch-Naturwissenschaftlichen Fakultät

der Rheinischen Friedrich-Wilhelms-Universität Bonn

1. Gutachter: Prof. Dr. Thomas Becker

2. Gutachter: Prof. Dr. Jörg Höhfeld

Tag der Promotion: 21.11.23

Erscheinungsjahr: 2024

Abbreviations

$\Delta\psi$	membrane potential
BN	blue native
BSA	bovine serum albumin
CCCP	carbonyl cyanide m-chlorophenyl hydrazine
CHX	cyclohexamide
Cyt.	cytosol
dH_2O	distilled water
$DiSC_3(5)$	3,3′-dipropylthiadicarbocyanine iodide
DTT	dithiothreitol
EDTA	ethylenediaminetetraacetic acid
ER	endoplasmic reticulum
ERAD	ER-associated degradation
GFP	green-fluorescent protein
HA	hemagglutinin
His	histidine
Hsp	heat shock protein
IM	inner membrane
IMP	mitochondrial inner membrane peptidase
IMS	intermembrane space
kDa	kilodalton
M	membrane of the endoplasmic reticulum
Mat.	Matrix
MIA	mitochondrial import and assembly
MIM	mitochondrial import
Mito.	mitochondria
mitoCPR	mitochondrial compromised protein import response
mitoRQC	mitochondrial ribosome-associated quality control
mitoTAD	mitochondrial protein translocation-associated degradation
MitCOM	mitochondrial complexosome
mPOS	mitochondrial precursor overaccumulation stress
MPP	mitochondrial processing peptidase
mtDNA	mitochondrial DNA

NAC	nascent polypeptide-associated complex
NADP	nicotinamide adenine dinucleotide phosphate
Ni^{2+}-NTA	nickel nitrilotriacetic acid
OD_{600}	optical density at 600 nm
OM	outer membrane
OXPHOS	oxidative phosphorylation
PAGE	polyacrylamide gel electrophoresis
PAM	presequence-translocase associated motor
PMSF	phenylmethylsulfonyl fluoride
PNS	post-nuclear supernatant
PVDF	polyvinylidene fluoride membranes
rpm	revolutions per minute
ROS	reactive oxygen species
s.e.m	standard error of mean
SAM	sorting and assembly machinery
SDS	sodium dodecyl sulfate
TCA	trichloroacetic acid
TIM22	translocase of the inner membrane (carrier translocase)
TIM23	translocase of the inner membrane (presequence translocase)
TOM	translocase of the outer membrane
TM	transmembrane
UBA	ubiquitin-associated domain
UBL	ubiquitin-like
UBX	ubiquitin regulatory X domain
UBQLN	ubiquilin
UPRam	unfolded protein response activated by mistargeting of proteins
UPRmt	mitochondrial unfolded protein response
WT	wild-type

Table of Contents

1. Summary

Mitochondria perform crucial functions for cell survival. In order to fulfill these functions, mitochondria contain about 1,000-1,300 proteins. Approximately, 99% of the mitochondrial proteins are synthesized as precursors on cytosolic ribosomes and imported into mitochondria via sophisticated import machineries. The translocase of the outer membrane complex (TOM complex) forms an entry gate for most mitochondrial precursors. Defects in protein import via the TOM complex lead to the accumulation of mitochondrial precursor proteins, which in turn cause massive proteotoxic stress. To ensure correct mitochondrial function, a plethora of quality control factors govern mitochondrial protein import at various steps, thereby ensuring proper protein import into mitochondria. However, our understanding of quality control mechanisms is still limited. In this research study, we aimed to identify quality control factors that monitor the TOM complex.

Using affinity purifications, we identified a new quality control factor, Pth2, which operates at the TOM complex and promotes the removal of accumulated precursor proteins. Upon clogging of the TOM complex, Pth2 interacts with the ubiquitin-binding protein Dsk2 (sole yeast homolog of human, ubiquilins) which delivers ubiquitylated substrates to the proteasome for degradation. We observed two experimentally independent functions of Pth2 in quality control. One related to its role in the removal of non-imported precursor proteins during mitochondrial import. The other function of Pth2 was related to its peptidyl tRNA hydrolase activity linked to the quality control pathway in clearing translation-stalled polypeptides from the ribosome. In addition, our data led to the discovery of Fmp52, a novel regulatory protein at the TOM complex. We observed that Fmp52 is present both in mitochondria as well as in the cytosol. Furthermore, we observed that Fmp52 is stabilized upon proteasomal inhibition and clogging of the TOM complex. Thus, Fmp52 plays a regulatory role in mitochondrial quality control.

In conclusion, we identified two new factors operating at the TOM complex. These factors play an essential role in maintaining the TOM complex in an import-competent state, allowing efficient protein import via the cellular gateway.

2. Introduction

2.1 Mitochondria

Mitochondria emerged from an endosymbiotic event about 1.5 billion years ago. α-proteobacteria were then engulfed by an ancestral eukaryotic cell that co-evolved within the host cell to form, what we refer to as the present-day, mitochondria. This theory of the endosymbiotic origin of mitochondria is a flagship example of prokaryotic endosymbiosis and qualifies as a unique event in evolution (Gray et al., 1999; Archibald, 2015; Zachar and Boza, 2020). Moreover, the discovery of a unique mitochondrial genome, a relic of the mitochondrion's evolutionary past, has further affirmed the eubacterial roots of the mitochondrial genome. The mitochondrial genome of yeast, *Saccharomyces cerevisiae,* the model organism used in this study, encodes eight mitochondrial proteins, two rRNAs, and twenty four tRNAs. In contrast, the human mitochondrial genome encodes thirteen proteins, two rRNAs, and twenty two tRNAs (Lang et al., 1999; Hällberg and Larsson, 2014; Ott et al., 2016). Mitochondria are surrounded by two membranes, the outer and the inner membrane, which enclose two aqueous compartments: the intermembrane space (IMS) and the inner matrix respectively (Figure 1). The inner membrane is folded and invaginated into the matrix to form the so-called cristae. The crista membrane is the main site of oxidative phosphorylation (OXPHOS), reactions by which adenosine triphosphate (ATP) is produced from the proton gradient generated across the inner membrane by the respiratory chain (Vogel et al., 2006; Zick et al., 2009). In addition to ATP production, mitochondria perform a variety of cellular functions. They are involved in metabolic pathways, such as the tricarboxylic acid cycle, biosynthesis of amino acids, heme, and iron-sulfur clusters, β-oxidation of lipids, and steroid synthesis (Demine et al., 2014; Marcero et al., 2016; Martinez-Reyes et al., 2016; Lill and Freibert, 2020;). Furthermore, mitochondria participate in signaling processes involving reactive oxygen species (ROS), calcium ions, and programmed cell death (Joza et al., 2001; McBride et al., 2006; Galluzzi et al., 2012; Nunnari and Suomalainen, 2012). The multifaceted role of mitochondria in cellular metabolism has been illustrated by the fact that mitochondrial dysfunction has been implicated in a wide range of common diseases including neurodegenerative disorders, metabolic syndromes, cancer, cardiomyopathies, and obesity (Nunnari and Suomalainen, 2012; Picard et al., 2016; Wallace, 2018). To fulfil the various functions, mitochondria consist of ~1,000 different proteins in *Saccharomyces cerevisiae* and

~1,300 different proteins in human cells (Sickmann et al., 2003; Pagliarini et al., 2008; Morgenstern et al., 2017; Rath et al., 2021; Morgenstern et al., 2021). Approximately 99% of mitochondrial proteins are nuclear-encoded, that is they are produced on cytosolic ribosomes and subsequently need to be imported and transported to their destined location in the correct sub-cellular mitochondrial compartment (Harbauer et al., 2014; Pfanner et al., 2019).

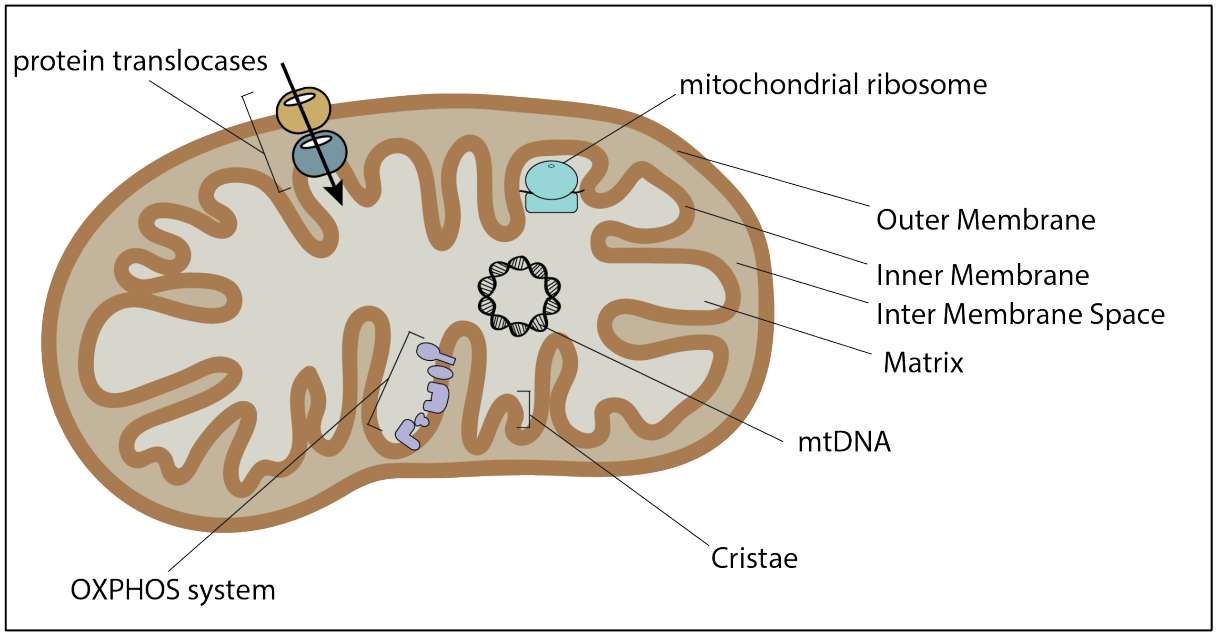

Figure 1. The general structure of mitochondria. Mitochondria consist of two membranes: the outer and the inner membrane that enclose two aqueous compartments: the intermembrane space and the inner matrix respectively. The inner membrane is folded into characteristic invaginations called cristae. The inner cristae membrane harbors the OXPHOS complexes for the production of ATP. Within the matrix lies the circular mitochondrial DNA. Only a few genes are transcribed from mtDNA, followed by translation on mitochondrial ribosomes, and subsequently integrated into the inner membrane. Mitochondria imports precursor proteins from the cytosol using a sophisticated network of import machineries located on the outer and inner membrane. mt DNA., mitochondrial DNA; OXPHOS., oxidative phosphorylation.

2.2 Protein import pathways into yeast mitochondria

The translocase of the outer membrane (TOM) complex forms an entry gate for almost all the mitochondrial precursor proteins. It consists of seven subunits, including a single β-barrel and six α-helical integral trans-membrane proteins. The β-barrel protein Tom40 forms the central protein conducting channel of the TOM complex. Three α-helical proteins serve as precursor receptors for incoming precursor proteins (Tom20, Tom22, and Tom70). Three α-helical small Tom proteins, Tom5, Tom6, and Tom7, are closely associated with Tom40 and are involved in

the assembly and stability of the TOM complex (Hill et al., 1998; Becker et al., 2005; Neupert and Herrmann, 2007; Shiota et al., 2015; Wiedemann and Pfanner, 2017; Araiso and Endo, 2022). Recent structural analyses using high-resolution cryo-electron microscopy of the yeast and human TOM complex corroborated these findings and revealed that the TOM pore is formed by a homodimer of Tom40 tethered together by two subunits of Tom22 (Bausewein et al., 2017; Araiso et al., 2019; Tucker and Park, 2019; Wang et al., 2020; Guan et al., 2021; Su et al., 2022). The two main receptor α-helical proteins Tom20 and Tom70 recognize the incoming precursor proteins and associated chaperones. Tom20 preferentially binds to precursor proteins with a cleavable presequence (Abe et al., 2000; Yamano et al., 2008). On the other hand, Tom70 recognizes proteins with internal mitochondrial targeting sequences and forms a docking site for hydrophobic precursor proteins such as multi-spanning outer and inner membrane proteins (Brix et al., 1997; Yamamoto et al., 2009; Backes et al., 2018; den Brave et al., 2021).

After passing through the TOM complex, specific protein translocases sort the precursor proteins into their destined mitochondrial compartments (Figure 2). First, precursors with a cleavable N-terminal, positively charged, amphipathic α-helical presequence are handed over to the translocase of the inner membrane (TIM23 complex) and are transported into the inner membrane or the matrix in a membrane potential-dependent manner (Chacinska et al., 2003; van der Laan et al., 2010; Gupta and Becker, 2021). Inner membrane-sorted preproteins contain a hydrophobic sequence that serves as a stop-transfer signal to these proteins and are laterally released into the inner membrane. Matrix-imported proteins additionally require the cooperation of the presequence translocase-associated motor (PAM). The central component of the PAM machinery is mitochondrial Hsp70 (mtHsp70) which is controlled by its five co-chaperones: Tim44, Mge1, Pam18 (Tim14), Pam16 (Tim16) and Pam17. As an ATP-driven chaperone, mtHsp70 in cooperation with its co-chaperones pulls precursor proteins from the TIM23 complex, facilitating their translocation into the matrix (De Los Rios et al., 2006; Eppinger et al., 2008; van der Laan et al., 2010). After protein import, the presequence of both inner membrane and matrix-located preproteins is cleaved off by the mitochondrial processing peptidase (MPP) (Taylor et al., 2001; Vögtle et al., 2009).

Second, precursors of multi-spanning, inner-membrane proteins that have internal targeting signals such as carrier proteins are inserted into the inner membrane by the carrier translocase of the inner membrane (TIM22 complex) in a membrane potential-dependent manner (Neupert and Herrmann, 2007; Chacinska et al., 2009). After passage through the TOM complex, the hydrophobic sequences are shielded from the aqueous intermembrane space by hexameric

small TIM chaperones which also guide the transfer of the precursor proteins for their final insertion into the inner membrane. The transport of proteins to the carrier translocase (TIM22) is aided by interactions with outer membrane proteins involving the metabolite channel porin in yeast. (Ellenrieder et al., 2019; Grevel and Becker, 2020; Horten et al., 2020).

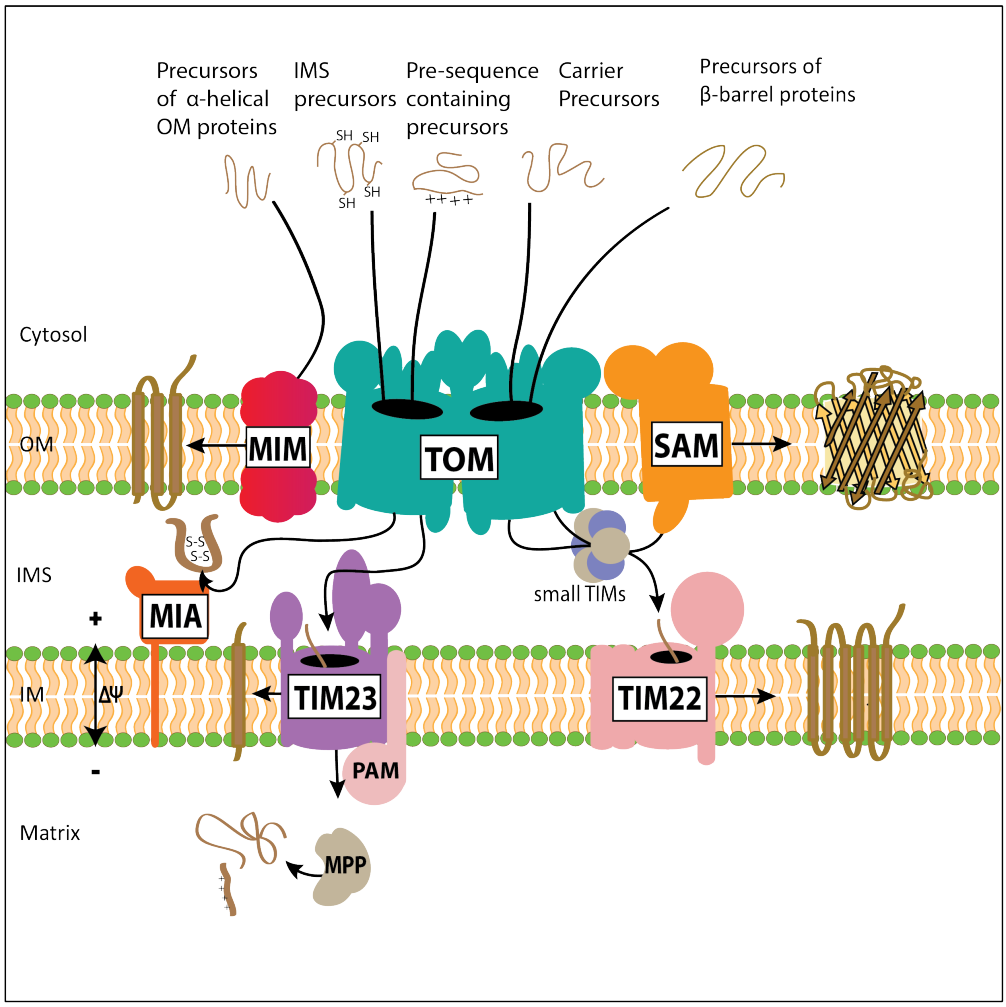

Figure 2. Protein Import Pathways into Mitochondria. The majority of the precursor proteins are imported through the translocase of the outer member (TOM) complex. Proteins containing a cleavable N-terminal, positively charged amphiphilic presequence are handed over to the translocase of the inner membrane (TIM23 complex) for either lateral release into the inner membrane (IM) or are imported into the matrix. The presequence translocase-associated motor (PAM) cooperates in the import of matrix-destined proteins. Mitochondrial processing peptidase (MPP) cleaves off the presequence after import. Small TIM chaperones in the intermembrane space (IMS) guide hydrophobic carrier precursors to the carrier translocase of the inner membrane (TIM22). The mitochondrial intermembrane space import and assembly (MIA) machinery in the intermembrane space (IMS) coordinates the import and oxidation of precursor proteins containing cysteine-rich motifs. The sorting assembly machinery (SAM complex) integrates β-barrel proteins into the outer membrane. Precursors of α-helical proteins are inserted from the cytosol into the outer membrane with the help of mitochondrial import machinery (MIM complex). OM., outer membrane; IMS., intermembrane space; IM., inner membrane; Δψ., membrane potential. (Figure adapted from Gupta & Becker, 2021)

The TIM22 complex facilitates both the insertion and lateral release of carrier precursors into the inner membrane (Rehling et al., 2003).

Third, the mitochondrial import and assembly (MIA) machinery is involved in importing proteins destined for the intermembrane space. These precursor proteins harbor an internal-cysteine-rich motif, which also serves as a mitochondria-targeting signal. The precursors are kept in a reduced state in the cytosol and translocated across the outer membrane via the TOM complex. The MIA machinery promotes the import of incoming precursors by the formation of intermolecular disulfide bonds as soon as the precursors emerge from the TOM complex. Mia40, the core subunit of the MIA machinery, oxidizes the thiol groups of precursor proteins to disulfide bonds (Hell et al., 2001; Stojanovski et al., 2008). Re-oxidation of Mia 40 for another round of import is mediated by Erv1 which shuttles electrons from the MIA complex to the respiratory chain (Neupert and Herrmann, 2007; Chacinska et al., 2009).

The sorting assembly machinery (SAM complex) integrates β-barrel proteins into the outer membrane. Similar to the carrier pathway, small TIM chaperones bind to the β-barrel precursors to prevent their aggregation in the aqueous intermembrane space, thereby aiding their transfer from the TOM complex to the SAM complex. The most C-terminal β-strand of the precursor functions as a β-signal, inducing the opening of the lateral gate of the SAM complex and facilitating its insertion as the first step in the process. Subsequently, β-hairpins are inserted into the lateral gate in a stepwise manner until the β-barrel is formed (Kozjak et al., 2003; Wiedemann et al., 2003; Klein et al., 2012; Diederichs et al., 2020; Takeda et al., 2021).

Fifth, precursors of α-helical outer membrane proteins are imported by the mitochondrial import machinery (MIM complex) (Ishikawa et al., 2004, Becker et al., 2008, Dimmer et al., 2012). Different populations of MIM complexes promote the insertion of different types of outer membrane proteins (Doan et al., 2020; Gupta and Becker, 2021). Free MIM complex promotes the insertion of single-spanning α-helical proteins. The MIM complex associates with the TOM complex to receive precursors from the Tom70 receptor, and with the SAM complex to mediate the import and assembly of small Tom proteins (Becker et al., 2008; Doan et al., 2020; Gupta and Becker, 2021).

2.3 Targeting of proteins to mitochondria

The transport of proteins from the cytosol to the TOM receptors on the mitochondrial surface remains partially characterized. Mitochondrial precursor proteins can be imported via the TOM

complex, either co-translationally or post-translationally (Becker et al., 2019; Hansen and Herrmann, 2019).

In the case of co-translational import, the proteins are imported while they are being synthesized on cytosolic ribosomes. In such cases, the respective mRNAs are associated with the mitochondrial outer membrane (Lesnik et al., 2014; Gold et al., 2017; Qin et al., 2021; Uszczynska-Ratajczak et al., 2023). The RNA-binding protein, Puf3 which belongs to the Pumilio protein family has been shown to be involved in the transport of mRNAs to the mitochondrial periphery (Gadir et al., 2011; Quenault et al., 2011; Lapointe et al., 2018). Furthermore, the interaction between the translated mitochondrial targeting sequence and the Tom20 import receptor plays a crucial role in targeting the mRNAs to the surface of the mitochondria (Eliyahu et al., 2010). The nascent polypeptide-associated complex (NAC) ensures the accurate localization of precursor proteins to mitochondria at the ribosome exit tunnel (George et al., 1998; Funfschilling and Rospert, 1999). The mitochondrial outer membrane proteins Om14 and Sam37, cooperate with the NAC complex to further facilitate protein import (Lesnik et al., 2014; Ponce-Rojas et al., 2017).

The majority of mitochondrial precursor proteins are imported in a post-translational manner (Becker et al., 2019; Bykov et al., 2020). For proteins that are imported post-translationally, it is imperative that they are maintained in an import-competent confirmation in the cytosol. In order to prevent the aggregation and misfolding of these precursor proteins, a network of cytosolic chaperones belonging to the Hsp70 and Hsp90 families, guide the precursor proteins to the mitochondrial surface (Deshaies et al., 1988; Young et al., 2003; Endo and Yamano, 2009; Becker et al., 2019). It has been shown that Hsp70 and Hsp90, together with their co-chaperones bind to the Tom70 receptor of the TOM complex thereby targeting the mitochondrial precursors as well as initiating protein translocation. (Young et al., 2003; Backes et al., 2021; Song et al., 2021). The coordinated network of chaperones during protein targeting prevents the premature folding of misfolded proteins and protein aggregation in the cytosol. Among these chaperones, Hsp70s are ubiquitously present and participate in a wide range of cellular processes such as biogenesis of mitochondrial precursor proteins, protein folding, targeting, preventing aggregation, and protein turnover (Sheffield et al., 1990; Kampinga and Craig, 2010; Rosenzweig et al., 2019). Hsp70 chaperones are recruited by the Hsp40 chaperones. Hsp40 chaperones, also called J-proteins, due to the presence of a common J-domain, recruit Hsp70s by stimulating their ATPase activity thereby playing a pivotal role in various cellular processes. The Hsp40 co-chaperones, Xdj1, and Djp1 bind differentially to the receptors Tom22 and Tom70, respectively (Opaliński et al., 2018). Further, Hsp40 co-

chaperones like Ydj1 and Sis1 interact with newly synthesized precursor proteins thereby ensuring their proper biogenesis, targeting, and membrane insertion (Jores et al., 2018; Drwesh et al., 2022). Despite the sophisticated network of chaperones, protein targeting can fail for a proportion of precursor proteins even under optimal conditions.

2.4 Stress responses on impaired mitochondrial import

Mitochondria receives a large number of proteins that needs to be imported from the cytosol. The TOM complex positioned at the mitochondrial entry gate bears the responsibility for importing a substantial flow of proteins. If the TOM complex is overloaded or is undermined due to mitochondrial damage like loss of mitochondrial membrane potential or mutations in the translocon, this can result in the blocking and clogging of the TOM pore (Wang and Chen, 2015; Wrobel et al., 2015; Mårtensson et al., 2019). Precursor proteins need to be maintained in a predominantly unfolded state because the Tom40 pore channel exclusively allows the transport of helix-turn-helix structures, and is incapable of accommodating folded domains (Ahting et al., 2001; Wiedemann et al., 2001; Shiota et al., 2015; Kater et al., 2020). Consequently, proteins with folded domains pause at the import channel, leading to a delay or blockage of the translocation process (Chacinska et al., 2003; Gold et al., 2014). Precursors that stall at the translocase can span both the outer and inner membranes and form a highly stable super complex with the TOM and TIM translocases (Chacinska et al., 2003; Gomkale et al., 2021). In such cases, premature folding of precursor proteins obstructs their passage through the TOM channel, whereas their N-terminal presequence interacts with the TIM23 translocase of the inner membrane, resulting in clogging of the precursors at the TOM-TIM super complex (Boos et al., 2019; Mårtensson et al., 2019; Gomkale et al., 2021). Premature folding of precursor proteins can be exacerbated by cellular events like protein misfolding under conditions of stress and mitochondrial damage (Gregersen et al., 2006). Studies have shown that overexpression of precursor proteins particularly those containing bipartite signals composed of a mitochondria-targeting sequence and an inner-membrane sorting stop transfer signal, can clog the TOM complex (Weidberg and Amon, 2018). Overall mutations affecting protein import and conditions compromising the mitochondrial inner membrane integrity and function can further block protein import into the mitochondria leading to the accumulation of precursor proteins (Wang and Chen, 2015). Therefore, efficient response mechanisms are crucial to address the potentially severe physiological consequences of clogging the TOM channel.

In order to mitigate the proteotoxic stress caused by the accumulation of mitochondrial precursor proteins, cells have evolved a variety of mechanisms. Prolonged blockage of the TOM complex induces massive transcriptional remodeling to adapt to protein stress and is referred to by the umbrella term, mitoprotein-induced stress response (Boos et al., 2020). In yeast cells, the transcription factor Hsf1 is the key player of the mitoprotein-induced stress response, and triggers a variety of processes. Stress signals such as accumulation of mitochondrial precursors in the cytosol, compromised respiration, or perturbation in mitochondrial Hsp70, lead to a rapid increase in the expression of genes targeted by Hsf1 (Matilainen et al., 2017; Boos et al., 2019). Under non-stress conditions, Hsf1 binds to chaperones and its activity is repressed. However, under conditions when the cytosolic proteostasis is disturbed, chaperones preferentially bind to non-imported precursor proteins and are titrated away from Hsf1. Consequently, Hsf1 is released restoring cytosolic proteostasis (Krakowiak et al., 2018; Masser et al., 2019; Boos et al., 2020). Recent findings demonstrate a similar HSF1-HSP70 axis in mammalian cells in triggering the mitochondrial unfolded protein response (UPRmt) to protect the cells against protein misfolding. However, the activation of UPRmt in mammals is dependent on both the production of mitochondrial reactive oxygen species (mtROS) and the accumulation of non-imported precursor proteins (Sutandy et al., 2023). In yeast, Hsf1 promotes the expression of Rpn4, a transcription factor that controls proteasomal abundance and activity in a pathway referred to as the unfolded protein response activated by mistargeting of proteins (UPRam) (Hahn et al., 2006; Wrobel et al., 2015; Boos et al., 2019). Moreover, UPRam protects cells by inhibiting protein synthesis and proteasome activation (Wrobel et al., 2015).

Overaccumulation of mitochondrial precursor proteins causes the activation of the mitochondrial precursor overaccumulation stress (mPOS) pathway. The overall response to mPOS in cells is mediated by the downregulation of general protein synthesis, particularly mitochondrial genes encoding proteins involved in respiratory metabolism, as well as enhancing chaperone activity and protein turnover. The resulting stress can eventually lead to cell death if not rescued (Wang and Chen, 2015).

The mitochondrial import of precursor proteins is tightly regulated and is under the constant surveillance of the proteasome. The import of proteins into mitochondria is coordinated with their cytosolic degradation, thereby maintaining cellular homeostasis. To this end, mitochondrial proteins that are not efficiently imported are degraded by the ubiquitin proteasome system (UPS). (Bragoszewski et al., 2013; Kowalski et al., 2018; Mohanraj et al., 2019). Under these conditions, proteasomal abundance and activity is increased in response to

the accumulation of mitochondrial proteins in the cytosol (Wrobel et al., 2015). The underlying mechanisms of how precursor proteins are recognized and degraded are still largely unknown in yeast.

In mammals, the ubiquilin (UBQLN) family of proteins plays a crucial role in ensuring quality control of mislocalized proteins. Four ubiquilins (UBQLN1 to UBQLN4) are found in mammals, whereas only one homolog, Dsk2, is present in yeast (Chuang et al., 2016). UBQLNs contain two functional domains: a ubiquitin-associated (UBA) domain that interacts with ubiquitylated substrates, and a ubiquitin-like (UBL) domain that mediates interaction with the proteasome. Structural and functional analysis of UBQLNs identified a third, methionine-rich middle domain termed the M-domain that binds to the transmembrane domain (TMD) of mitochondrial proteins, prevents their aggregation in the cytosol, and drives them to the mitochondria. On import failure, UBQLNs recruit E3-ubiquitin ligase to ubiquitylate their substrate proteins and consequently, the ubiquitin-substrate complex is delivered to the proteasome for degradation. Thus, UBQLNs can function in the triage of tail-anchored mitochondrial proteins, supporting mitochondrial insertion and if targeting fails they facilitate the turnover of mislocalized membrane proteins (Itakura et al., 2016; Juszkiewicz and Hegde, 2018).

When chaperones and the ubiquitin-proteasome system are overburdened, cells utilize an additional layer of cell defense to deal with the toxicity of unimported mitochondrial precursor proteins by their spatial sequestration to aggregate-like deposits (Miller et al., 2015; Sonntag et al., 2017; Krämer et al., 2021; Nowicka et al., 2021; Schlagowski et al., 2021; Shakya et al., 2021; Xiao et al., 2021). In response to precursor aggregation, a cascade of cellular events is triggered, including the upregulation of cytosolic chaperones such as Hsp42 and Hsp104 (Specht et al., 2011; Mogk and Bukau, 2017; Nowicka et al., 2021). Hsp42 acts as an aggregase, promoting the recognition and sequestration of misfolded proteins into aggregates, preventing their interaction with other cellular components (Specht et al., 2011; Grousl et al., 2018). In contrast, Hsp104 acts as a dissagregase by either refolding the aggregated proteins or targeting them for degradation, thereby restoring cellular proteostasis (Grousl et al., 2018; Michalska et al., 2019; Shorter and Southworth, 2019). Recent research findings by Krämer et al., described that an imbalance in cellular proteostasis caused by protein accumulation in the cytosol led to the formation of granular structures in the cytosol, denoted as MitoStores. MitoStores were found to mainly contain mitochondrial precursor proteins containing matrix-targeting sequences and were regulated by the cytosolic chaperones, Hsp42 and Hsp104. Moreover, it

was demonstrated that MitoStores are transient in nature and the sequestered precursors could be imported back into mitochondria once the import capacity is recovered (Krämer et al., 2023).

2.5 Quality control at the TOM complex

To prevent clogging of the TOM complex by import-intermediates and maintain the translocase in an import-competent state, a variety of molecular mechanisms operate at the TOM complex to remove precursor proteins that got stalled during translocation in the TOM channel.

In the case of co-translationally imported mitochondrial proteins, nascent mitochondrial precursor proteins can stall at the ribosome during translation. Possible reasons are faulty mRNA, lack of STOP codon, strong secondary structures in the mRNA, and insufficient availability of charged tRNAs or amino acids (Brandman and Hegde, 2016). The ribosome-associated quality control (RQC) pathway removes such stalled nascent chains from the ribosomes and delivers the stalled nascent polypeptides to the proteasome for degradation (Brandman and Hegde, 2016; Joazeiro, 2019) (Figure 3).

In this pathway, the ribosomal subunits dissociate and the nascent protein remains bound to the 60S subunit. Subsequently, Rqc2 recruits the E3 ubiquitin ligase Ltn1 to promote ubiquitylation of the nascent polypeptides and mark it for proteasomal degradation (Bengtson and Joazeiro, 2010; Brandman et al., 2012). In some cases, the lysine residues of the nascent chain are buried in the ribosome exit tunnel and are not accessible for ubiquitylation. Here, Rqc2 adds C-terminally alanine and threonine residues (CAT-tail) to the nascent chain, thereby pushing the polypeptide out of the ribosomal tunnel to facilitate ubiquitylation by Ltn1 (Shen et al., 2015). The close contact of the 60S ribosomal subunit with the TOM complex during co-translational protein import could hinder Ltn1-dependent ubiquitylation. Consequently, lysine residues escape ubiquitylation by Ltn1 although CAT-tailing occurs. Such CAT-tail modified proteins are imported into mitochondria, where they can form toxic inclusions (Izawa et al., 2017).

To prevent the proteotoxic stress caused by the detrimental import of CAT-tail modified proteins, mitochondrial RQC employs the conserved protein Vms1. Vms1 like its human homolog, ANKZF1, functions as a peptidyl-tRNA hydrolase, and releases the nascent chain from the 60S ribosomal subunit (Izawa et al., 2017; Verma et al., 2018; Zurita Rendón et al., 2018). Furthermore, Vms1 hinders Rqc2 from binding to the ribosomes and therefore prevents CAT-tailing (Izawa et al., 2017). Subsequently, the released nascent chains are imported into

mitochondria and degraded by the mitochondrial proteases (Izawa et al., 2017; Matsuo et al., 2017; Verma et al., 2018).

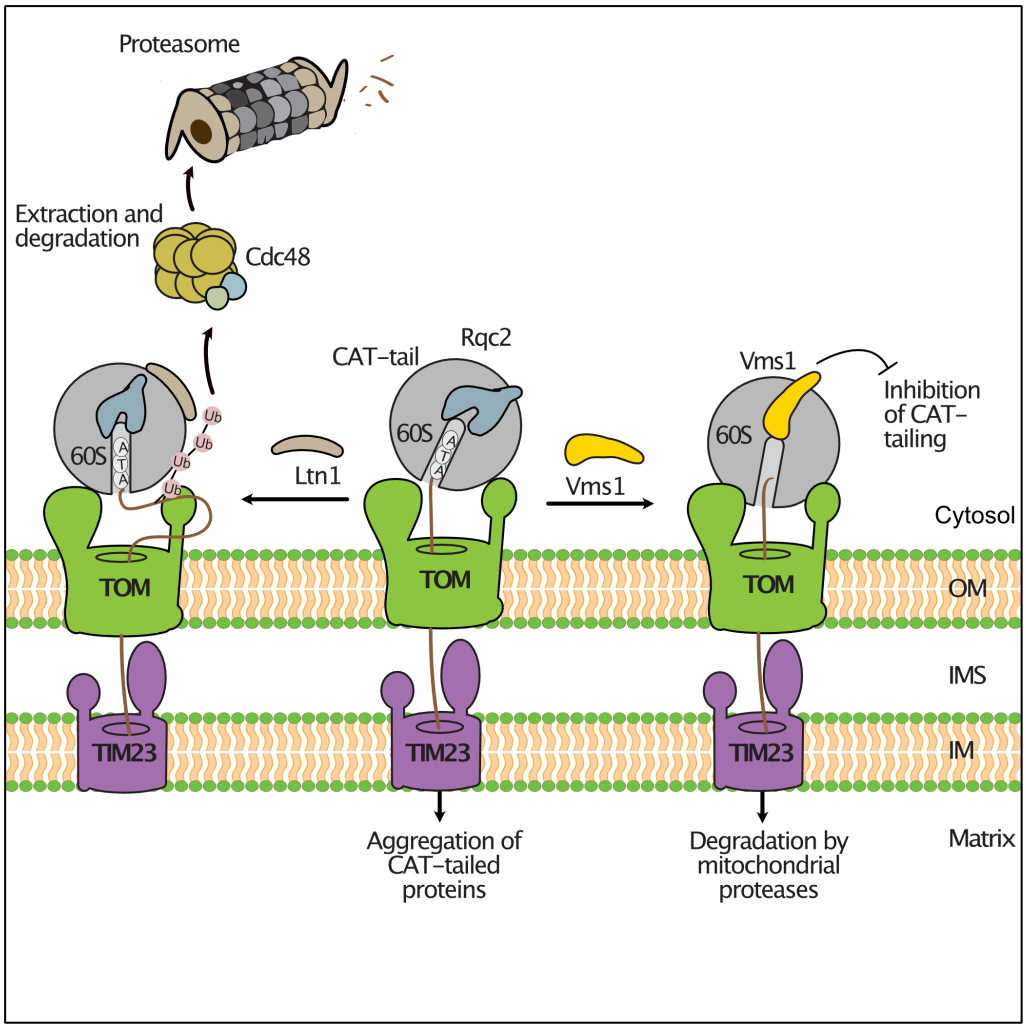

Figure 3. Ribosomal protein quality control during import. Co-translational protein import results in close proximity of the ribosome to the TOM complex. Stalling during translation could arise due to numerous reasons such as faulty mRNA, lack of stop codon, strong secondary structures in the mRNA, and insufficient availability of charged tRNAs. The ribosome-associated quality control (RQC) pathway removes the stalled polypeptide chains from the ribosomes and delivers the stalled polypeptide chains for proteasomal degradation. The RQC component Rqc2 adds C-terminal alanine threonine (CAT)-tails to the nascent chain. The CAT-tailed proteins when imported into the mitochondria, forms toxic aggregates. If accessible, nascent chains can be ubiquitylated by the ribosome-bound E3 ubiquitin-ligase Ltn1, thereby promoting proteasomal degradation (left). The toxic effect of CAT-tail formation can be prevented by the release of the nascent polypeptide from the ribosome mediated by the tRNA hydrolase Vms1 (right). OM., outer membrane; IMS., intermembrane space. (Figure adapted from den Brave et. al, 2021)

The mitochondrial compromised protein import stress response (mitoCPR) is launched upon conditions of prolonged import failure such as reduction of membrane potential and

accumulation of non-imported clogging-prone import intermediates at the mitochondrial protein translocase which induces the expression of *CIS1* (Weidberg and Amon, 2018; Boos et al., 2019) (Figure 4). The cytosolic adaptor protein, Cis1, in turn, recruits the outer membrane AAA-ATPase Msp1 (human homolog, ATAD1) to the Tom70 receptor (Weidberg and Amon, 2018). Msp1 facilitates ATP-driven extraction of translocon-arrested precursor proteins and delivers them to proteasomal degradation (Basch et al., 2020).

Altogether, both Vms1 and Msp1 monitor protein import under conditions of stress. However, it is still rather unclear how the mitochondrial entry gate is monitored under constitutive or non-stressed conditions.

Table 1: Components involved in quality control at the TOM complex

Protein factors		**Localization**	**Monitored mitochondrial proteins and functions**
Yeast	**Human**		
mitoTAD (mitochondrial translocation associated-degradation)			
Cdc48	p97/VCP	Cytosol	AAA-ATPase
Ubx2	UBXD8/FAF2	Mitochondria, ER, Lipid particles	Cdc48 recruitment
mitoCPR (mitochondrial comprised protein import responses)			
Msp1	ATAD1	Mitochondria, peroxisome	AAA-ATPase
Cis1		Cytosol	Linker of Msp1 and Tom70
mitoRQC (mitochondrial ribosomal quality control)			
Vms1	ANKZF1	Cytosol	Cdc48 recruitment, peptidyl tRNA hydrolase

The mitochondrial protein translocation-associated degradation (mitoTAD) pathway continuously monitors the TOM complex to prevent clogging of the translocation channel with precursor proteins (Mårtensson et al., 2019) (Figure 4). Ubx2, previously reported to function in the endoplasmic reticulum-associated degradation (ERAD), is the key component of this

pathway (Neuber et al., 2005; Schuberth and Buchberger, 2005). In addition, Ubx2 associates with lipid droplets, and plays a role in lipid homeostasis (Wang and Lee, 2012; Rajakumar et al., 2020). It has been reported that the lack of Ubx2 resulted in smaller lipid droplet morphology and altered protein composition. Conversely, the overexpression of Ubx2 resulted in lipid droplet aggregation. It was further shown that Ubx2 is important for the synthesis of triacylglycerols (TAGs), which forms the inner core of lipid droplets (Wang and Lee, 2012).

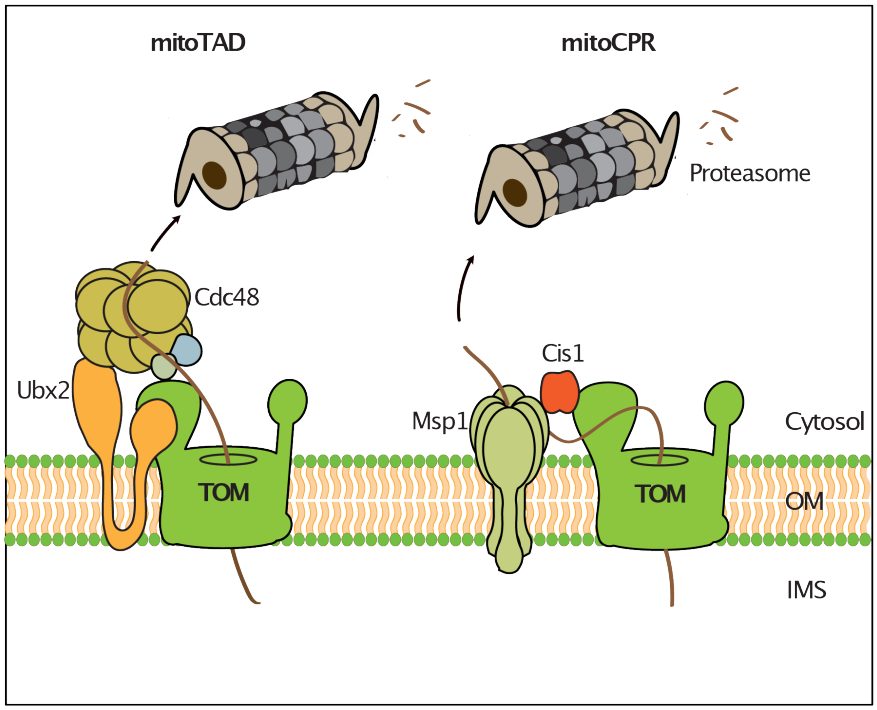

Figure 4. MitoTAD and MitoCPR. The TOM complex is constantly monitored by the mitochondrial translation-associated degradation (mitoTAD) pathway. Upon clogging of the TOM complex, Ubx2 recruits the AAA-ATPase Cdc48 for extraction of stalled precursor proteins from the TOM complex. Under stress conditions, the mitochondrial compromised protein import response (mitoCPR) induces the expression of Cis1. Cis1 in turn recruits membrane-bound AAA-ATPase Msp1 to the TOM complex, facilitating subsequent extraction and degradation of stalled precursor proteins. OM., outer membrane; IMS., intermembrane space. (Figure adapted from den Brave et. al, 2021)

Ubx2 contains two crucial domains for its function: a ubiquitin-regulatory X (UBX) domain and a ubiquitin-associated (UBA) domain. The UBX domain serves as a docking site for the cytosolic AAA-ATPase Cdc48 and the UBA domain for recognizing and binding ubiquitylated proteins. Comparable to its function described in the ERAD pathway, Ubx2 recruits Cdc48 and its cofactors Np14 and Ufd1 to the clogged TOM complex. Cdc48 promotes the extraction of clogged-precursor proteins and subsequently facilitates their proteasomal degradation

(Mårtensson et al., 2019). However, the mechanisms behind how the stalled precursor proteins stuck at the translocon are recognized and ubiquitylated are still largely unknown. In this context, studies with mammalian cell lines have shown that protein import in mitochondria is regulated by the coordinated action of ubiquitylation and deubiquitylation under non-stress conditions. Here, the E3-ubiquitin ligase, MARCH5, ubiquitylates mitochondrial precursor proteins targeting them for degradation by the proteasome. In contrast, the deubiquitylating enzyme, USP30, removes ubiquitin from mitochondrial precursor proteins, allowing them to undergo protein import (Ordureau et al., 2020; Phu et al., 2020). It will be of high relevance to investigate if such a pathway exists in yeast.

So far, the mitoTAD pathway is the only pathway that continuously monitors the TOM channel under non-stressed conditions. The TOM complex imports a substantially large number of precursor proteins raising the possibility if additional quality control pathways that govern mitochondrial protein import quality control exist. However, our understanding of quality control mechanisms at the TOM complex under standard conditions is relatively limited.

3. Aim of Study

The translocase of the outer membrane (TOM complex) imports about 1000 different proteins into mitochondria that are produced on cytosolic ribosomes. Precursor proteins are imported in an unfolded state to pass the TOM channel. Prematurely folded or misfolded precursor proteins can arrest during translocation at the TOM complex and cause clogging of the translocon. Defects in protein import via the TOM complex lead to the accumulation of mitochondrial precursor proteins, which in turn cause various cellular stress responses like altered cytosolic protein biogenesis and increased proteasomal activity. However, it is not well understood how the TOM complex is monitored under non-stressed conditions.

The mitochondrial protein translocation-associated degradation (mitoTAD) pathway continuously clears arrested precursor proteins from the TOM complex to regenerate the translocase for protein import. In this pathway, Ubx2 recruits the cytosolic AAA-ATPase Cdc48 to the TOM complex, which extracts clogged precursor proteins and facilitates proteasomal degradation. So far, the mitoTAD pathway is the only mechanism that is permanently monitoring the TOM complex under constitutive non-stressed conditions.

Conducting thorough investigations in quality control under constitutive non-stress conditions would contribute significantly to our overall understanding and comprehension of mitochondrial quality control mechanisms. This study aimed to characterize the molecular quality control mechanisms that safeguard the protein entry gate of mitochondria under non-stressed conditions. The activation and recruitment of cytosolic and membrane-bound quality control factors in response to the arrest of precursor proteins at the TOM channel were investigated.

Altogether, the aim of the study was to provide new insights and increase our understanding of protein quality control at the TOM complex.

4. Results

4.1 Surveillance of the mitochondrial protein entry gate

To ensure the proper functioning of cellular processes, mitochondria need to correctly import and sort more than 1,000 different proteins. Approximately 99% of mitochondrial proteins are synthesized as precursors on cytosolic ribosomes, and consequently enter the mitochondria via the TOM complex positioned at the mitochondrial entry gate (Neupert and Herrmann, 2007; Pagliarini et al., 2008; Pfanner et al., 2019; Morgenstern et al., 2021). Defects in protein import lead to the accumulation of mitochondrial precursor proteins, which in turn induce stress responses to maintain mitochondria in a functional state (Wang and Chen, 2015; Wrobel et al., 2015; Boos et al., 2019; Shakya et al., 2021). The TOM complex is continuously monitored under non-stress conditions by the mitochondrial protein translocation-associated degradation (mitoTAD) pathway. The mitochondrial population of Ubx2 recruits Cdc48 along with its cofactors Np14 and Ufd1 to the clogged TOM complex. Cdc48 promotes the extraction of clogged-precursor proteins and subsequently facilitates proteasomal degradation (Mårtensson et al., 2019). However, no further quality control factors operating under non-stressed conditions have been reported so far.

4.1.1 Mitochondrial Ubx2 interacts with peptidyl tRNA hydrolase, Pth2

Ubx2 is a dynamic protein that is localized in the ER membrane, lipid droplets, and the TOM complex in the outer mitochondrial membrane (Figure 5A) (Neuber et al., 2005; Schuberth and Buchberger, 2005; Wang and Lee, 2012; Mårtensson et al., 2019). We focused on the mitochondrial population of Ubx2 to investigate new mitochondrial quality control factors using a quantitative mass spectrometry-based approach (Figure 5B). Crude mitochondria were isolated from both wild-type (WT) and HA-tagged Ubx2 expressing strains in a medium containing a non-fermentable carbon source. Mitochondria were lysed with the non-ionic detergent digitonin and then subjected to affinity purification. The eluted samples were subsequently analyzed using label-free proteomics. Consistent with the previous findings, proteins that were co-purified with high enrichment were predominantly TOM subunits (Mårtensson et al., 2019). In addition, we observed that the components of ERAD (Hrd3, Yos9, subunit of Sec complex- Sec61) and lipid droplets (Hfd1) were enriched in the elution fractions

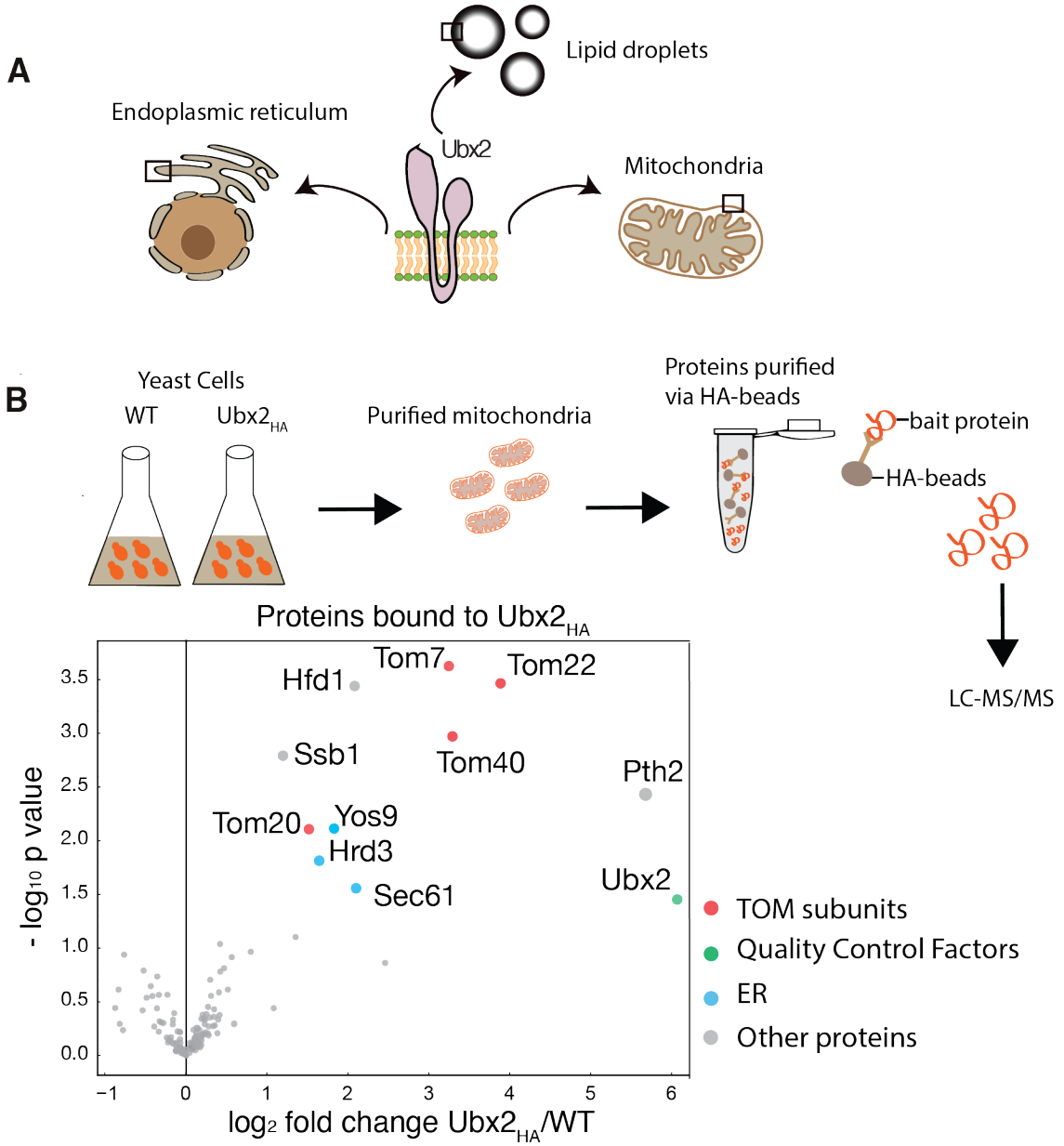

Figure 5. Mass spectrophotometry analysis of HA-tagged Ubx2 mitochondria. (A) Cartoon depicting the localization of Ubx2 in the ER membrane outer mitochondrial membrane. **(B)** Mitochondria from wild-type (WT) and $Ubx2_{HA}$ yeast strains were subjected to affinity purification via anti-HA affinity matrix, and elution samples were analyzed by mass spectroscopy. Shown here is the volcano plot of the proteins co-precipitated with $Ubx2_{HA}$ and identified by label-free proteomics. Depicted are the log_2 fold changes of $Ubx2_{HA}$-bound proteins versus WT background mitochondria of four replicates, plotted against their statistical significance (-log10 p-value). Proteins of interest are highlighted with colors (red, green, blue and gray). ER., Endoplasmic Reticulum; LC-MS., Liquid chromatography-mass spectrometry.

from yeast strains expressing HA-tagged Ubx2. Excitingly the peptidyl tRNA hydrolase, Pth2, was also highly enriched in the HA-tagged Ubx2 mitochondria elution fraction. Pth2 has been reported as an α-helical mitochondrial outer membrane protein that interacts with cytosolic

factors, such as Dsk2 and Rad23, of the ubiquitin-proteasome system (Ishii et al., 2006; Doan et al., 2020). However, Pth2 function linked to mitochondrial protein biogenesis has not been described thus far.

4.1.2 Pth2 binds to the TOM complex

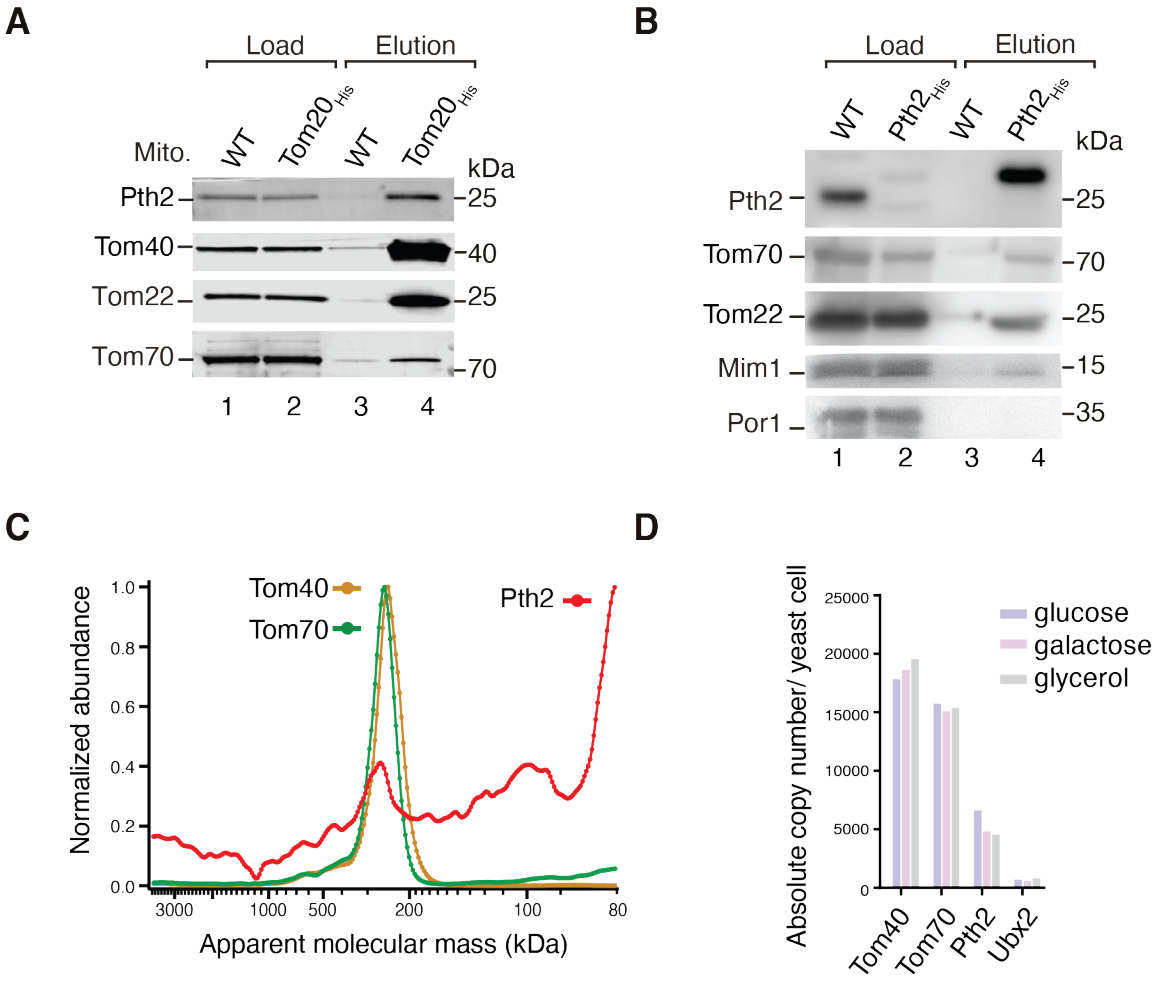

Figure 6. Pth2 interacts with the TOM subunits. (A) Mitochondria isolated from wild-type (WT) and $Tom20_{His}$ yeast cells were solubilized with digitonin and used for affinity purification with Ni^{2+}-NTA agarose beads. After the washing steps, samples were eluted with SDS-sample buffer. Samples were analyzed by SDS-PAGE and immunodetection with the indicated antisera. Load: 0.2%; elution: 100%. **(B)** Wild-type (WT) and $Pth2_{His}$ yeast cells were solubilized with digitonin and used for affinity purification with Ni^{2+}-NTA agarose beads. Samples were analyzed with SDS-PAGE and immunodetection with the indicated antisera. Load: 0.2%; elution: 100%. **(C)** Comparison of the normalized abundance-mass profiles of Tom40, Tom20, and Pth2, obtained from Schulte et al., the MitCOM data set (Schulte et al., 2023). **(D)** Absolute copy number per yeast cell of the indicated proteins. Values are based on the quantification of mitochondrial proteins grown on different carbon sources by Morgenstern et al., 2017.

We wondered whether Pth2, like Ubx2, binds to the TOM complex and is involved in the mitochondrial protein translocation-associated degradation (mitoTAD) pathway. To this end, we performed affinity purification assays using purified mitochondria from yeast strains expressing wild-type (WT) and His-tagged Tom20, and subsequently analyzed the samples by SDS-PAGE followed by immunodetection. Indeed, Pth2 was efficiently co-purified with His-tagged Tom20 (Figure 6A). In addition, subunits of the TOM complex such as Tom40, Tom22 and Tom70 were efficiently co-purified with $Tom20_{His}$ as previously described (Qiu et al., 2013; Mårtensson et al., 2019). Furthermore, we performed reciprocal affinity purification assays using purified mitochondria expressing His-tagged Pth2 to confirm the TOM-Pth2 interaction (Figure 6B). As expected, subunits of the TOM complex (Tom22 and Tom70) were found in the elution fraction. In addition, Mim1, a subunit of the MIM complex, involved in the insertion of α-helical outer membrane proteins was also co-purified in the elution fraction of $Pth2_{His}$ (Doan et al., 2020).

We employed the high-resolution mitochondrial complexome (MitCOM) analysis to compare the mitochondrial protein assembly profile of Pth2 with other proteins (Figure 6C). In this analysis, crude mitochondria were lysed with a non-ionic detergent digitonin, processed via blue native gel electrophoresis, followed by high-resolution cryo-slicing and quantitative mass spectroscopy (MS). Subsequently, using elaborate MS quantification and profile building, abundance-mass profiles for different proteins were determined (Schulte et al., 2023). On comparing the MitCOM profiling of Pth2 and TOM subunits, we observed a co-migration of the peptidyl tRNA hydrolase Pth2 with the main peak of the TOM complex indicating a role of Pth2 at the TOM complex (Figure 6C). We compared the absolute copy number per yeast cell based on the quantification of mitochondrial proteins grown on different carbon sources by Morgenstern et al., 2017 (Figure 6). The absolute copy number of Pth2 is approximately three times less than that of Tom40. However, Pth2 exhibits a higher copy number compared to the mitoTAD component, Ubx2. Overall, our results indicate that Pth2 associates with the TOM complex under constitutive conditions.

The co-purification of Pth2 with mitochondria from yeast strains expressing HA-tagged Ubx2, raised the possibility that Pth2 functions in supporting the mitochondrial protein translocation-associated degradation (mitoTAD) pathway. To evaluate whether Pth2 co-operates with Ubx2 in TOM binding, we performed affinity purification assays using *UBX2* deletion yeast strains expressing HA-tagged Tom40.

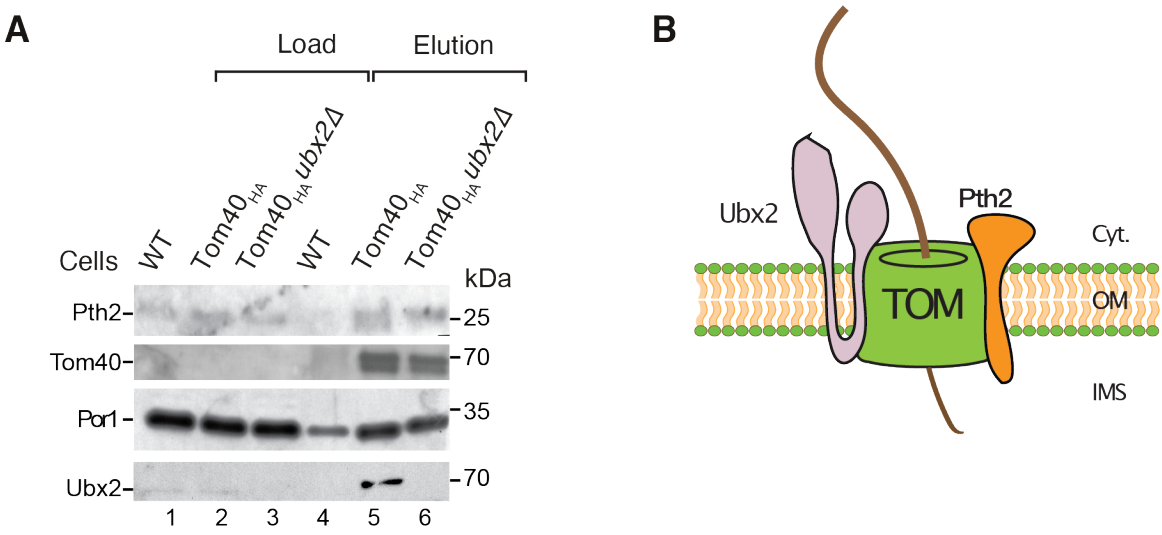

Figure 7. Pth2 interacts with TOM subunits independent of Ubx2. (A) Wild-type (WT), $Tom40_{HA}$, and $Tom40_{HA}$*ubx2*Δ yeast cells were solubilized with digitonin and used for affinity purification using an anti-HA affinity matrix. After washing steps, samples were eluted with SDS-sample buffer. Samples were analyzed by SDS-PAGE and immunodetection with the indicated antisera. Load., 0.2%; elution., 100%. **(B)** Model representing that Pth2 binds to the TOM complex independent of Ubx2. Cyt., cytosol; OM., outer membrane; IMS, intermembrane space.

Our results indicated that the TOM-Pth2 interaction does not depend on Ubx2. Moreover, Pth2 binds to the TOM complex independent of Ubx2 (Figure 7). Taken together, Pth2 is permanently associated with the TOM complex, and its association with the TOM complex does not depend on the key component of the mitoTAD pathway, Ubx2.

4.1.3 Pth2 promotes the removal of arrested precursor proteins from the clogged TOM complex

Next, we reasoned the quality control role of the interaction between Pth2 and the TOM complex. We asked whether Pth2 associates with the TOM complex to ensure the efficient removal of clogged precursor proteins. Prematurely folded proteins can get stuck at the TOM complex during mitochondrial protein import, resulting in clogging of the protein translocon and subsequent accumulation of mitochondrial precursor proteins. To study the response triggered by the accumulation of these precursor proteins, we attempted to artificially mimic the cellular conditions at the TOM pore, induced by import stress, by increasing the amount of faulty translocation states at the TOM complex. To this end, we deleted *PAM17* in yeast cells to compromise protein import (Figure 8A).

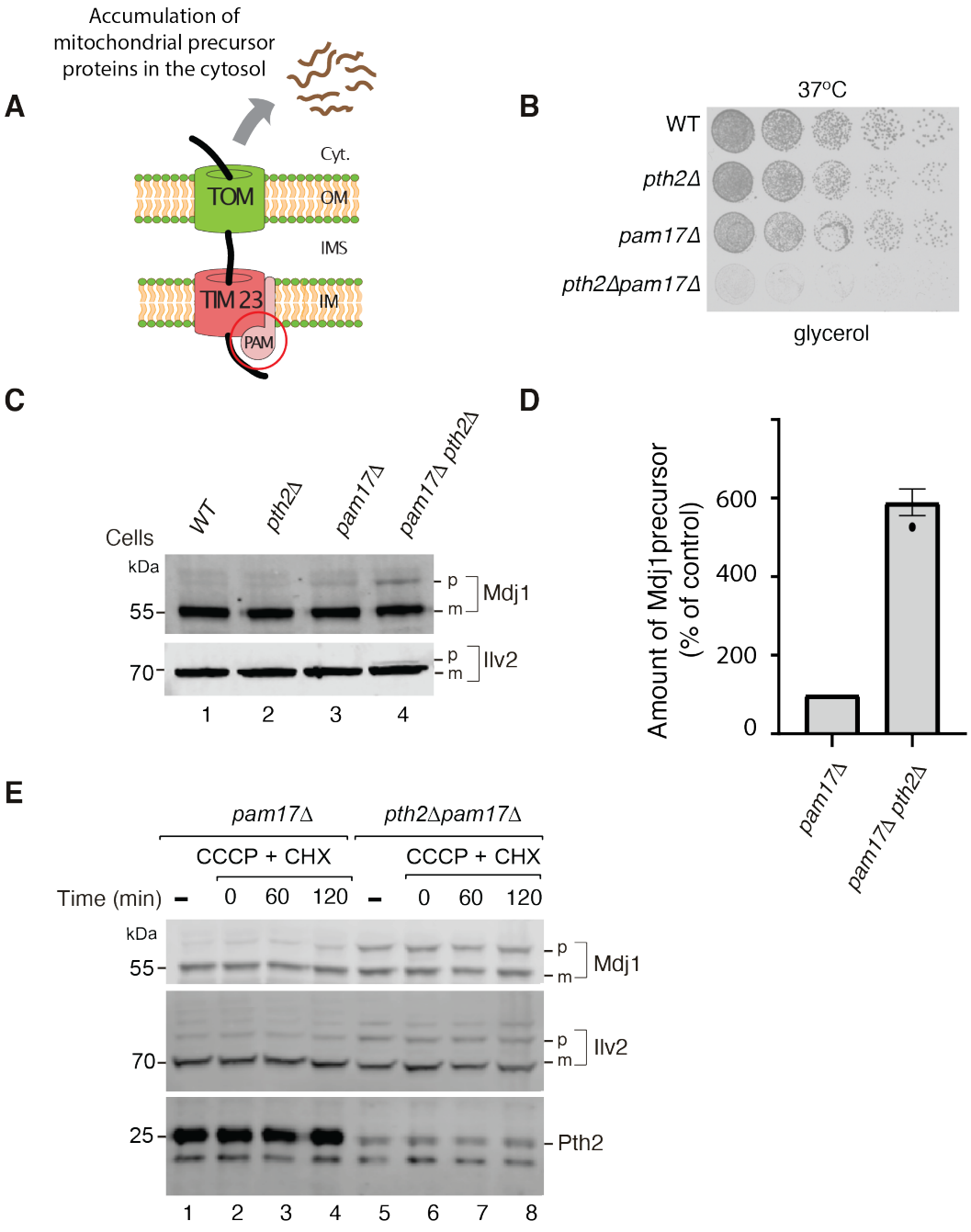

Figure 8. Pth2 promotes the clearance of arrested precursor proteins from the TOM complex. (A) Model showing the effect of deletion of *PAM17*, a non-essential component of the PAM motor. Deletion of *PAM17* impairs import and subsequently leads to the accumulation of mitochondrial precursor proteins in the cytosol. Cyt., cytosol; OM., outer membrane; IMS, intermembrane space. **(B)** Serial dilutions of wild-type (WT), *pth2Δ, pam17Δ*, and *pth2Δpam17Δ* yeast cells were spotted on full medium with glycerol as the carbon source and grown at 37°C. **(C)** Mdj1 and Ilv2 precursor levels in cell extracts from the indicated strains were analyzed by SDS-PAGE and immunodetection with indicated antisera**.** p, precursor; m, mature form of Mdj1 or Ilv2 precursor. **(D)** Quantification of the Mdj1 precursor levels. The amount of Mdj1 in pam17Δ cells was set to 100% (control). Mean ± s.e.m (n=3). **(E)** Degradation kinetics of the Mdj1 and Ilv2 precursor was analyzed in cell extracts from the indicated mutant strains after treatment with CCCP followed by cycloheximide (CHX) chase for the indicated time periods. CCCP, carbonyl cyanide m-chlorophenyl hydrazine.

Pam17 is a non-essential subunit of the precursor translocase-associated motor (PAM) and is required for driving protein import into the matrix (van der Laan et al., 2005). As a result, protein transport into the mitochondrial matrix is comprised in cells lacking *PAM17* and has been associated with the accumulation of precursor forms of several mitochondrial proteins on the mitochondrial surface (Mårtensson et al., 2019). Mdj1 and Ilv2 precursors are substrates of the PAM machinery and can thereby serve as good readouts to study the defects in mitochondrial import machinery by monitoring the accumulation of their precursor forms (Sahi et al., 2013).

In the context of *PAM17* deletion strain, where protein import is impaired, we further deleted *PTH2* to study its involvement in clearing non-imported precursor proteins in cells. We performed a growth assay with the double mutant strain *pth2*Δ*pam17*Δ along with respective single deletion strains and wild-type (Figure 8B). While the single mutant strains displayed only mild growth defects, the growth of the *pth2*Δ*pam17*Δ double mutant strain was profoundly reduced on a non-fermentable carbon source at elevated temperatures. These results led us to check for precursor protein accumulation in the double mutant strain (Figure 8C). Precursor proteins are not processed by mitochondrial proteases and thereby exhibit a slower migration on SDS-PAGE. As a result, precursor forms can be differentiated from the mature protein on SDS-PAGE followed by immunodetection. We observed a strong accumulation of the precursor forms of both Mdj1 and Ilv2 in *pth2*Δ*pam17*Δ yeast cells compared to single deletion cells thereby indicating that Pth2 functions in the degradation of non-imported precursor proteins from the TOM complex. To better characterize the degradation kinetics of the precursor form of Mdj1 and Ilv2, we conducted time-dependent pulse-chase experiments with the addition of carbonyl cyanide m-chlorophenyl hydrazine (CCCP) before the onset of the chase period (Figure 8E). Treatment of cells with CCCP, which is an uncoupler of oxidative phosphorylation, depletes membrane potential and consequently blocks protein import across the inner mitochondrial membrane (Wrobel et al., 2015). Our results indicated stabilization of the precursor form of both Mdj1 and Ilv2 in *pth2*Δ*pam17*Δ yeast cells compared to single deletion cells. In all, our results revealed that Pth2 plays a critical role in the removal of arrested precursor proteins from the TOM complex.

In order to exclude the possibility that the accumulation and stabilization of precursor proteins observed in *pth2*Δ*pam17*Δ yeast cells is not an indirect effect caused by the loss of mitoTAD components or loss of mitochondrial membrane potential, we characterized the steady-state

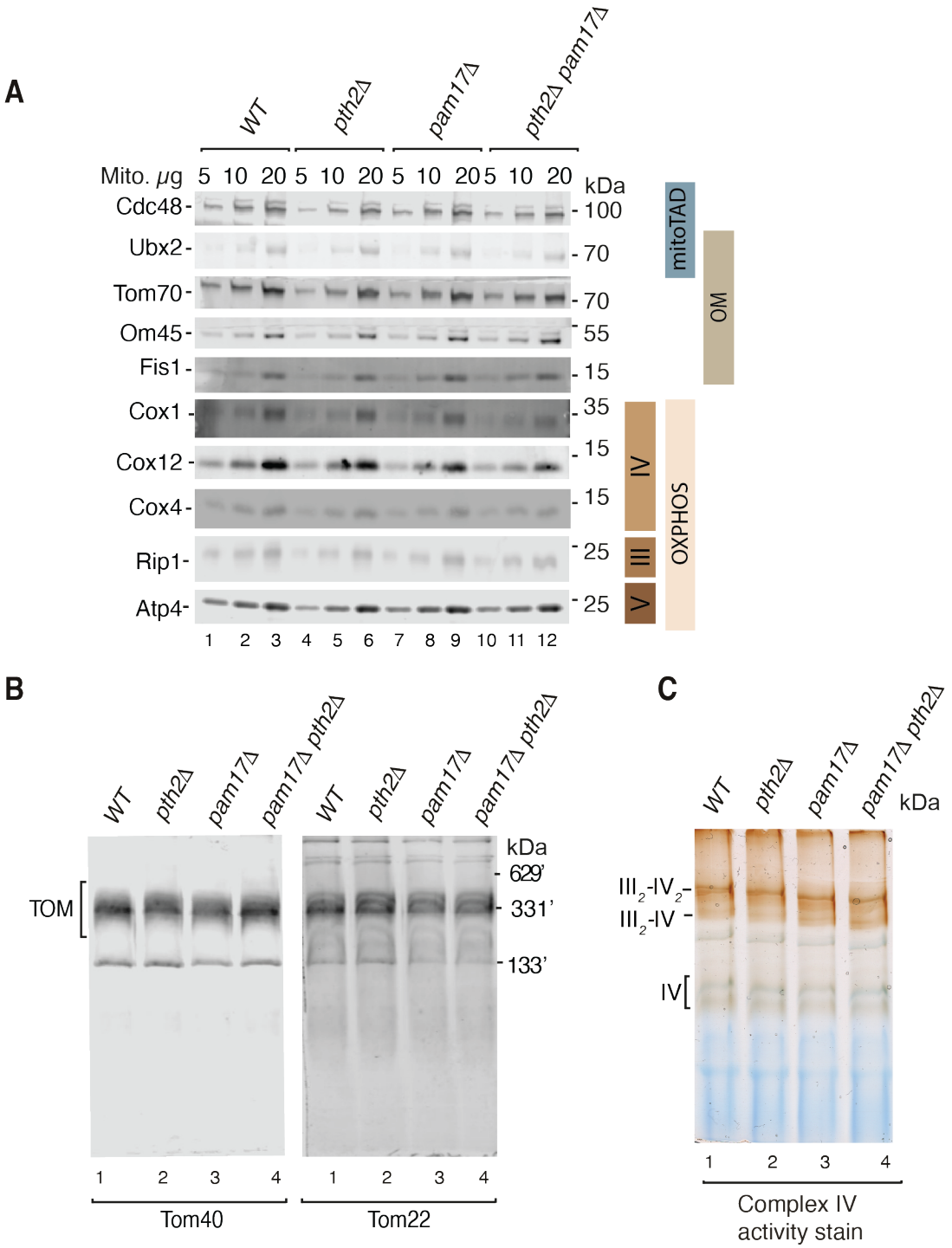

Figure 9. Characterization of steady-state protein levels of Pth2 and Pam17 deficient mitochondria. (A) Mitochondria isolated from wild-type (WT), *pth2*Δ*, pam17*Δ, and *pth2*Δ*pam17*Δ yeast cells were analyzed by SDS-PAGE and immunodetection with the indicated antisera. **(B)** Mitochondria from the indicated strains were lysed with digitonin and analyzed by BN-PAGE, followed by immunodetection with indicated antisera**. (C)** In-gel activity staining of complex IV in mitochondria from the indicated strains on BN-PAGE. II**,** complex II (succinate dehydrogenase); III, complex III (cytochrome c reductase); IV, complex IV (cytochrome c oxidase); V, complex V (F_1-F_o-ATP synthase) of mitochondrial oxidative phosphorylation machinery. OXPHOS., oxidative phosphorylation., OM., outer membrane; mitoTAD., mitochondrial protein translocation-associated degradation.

levels of mitochondrial proteins by SDS-PAGE and immunodetection (Figure 9A). The steady-state levels of Ubx2-Cdc48 (mitoTAD components) and the TOM subunits were not substantially altered in mitochondria isolated from *pth2*Δ*, pam17*Δ, and *pth2*Δ*pam17*Δ yeast strains with respect to WT. Moreover, the steady-state protein levels of mitochondrial respiratory chain subunits on SDS-PAGE remained unchanged. To examine that the TOM complex does not fall apart in the mutant strains, mitochondria were analyzed on blue native polyacrylamide gel electrophoresis (BN-PAGE) followed by immunodetection. BN-PAGE is a powerful analytical technique that allows protein separation under native conditions and preserves protein-protein interactions (Schägger and von Jagow, 1991). The TOM complex migrates at around 440 kDa in mitochondria from the WT strain (Becker et al., 2011). In mitochondria from both the single and double mutant strain, the TOM complex migrated comparable to the WT strain reflecting that the assembly of the TOM complex on BN-PAGE remained unaffected (Figure 9B). Furthermore, the assembly of oxidative phosphorylation complexes III, IV and V was intact in the double and single deletion strains on BN-PAGE. Subsequent staining of BN-PAGE for complex IV activity showed no change as compared to WT indicating the mitochondrial respiratory function was still active (Figure 9C).
All these results led us to conclude that the accumulation of precursor proteins observed in the *pth2*Δ*pam17*Δ yeast cells was not an indirect effect due to the loss of essential mitochondrial components but was caused due to the lack of the quality control role of Pth2.

4.1.4 Pth2 removes ubiquitylated precursor proteins

We wondered whether the absence of Pth2 leads to increased ubiquitylation of precursor proteins at the TOM complex. To define the involvement of Pth2 in the ubiquitylation of precursor proteins at the TOM complex, we utilized a second strategy of increasing the number of faulty translocation states at the TOM complex. We employed the overexpression of artificial cytochrome b_2-DHFR-HB construct to clog the TOM complex (Figure 10A). The b_2-DHFR-HB construct consists of an intermembrane mitochondrial targeting sequence from cytochrome b_2 fused to mouse dihydrofolate reductase (DHFR), followed by a heme group from cytochrome b_2. The DHFR moiety folds stably in the cytosol whereas the mitochondrial targeting sequence targets the constructs to the TOM-TIM23 complex in the mitochondria (Bömer et al., 1997; Chacinska et al., 2005; Boos et al., 2019). The b_2-DHFR-HB construct is prone to arrest at the TOM complex *in vitro* and *in vivo* (Gärtner et al., 1995; Bömer et al., 1997; Boos et al., 2019). Studies have shown that the overexpression of this fusion construct

from a regulatable galactose promoter resulted in reduced cell growth and cytosolic accumulation of mitochondrial precursor proteins (Boos et al., 2019; Mårtensson et al., 2019).

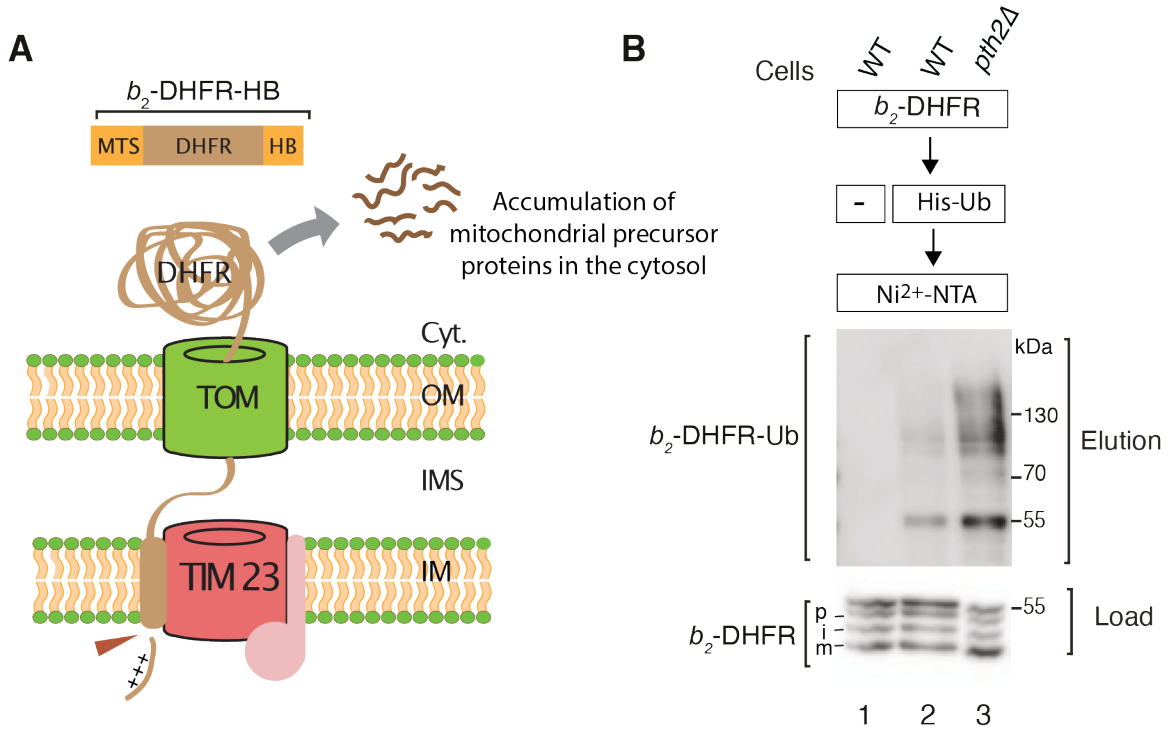

Figure 10. Ubiquitylation of b_2-DHFR in cells lacking Pth2. (A) Schematic representing the linear structure of cytochrome b_2-DHFR-HB construct that adopts an intermembrane mitochondrial targeting sequence from cytochrome b_2, a moiety of DHFR, and a heme group. Since the mitochondrial targeting sequence of cytochrome b_2 consists of a sorting signal, the precursor is laterally released into the inner membrane. The mitochondrial processing peptidase (MPP) cleaves the presequence and subsequently the sorting signal is cleaved. The DHFR domain stably folds in the cytosol, thereby delaying the import of precursors, and subsequently clogging the TOM complex. MTS., mitochondrial targeting sequence; DHFR., dihydrofolate reductase; HB, heme-binding domain. Cyt., cytosol; OM., outer membrane; IMS, intermembrane space; IM, intermembrane. **(B)** Wild-type (WT) and *pth2*Δ yeast cells co-expressing b_2-DHFR and His-tagged ubiquitin, as indicated, were lysed under denaturing conditions followed by affinity purification with Ni^{2+}-NTA agarose beads. After washing steps, samples were analyzed by SDS-PAGE and immunodetection with the indicated antisera. Load, 0.2%; elution, 100%. p., precursor; i., intermediate form; m, mature form of b_2-DHFR-HB precursor.

To subsequently detect ubiquitylated species of b_2-DHFR, we expressed a His-tagged ubiquitin construct along with the overexpression of artificial clogging-prone construct cytochrome b_2-DHFR-HB, in collaboration with Dr. Fabian den Brave (Figure 10B). This method relies on the use of N-terminal His-tagged ubiquitin, which is compatible with the Ni^{2+}-NTA agarose beads and thereby allows the purification of His-tagged ubiquitin conjugates. As control, WT yeast cells expressing His-tagged ubiquitin and b_2-DHFR-HB were used to ensure the

specificity of the assay. In WT cells, b_2-DHFR was ubiquitylated which could be observed as higher molecular weight species on SDS-PAGE. Thus, ubiquitylation of b_2-DHFR gave rise to a slower migrating protein form that could be specifically detected on SDS-PAGE followed by immunodetection. Interestingly, in cells lacking *PTH2,* ubiquitylation of b_2-DHFR was further enhanced. As observed with the accumulation of ubiquitylated precursor proteins in *pth2*Δ mutant cells, we conclude that Pth2 is involved in the removal of accumulated ubiquitylated precursor proteins.

4.1.5 Overlapping regulatory functions of Pth2 and Ubx2

To further define the role of Pth2 in quality control, its interaction with the mitoTAD key component, Ubx2 was investigated in further detail in collaboration with Dr. Fabian den Brave. Pth2 was deleted in cells lacking Ubx2 and growth assays were performed (Figure 11A). The phenotype of the single Ubx2 and Pth2 deletion strains displayed only milder growth defects due to the presence of overlapping compensatory functions of both proteins. Remarkably, the double deletion strain *pth2*Δ*ubx2*Δ showed a prominent growth defect in media containing non-fermentable carbon sources when mitochondrial function became particularly important.

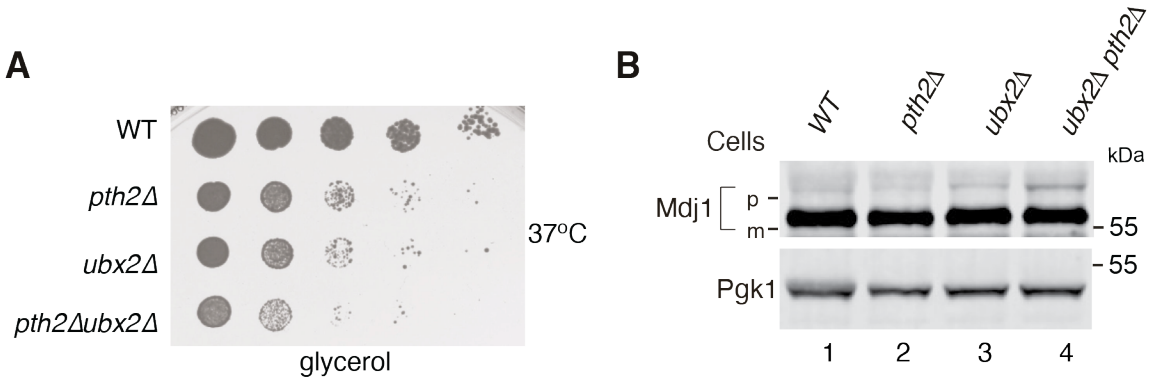

Figure 11. Double deletion of Pth2 and Ubx2 shows synthetic growth defects. (A) Serial dilutions of wild-type (WT), *pth2*Δ*, ubx2*Δ, and *pth2*Δ*ubx2*Δ yeast cells were spotted on full medium with glycerol as the carbon source and grown at 37°C. **(B)** Mdj1 precursor levels in cell extracts from the indicated strains were analyzed by SDS-PAGE and immunodetection with indicated antisera. Pgk1 was used as a loading control. p, precursor; m, mature form of Mdj1 or Ilv2 precursor.

We analyzed the cell extracts from the WT, *pth2*Δ*, ubx2*Δ*, and pth2*Δ*ubx2*Δ strains on SDS-PAGE followed by immunodetection. Strikingly, a strong accumulation of the precursor

form of Mdj1 was observed in the double mutant strain lacking *PTH2* and *UBX2* under permissive conditions, indicating that both proteins play a role in the degradation of non-imported precursor proteins from the TOM complex (Figure 11B).

To exclude the indirect effects caused by the deletion of *PTH2* and *UBX2* on essential mitochondrial functions, outer and inner mitochondrial membrane proteins as well as mitoTAD components were analyzed by SDS-PAGE followed by immunodetection (Figure 12). The levels of Cdc48 were reduced in *UBX2* deletion cells as previously described (Mårtensson et al., 2019). Interestingly, Cdc48 levels were partially rescued in the double deletion strain *pth2*Δ*ubx2*Δ suggesting compensatory functions of Pth2 with Ubx2 in quality control under non-stress conditions. The steady-state levels of mitochondrial outer membrane, inner membrane and matrix proteins were not significantly altered and remained similar in the single and double-deletion strains of *PTH2* and *UBX2* respectively. The steady-state levels of the TOM subunits were unaffected in the double deletion strain with respect to the single deletion strains on SDS-PAGE. All these results indicated that the precursor accumulation observed in the *pth2*Δ*ubx2*Δ strain was not an indirect effect caused by the loss of essential mitochondrial proteins.

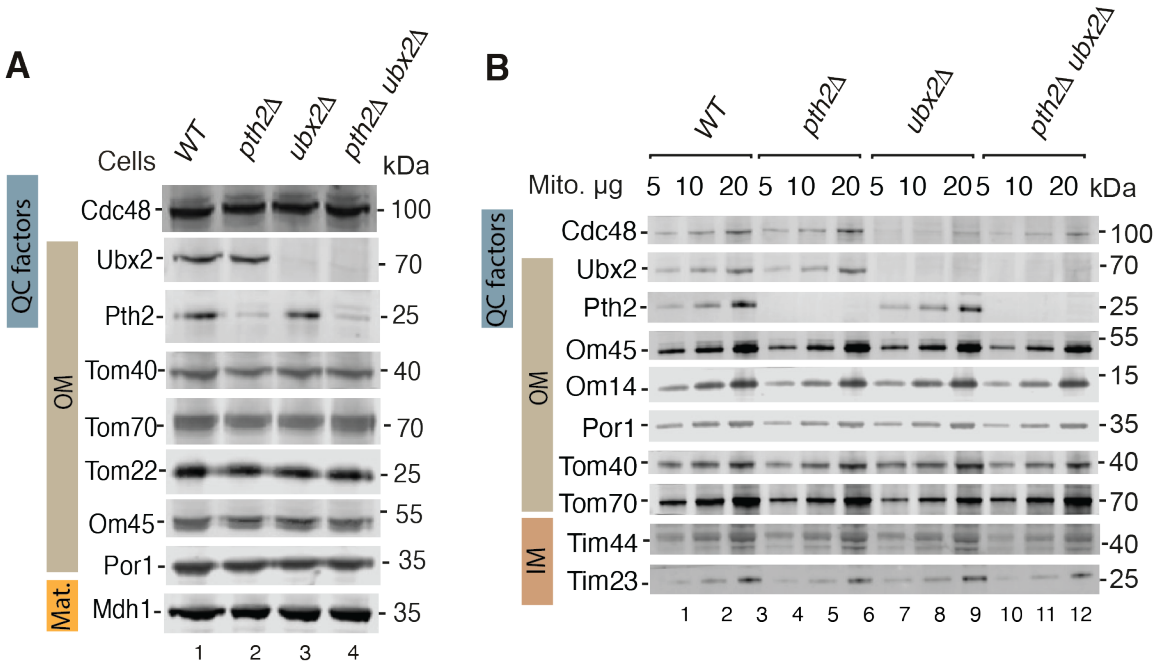

Figure 12. Steady-state levels in Pth2 and Ubx2 deficient mitochondria. (A) Cell extracts from wild-type (WT), *pth2*Δ, *ubx2*Δ, and *pth2*Δ*ubx2*Δ yeast cells were analyzed by SDS-PAGE and immunodetection. **(B)** Mitochondria isolated from the indicated strains were analyzed by SDS-PAGE and immunodetection with the indicated antisera. QC factors., quality control factors; OM., outer membrane; IM., inner membrane; Mat., Matrix of mitochondria.

4.1.7 Pth2 is N-terminally anchored to the mitochondrial outer membrane

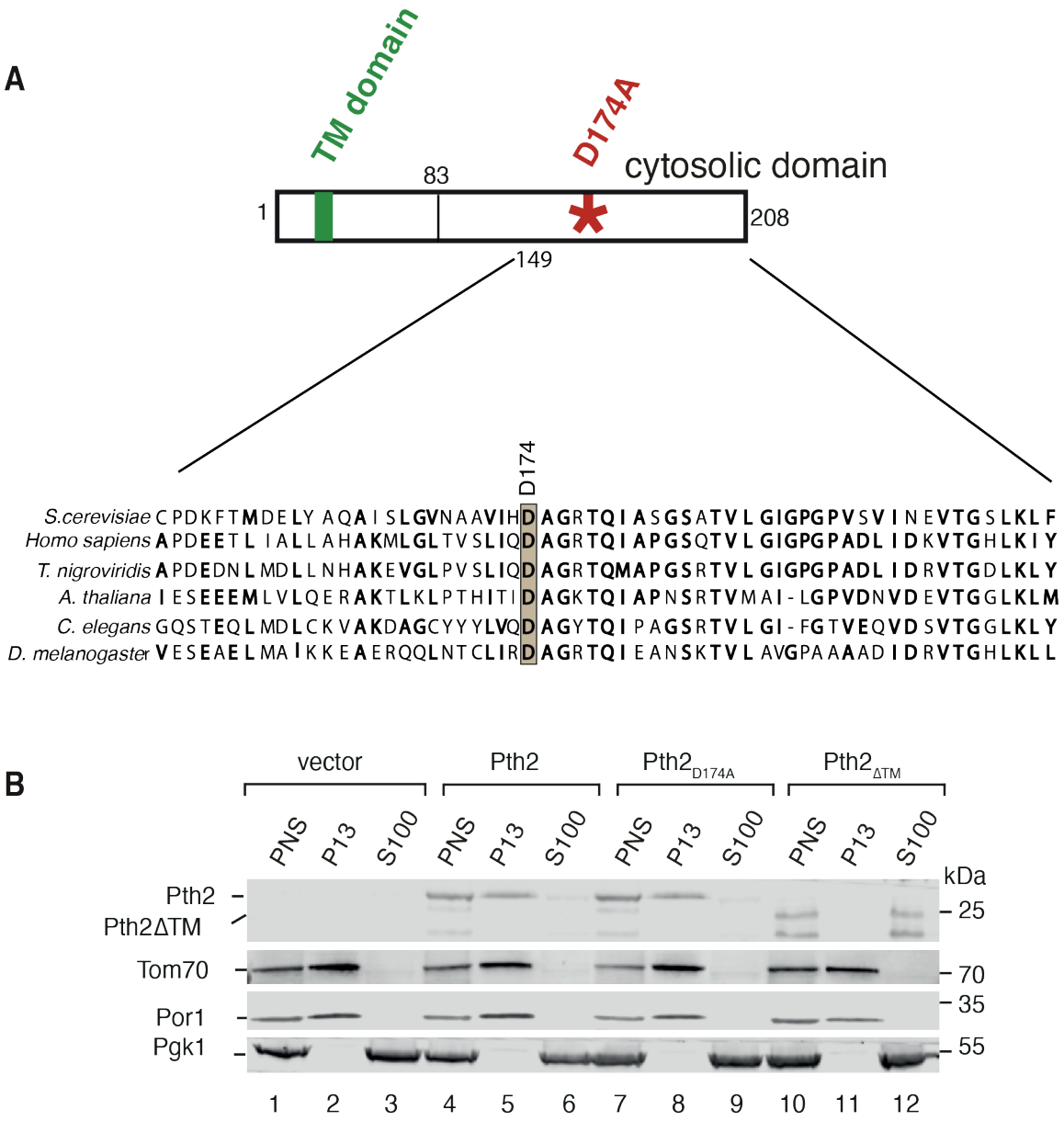

Figure 13. Characterization of Pth2 mutants. (A) Schematic representation of Pth2 and multiple sequence alignment of different Pth2's from archaeal and eukaryotic organisms. Protein sequences were aligned using Clustal omega. Conserved amino acid residues are labelled as bold. The box indicates the conserved aspartic acid residue in the tRNA hydrolase active site. *S. cerevisiae., Saccharomyces cerevisiae H. sapiens., Homo sapiens, T. nigroviridis., Tetraodon nigroviridis, A. thaliana., Arabidopsis thaliana, C. elegans.,Caenorhabditis elegans, , D. melanogaster., Drosophila melanogaster.* In the linear structure of Pth2, the trans-membrane (TM) domain is represented in green and the amino acid exchange D174A by a red asterisk. **(B)** Cellular fractionation samples of the indicated strains were analyzed by SDS-PAGE and immunodetection with indicated antisera. PNS, post-nuclear supernatant fraction; P13, mitochondria enriched; S100, cytosolic fraction.

Peptidyl-tRNA hydrolase, Pth2, is an enzyme that cleaves off peptidyl-tRNA into tRNA and peptides during translation, thereby renewing the cellular pool of ribosomes for protein biosynthesis (Hernandez-Sanchez et al., 1998; Das and Varshney, 2006). The structure of human Pth2 has been solved by crystallography and provides insights into its catalytic tRNA hydrolase activity and its α/β fold structure (De Pereda et al., 2004). Yeast Pth2 consists of 208 amino acid residues and contains two domains: a conserved C-terminal part that harbors the catalytic domain and a divergent N-terminal part (De Pereda et al., 2004; Ishii et al., 2006). The C-terminal part of Pth2 exhibits a high degree of conservation across a wide range of organisms, spanning from archaea to eukaryotes (Figure 13A). To date, no function has been attributed to the N-terminal part of Pth2, but it could be likely that it renders species selectivity to Pth2 (Ishii et al., 2006).

The trans-membrane domain of Pth2 was predicted using online prediction softwares (CCTOP, TMpred, TMHMM) and was found to scan approximately the first 10 to 20 amino acids of the Pth2 protein. The conserved residue of the peptidyl-tRNA hydrolase active site (D174) was mutated to alanine using site-directed mutagenesis (Ishii et al., 2006).
Pth2 is a α-helical signal-anchored outer mitochondrial membrane protein imported via the MIM complex (Doan et al., 2020). Cellular fractionation experiments were performed to determine the localization of the Pth2-mutant constructs (Figure 13B). In line with previous studies, Pth2 was localized in the mitochondrial enriched fraction (P13) (Doan et al., 2020). In strains expressing the Pth2 mutant lacking the TM region (Pth2TMΔ), Pth2 was found in the cytosolic fraction (S100), indicating that the TM region of Pth2 is required for its mitochondrial localization. Pth2 was also found in the mitochondrial fraction (P13) in the strains expressing Pth2 mutant form with a mutation in the tRNA hydrolase active site (Pth2D174A).

4.2 Pth2 functions in quality control at mitochondria

4.2.1 Dual role of Pth2 in quality control

Pth2 and Vms1 have been characterized as peptidyl tRNA hydrolases (Verma et al., 2018; Zurita Rendón et al., 2018). Vms1 functions in the mitochondrial ribosome-associated quality control (mitoRQC) pathway and mediates the removal of stalled peptides from the ribosomal subunits (Izawa et al., 2017; Matsuo et al., 2017; Su et al., 2019). In addition, the cytosolic

protein Vms1 has been described to recruit Cdc48 to the mitochondrial surface in response to oxidative stress (Heo et al., 2013).

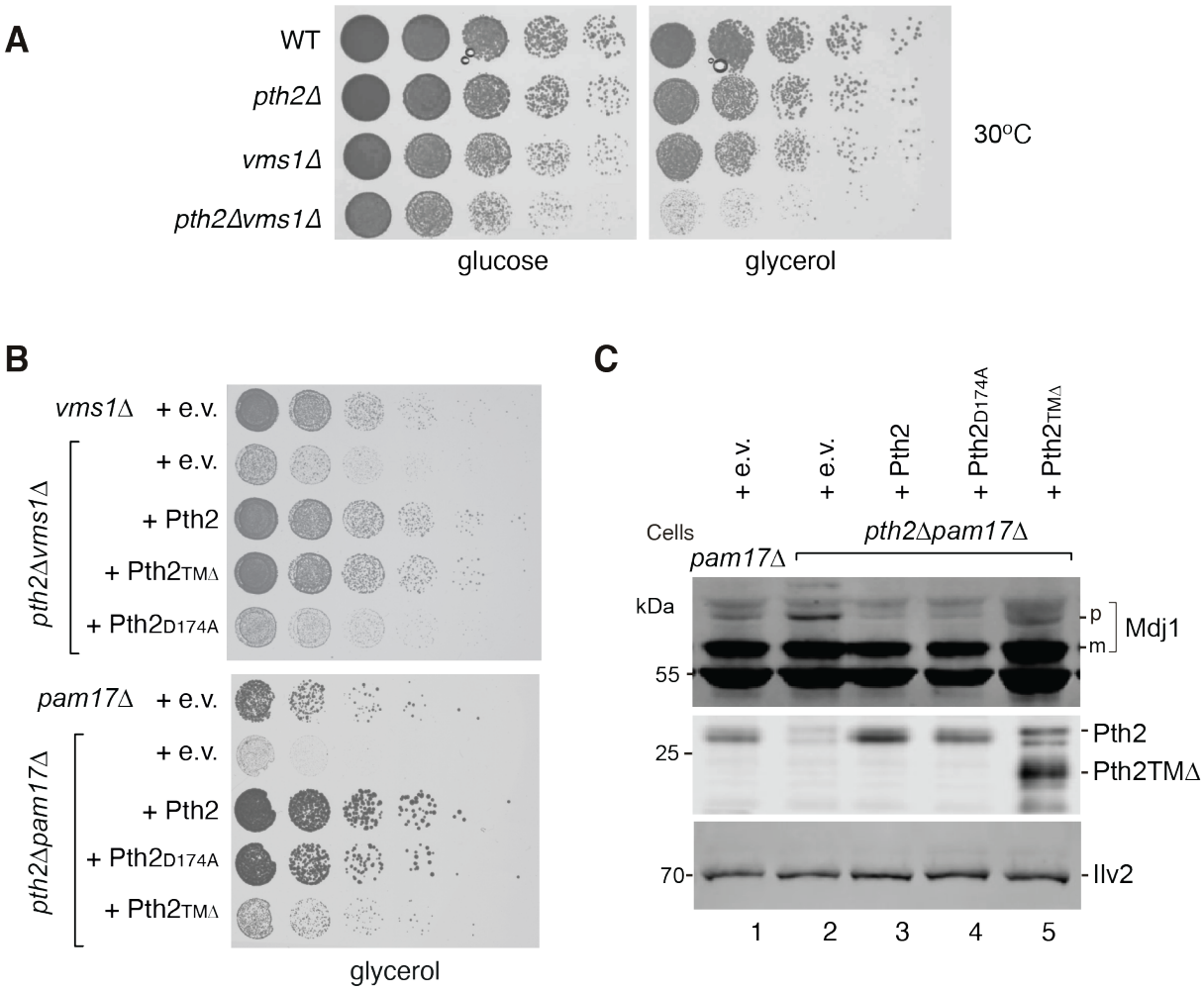

Figure 14. Dual role of Pth2 in quality control. (A) Serial dilutions of wild-type (WT), *pth2*Δ, *vms1*Δ, and *pth2*Δ*vms1*Δ yeast cells were spotted on full medium with glucose or glycerol as carbon source and grown at 30°C. **(B)** Serial dilutions of the indicated strains were spotted onto selective medium with glycerol as the carbon source and grown at 37°C. **(C)** Cell extracts from the indicated strains cells were analyzed by SDS-PAGE and immunodetection with indicated antisera**.** e.v., empty vector; p, precursor; m, mature form of Mdj1 precursor.

To elucidate the physiological connection between Pth2 and Vms1, we created a double deletion yeast strain, *pth2*Δ*vms1*Δ which exhibited a strong growth defect in both glucose and glycerol media. This was contrary to the growth phenotype observed in single deletions strains where growth was not altered (Figure 14A). We then utilized the observed growth phenotypes for *pth2*Δ*pam17*Δ and *pth2*Δ*vms1*Δ cells as readouts to study Pth2 function with the help of the

Pth2 mutant constructs, Pth2TMΔ and Pth2D174A. The expression of the Pth2D174A construct did not rescue the growth defect observed in *pth2*Δ*vms1*Δ cells, in contrast to the Pth2TMΔ construct that was able to rescue *pth2*Δ*vms1*Δ cells. This suggested that Pth2 functions as a peptidyl-tRNA hydrolase independent of the mitochondrial localization of Pth2 (Figure 14B). On contrary to these findings, the Pth2TMΔ construct was able to rescue the growth defect observed in the *pth2*Δ*vms1*Δ yeast strain, whereas the Pth2D174A construct was unable to rescue these cells. Thus, two experimentally separable functions of Pth2 were discovered. One related to its peptidyl tRNA hydrolase activity in the Vms1-linked quality control pathway at ribosome stalled polypeptides and the other related to mitochondrial localization of Pth2 required for the removal of non-imported precursor proteins during mitochondrial import. Furthermore, we analyzed cell extracts of yeast cells expressing Pth2 mutant forms along with appropriate controls using SDS-PAGE and immunodetection (Figure 14C). Re-expression of the *PTH2* from a plasmid rescued both the observed growth phenotypes and precursor accumulation of Mdj1. Pth2TMΔ exhibited a faster migration on SDS-PAGE as the trans-membrane region was cleaved, and thus could be differentiated from the mature Pth2 protein. These results highlight the role of Pth2 in the removal of stuck non-imported precursors from the TOM complex.

4.2.2 Pth2 co-operates with Vms1 in the clearance of stalled ribosomes

It was previously shown that detergent-insoluble protein aggregates were formed in *ltn1*Δ*vms1*Δ cells due to the accumulation of mitochondrial proteins that were otherwise removed by the ribosome-associated quality control (RQC) pathway (Izawa et al., 2017). To examine the role of Pth2 in the Vms1-linked pathway, we checked for detergent-insoluble protein aggregates in *pth2*Δ*vms1*Δ cells, using *ltn1*Δ*vms1*Δ cells as a positive control (Figure 15A). We lysed the cells with a non-ionic detergent, followed by centrifugation, and analyzed total, soluble, and pellet fractions by SDS-PAGE and immunoblotting with antibodies against Rip1, Sod2 and Pgk1. Strikingly, we observed the accumulation of proteins in the insoluble pellet fraction of the *pth2*Δ*vms1*Δ sample, as well as in the *ltn1*Δ*vms1*Δ sample which was in line with previous findings (Izawa et al., 2017).

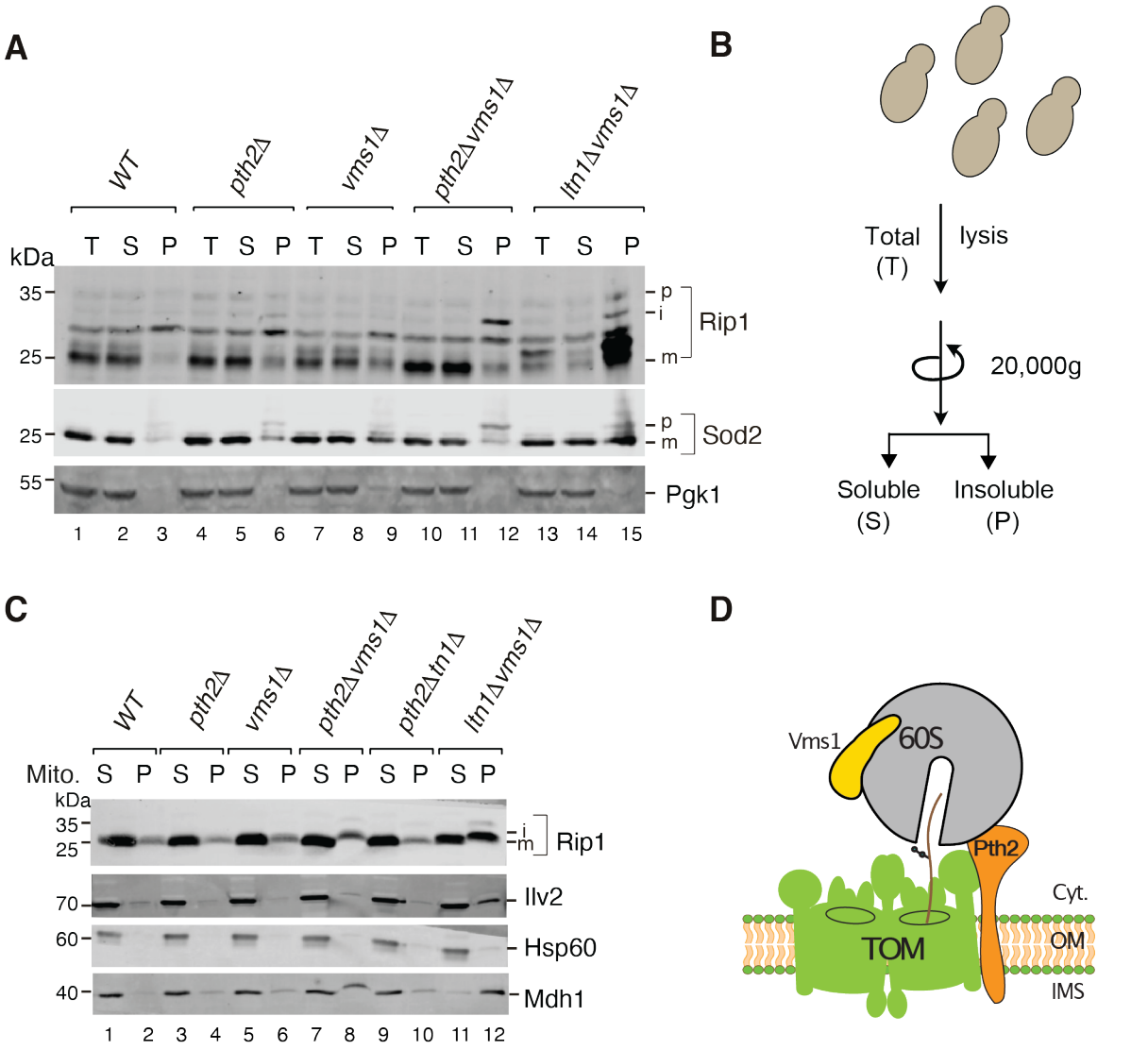

Figure 15. The relationship of Pth2 with Vms1 (A) Wild-type (WT), *pth2*Δ, *vms1*Δ, *pth2*Δ*vms1*Δ, and *ltn1*Δ*vms1*Δ yeast cells were grown in a medium containing galactose as a carbon source at 37°C and lysed with a non-ionic detergent. Total lysates (T) were separated into pellet (P) and supernatant (S) fractions by centrifugation (20,000g, 15 min) and analyzed by SDS-PAGE and immunodetection with indicated antisera. p., precursor; i., processing intermediate., m., mature form of Rip1 or Sod2 precursor. **(B)** Schematic representation of the experimental setup used to separate yeast cells into soluble (S) and insoluble pellet (P) fractions. **(C)** Mitochondria isolated from the indicated strains were grown under respiratory conditions at permissible temperatures and analyzed by SDS-PAGE and immunodetection with the indicated antisera. **(D)** Model showing that both Pth2 and Vms1 associate with ribosomal subunits at the mitochondrial outer membrane. Rqc2, components of the ribosomal quality control (RQC) adds C-terminal alanine threonine (CAT)-tails to the nascent chains. The CAT-tailed proteins when imported into mitochondria form toxic aggregates. Vms1 protects mitochondria from the toxic effect of CAT-tailed proteins by releasing the nascent polypeptides from the ribosome (Izawa et al., 2017). OM., outer membrane; IMS., intermembrane space; Cyt., cytosol.

After being imported into mitochondria, Rip1 is processed in two steps by mitochondrial processing peptidase (MPP), generating an intermediate and mature form of Rieske Fe-S protein (Rip1) (Fernandez-Vizarra and Zeviani, 2018; Hartl et al., 1986). In *pth2*Δ*vms1*Δ and *ltn1*Δ*vms1*Δ yeast cells, we observed the intermediate form of Rip1 in the pellet fraction suggesting that aggregation occurred after import into mitochondria (Izawa et al., 2017). Aggregation was restricted to mitochondrial proteins as the cytosolic protein phosphoglycerate kinase (Pgk1) was enriched only in the soluble fractions. In contrast to *pth2*Δ*vms1*Δ and *ltn1*Δ*vms1*Δ yeast cells, WT, *pth2*Δ, and *vms1*Δ samples did not accumulate aggregated proteins in the pellet fraction.

We further performed the same assay with purified mitochondria grown under respiratory conditions and analyzed soluble and pellet fractions by SDS-PAGE and immunoblotting with antibodies against Rip1, mitochondrial chaperone Hsp60 and mitochondrial matrix proteins, Mdh1 and Ilv2 (Figure 15C). Indeed, we found a large amount of protein in the insoluble pellet fraction of the *pth2*Δ*vms1*Δ sample. These results suggested a potential link between Pth2 and Vms1 in the clearance of aggregated proteins during co-translational mitochondrial import.

4.2.3 Pth2 recruits quality control factor Dsk2

Pth2 interacts with Ubiquitin-like (UBL)-Ubiquitin associated (UBA) proteins, Dsk2 and Rad23, that serve as delivery factors for targeting polyubiquitylated substrates to the proteasome for degradation (Ishii et al., 2006). The UBL domain of these proteins interacts with polyubiquitin receptors located on the 19S proteasome and helps to direct the ubiquitylated substrates toward the proteasome for degradation. Furthermore, the UBA domain is capable of binding to polyubiquitin chains. This allows the UBL-UBA proteins to recognize and capture ubiquitinated substrates that need to be degraded (Chen and Madura, 2002; Rao and Sastry, 2002). Members of these protein families possess an N-terminal UBL domain and one or more UBA domains at the C-terminus (Raasi and Pickart, 2003).

The human homolog of Dsk2, ubiquilins (UBQLNs), plays a crucial role in recognizing and targeting misfolded proteins and facilitating their degradation (Itakura et al., 2016). We investigated the involvement of Dsk2 in mitochondria-located quality control in yeast. To this end, we performed growth assays using yeast cells lacking *DSK2*. Mutant cells deficient in

DSK2 displayed growth defects under respiratory conditions, especially at elevated temperatures indicating mitochondrial dysfunction (Figure 16A).

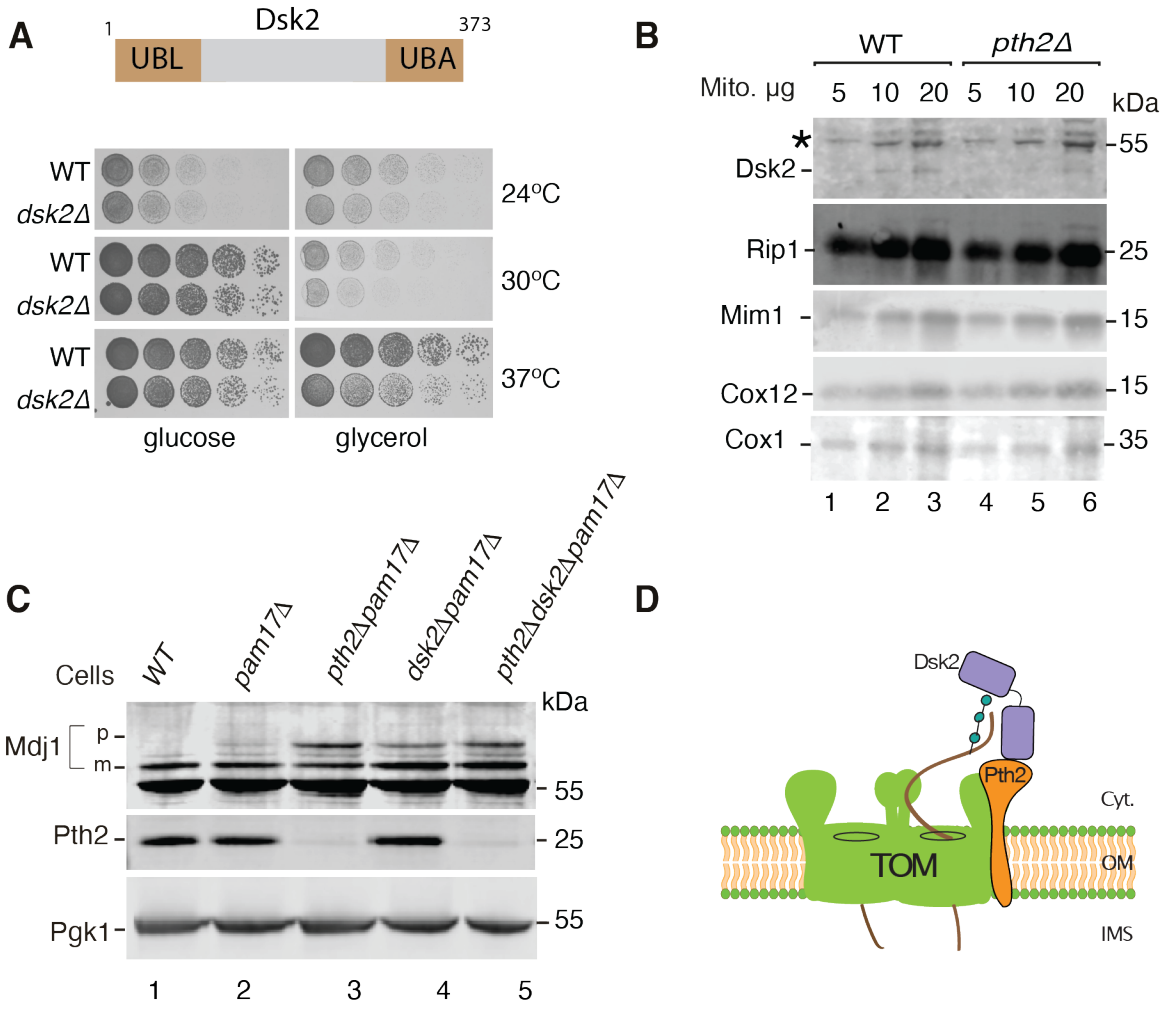

Figure 16. Pth2 recruits the quality control factor Dsk2. (A) Cartoon showing the linear structure of Dsk2 with a UBL domain at the N-terminus and a UBA domain at the C-terminus (above). Serial dilutions of wild-type (WT) and *dsk2*Δ yeast strains were spotted onto full medium with glucose or glycerol as the carbon source and grown at the indicated temperature conditions (below). **(B)** Dsk2 levels were analyzed in mitochondria isolated from WT and *pth2*Δ yeast strains, subsequently analyzed by SDS-PAGE, and immunodetection with the indicated antisera. The asterisk marks an unspecific signal of anti-Dsk2. **(C)** Mdj1 precursor levels in cell extracts from WT, *pam17*Δ, *pth2*Δ*pam17*Δ, *dsk2*Δ*pam17*Δ, and *pth2*Δ*dsk2*Δ*pam17*Δ yeast cells were analyzed by SDS-PAGE and immunodetection with the indicated antisera. UBL., ubiquitin-like; UBA., ubiquitin-associated; p., precursor; m., mature form of Mdj1 precursor. **(D)** Model showing that Pth2 serves as a mitochondrial receptor for recruiting Dsk2 to the TOM complex. OM., outer membrane; IMS., intermembrane space; Cyt., cytosol.

Under these conditions, there is an increased demand for metabolic processes, thereby increasing the reliance on mitochondrial function. Our results revealed that Dsk2 is involved in

mitochondrial quality control. Next, we speculated whether Pth2 recruits Dsk2 to mitochondria. To address this, we characterized the steady-state protein levels of Dsk2 in mitochondrial samples from strains deficient in *PTH2* (Figure 16B). Remarkably, the levels of Dsk2 were reduced in mitochondria from yeast cells lacking *PTH2*, suggesting that Dsk2 is recruited to the mitochondria via Pth2. The role of Dsk2 in the clearance of stuck precursors from the TOM channel was analyzed using the strategy of creating import stress by parallel deletion of *PAM17* (see chapter 4.1.3). We analyzed the cell extracts from WT, *pam17*Δ, *pth2*Δ*pam17*Δ, *dsk2*Δ *pam17*Δ, and *pth2*Δ*dsk2*Δ *pam17*Δ yeast strains on SDS-PAGE followed by immunodetection (Figure 16C). Interestingly, a strong accumulation of the precursor form of Mdj1 was seen in *dsk2*Δ*pam17*Δ and *pth2*Δ*dsk2*Δ*pam17*Δ yeast cells, as well as in *pth2*Δ*pam17*Δ (previously seen in Figure 8) indicating that Dsk2 plays a quality control role in the removal of non-imported precursor proteins from the TOM complex. Taken together, these results highlight the role of the Pth2-Dsk2 pathway in the removal of accumulated proteins as an additional layer of quality control under non-stress conditions.

4.3 Fmp52 as a novel interaction partner of Pth2

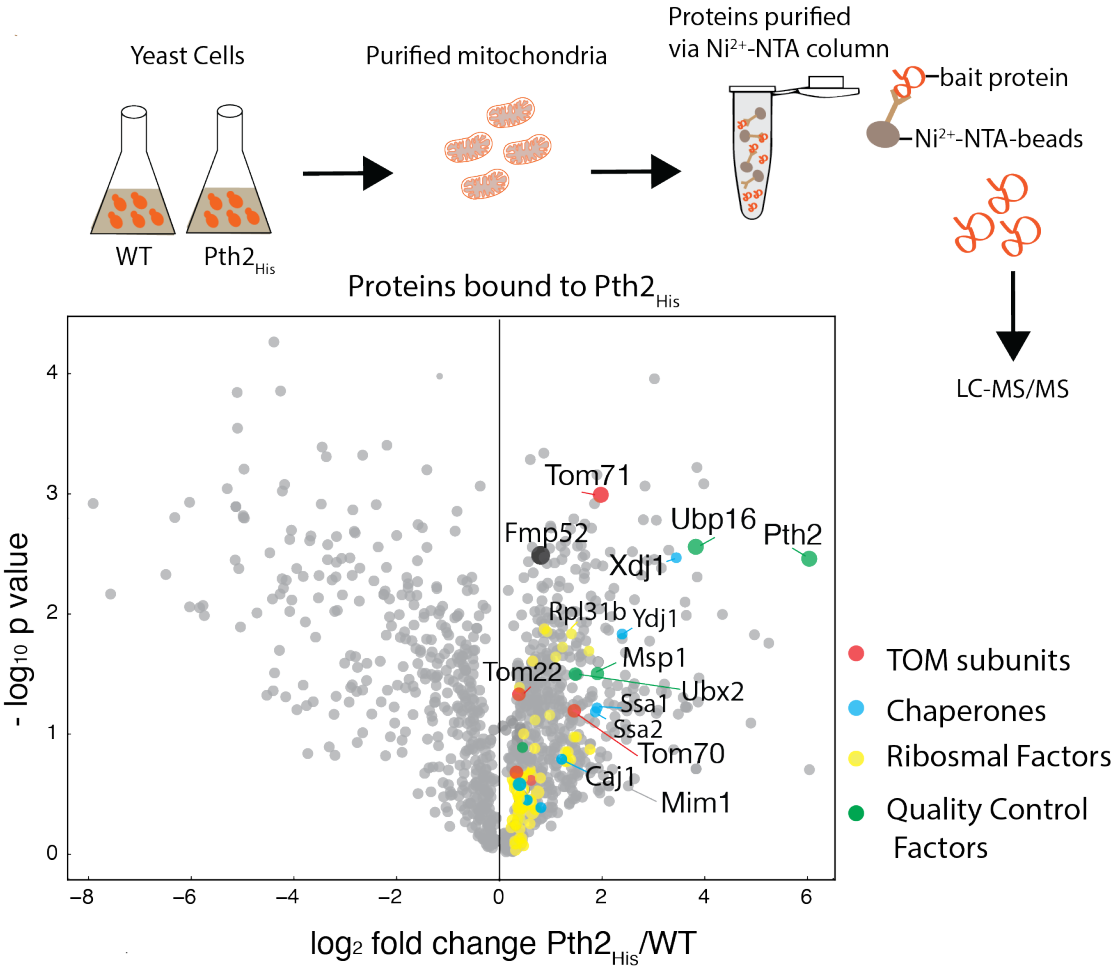

Figure 17. Mass spectrophotometry analysis of His-tagged Pth2 mitochondria. Wild-type (WT) and $Pth2_{His}$ mitochondria were subjected to affinity purification using Ni^{2+}-NTA agarose beads, and the eluted samples were analyzed by mass spectroscopy. Shown here is the volcano plot of the proteins co-precipitated with $Pth2_{His}$ and identified by label-free proteomics. Depicted are the log_2 fold changes of $Pth2_{His}$-bound proteins versus WT background mitochondria of four replicates, plotted against their statistical significance ($-log_{10}$ p-value). Proteins of interest are highlighted with colors (red, green, and blue). LC-MS., Liquid chromatography-mass spectrometry.

To gain further insights into Pth2 functions, we analyzed binding partners of Pth2 with quantitative mass spectroscopy (Figure 17). Crude mitochondria were isolated from both wild-type and mutant strain expressing His-tagged Pth2, in a medium containing a fermentable carbon source at permissive temperature conditions. Mitochondria were lysed with the non-ionic detergent digitonin and then subjected to affinity purification, and the eluted samples were subsequently analyzed using label-free proteomics.

As expected TOM and MIM subunits were enriched in mitochondrial samples from yeast strains expressing His-tagged Pth2. In addition, we observed that chaperones (Xdj1, Caj1, Ydj1), ribosomal factors (60S and 40S ribosomal subunits), and quality control factors (Msp1, Ubp16, and Ubx2) were also co-purified. Interestingly, we observed a notable increase in the abundance of the unknown protein, Fmp52, in the $Pth2_{His}$ elution fraction. Systemic studies with yeast mitochondria suggest that Fmp52 is localized to the mitochondrial outer membrane (Zahedi et al., 2006; Morgenstern et al., 2017; Vögtle et al., 2017). It has been observed that DNA damage with UVA irradiation, induced the expression of *FMP52,* a previously uncharacterized gene (Dardalhon et al., 2007). The role of Fmp52 however remained elusive. Nonetheless, the interesting observation that Fmp52 binds to Pth2, an outer mitochondrial membrane protein involved in the degradation of precursor proteins, provided a starting point for further functional characterization and understanding of the biological significance of Fmp52.

4.3.1 Fmp52 binds the TOM complex

To define the mitochondria-specific function of Fmp52, we began with affinity purification assay with cell extracts from yeast strains expressing HA-tagged Tom40 (Figure 18A). Indeed, Fmp52 was efficiently co-purified with Tom40, the core component of the TOM complex, under non-stressed conditions. In addition, various control proteins such as Tom20, Ubx2, and Tom70 were also co-purified with HA tagged Tom40, validating the successful functioning and reliability of the affinity-purification assay.

We analyzed cell extracts from WT and *fmp52*Δ yeast strains by SDS-PAGE followed by immunodetection with anti-Fmp52 antisera to validate the Fmp52-specific band (Figure 18B). An unspecific band denoted by an asterisk was observed below the specific Fmp52 signal.

To further corroborate our results, we compared the mitochondrial protein assembly profiles of Fmp52 and TOM subunits over an extended molecular mass range and observed the co-migration of Fmp52 with the main peak of the TOM complex (Figure 18C) (Schulte et al., 2023). Taken together, the interaction of Fmp52 with the core component of the main entry gate, Tom40 indicated towards a mitochondria-specific function of Fmp52.

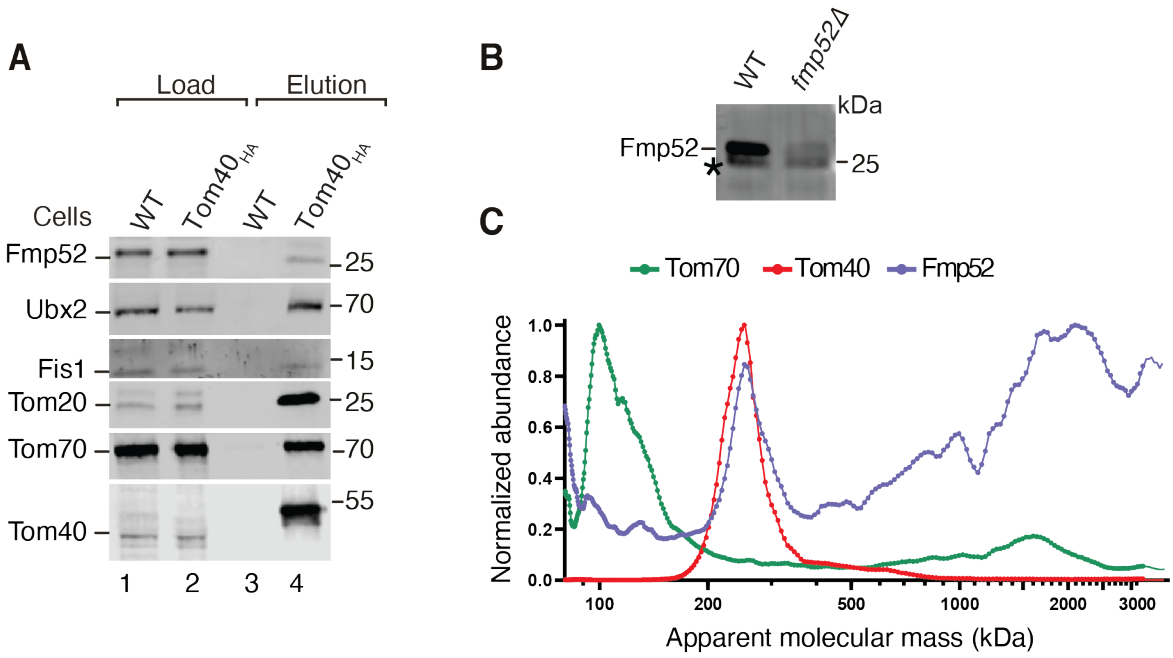

Figure 18. Fmp52 interacts with the TOM subunits. (A) Wild-type (WT) and Tom40$_{HA}$ yeast cells were solubilized with digitonin and used for affinity purification with anti-HA affinity matrix. After the washing steps, samples were eluted with SDS-sample buffer. The samples were analyzed by SDS-PAGE and immunodetection with the indicated antisera. **(B)** Cell extracts from WT and *fmp52*Δ yeast cells were analyzed by SDS-PAGE and immunodetection with the anti-Fmp52 antisera. The asterisk marks an unspecific signal of anti-Fmp52. **(C)** Comparison of the normalized abundance-mass profiles of Tom70, Tom40, and Fmp52 obtained from Schulte et al., MitCOM data set (Schulte et al., 2023).

We wondered how Fmp52 was recruited to the TOM complex and to this extent analyzed steady-state protein levels in the mitochondria of yeast cells lacking *TOM20* and *TOM70* (Figure 19A). Tom20 and Tom70 are the two main import receptors for the recognition of incoming precursor proteins by the TOM complex. No significant alterations were observed in mitochondrial Fmp52 steady-state protein levels in cells lacking *TOM20* or *TOM70*. Further affinity purification through HA-tagged Tom40 in *tom20*Δ and *tom70*Δ backgrounds revealed no major changes in the interaction of Fmp52 with Tom40 upon deletion of *TOM20* or *TOM70* (Figure 19B). The interaction of Ubx2 with Tom40 was reduced when *TOM20* was deleted and was completely blocked when *TOM70* was deleted as previously seen (Mårtensson et al., 2019). The binding of Msp1 with Tom40 was diminished upon loss of *TOM70* (Weidberg and Amon, 2018). Interestingly, increased binding of Msp1 with Tom40 was observed upon deletion of *TOM70*.

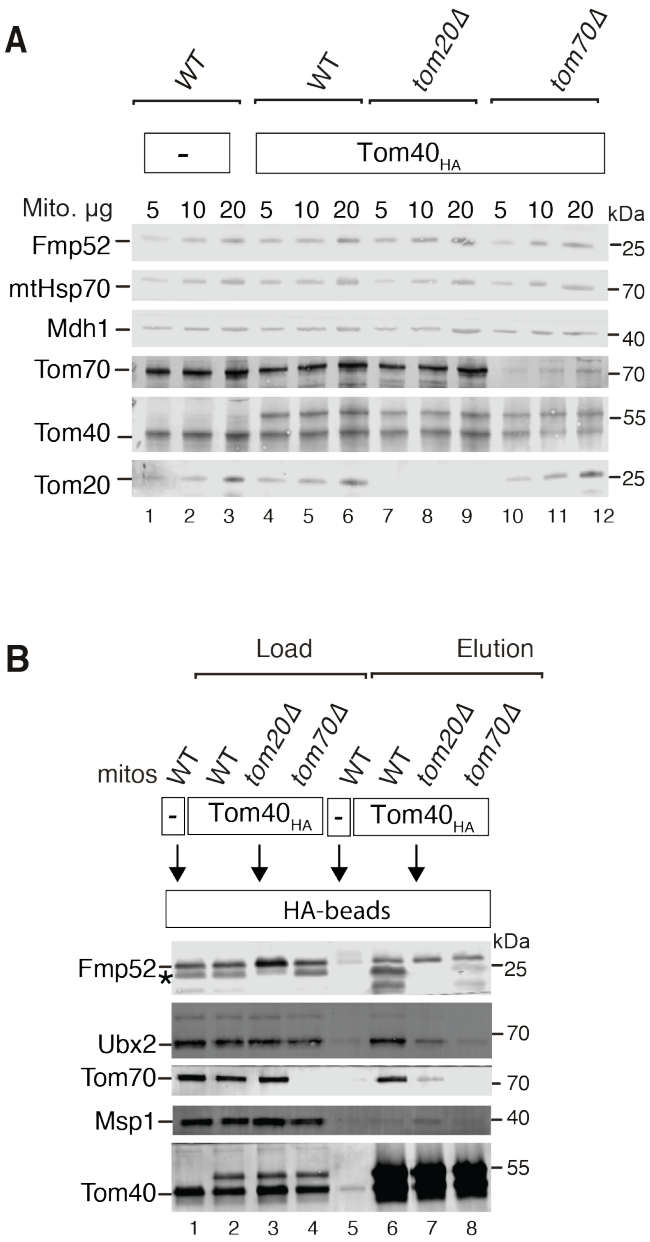

Figure 19. Fmp52 is recruited to the TOM complex independent of Tom20 and Tom70. (A) Mitochondria were isolated from the indicated yeast strains grown under permissive conditions, and subsequently analyzed by SDS-PAGE and immunodetection with the indicated antisera. **(B)** Mitochondria isolated from strains expressing HA-tagged Tom40 were solubilized with digitonin and subjected to affinity purification using an anti-HA affinity matrix (left). After the washing steps, samples were eluted with SDS-sample buffer. Load., 0.2%; elution., 100%. The asterisk marks an unspecific signal of anti-Fmp52. WT., wild-type.

4.3.2 Characterization of Fmp52

Fmp52 was predicted to possess an NADP-binding Rossmann fold in its structure. Nicotinamide adenine dinucleotide phosphate (NADP)-binding domain was determined by comparing it with canonical motifs commonly associated with such domains (Figure 20A) (Chen et al., 2010). Rossmann fold belongs to the general class of β/α proteins and comprises four α-helices and six consecutive β-strands (arranged in the 3-2-1-4-5-6 order) forming a parallel pleated sheet (Kamiński et al., 2022). In addition, the Rossmann-fold enzyme families are characterized by their use of co-factors, in particular nucleoside-containing co-factors (Laurino et al., 2016; Kamiński et al., 2022). The modeled structure of Fmp52 resembles the architecture of the Rossmann fold, with a similar arrangement and orientation of the β-strands.

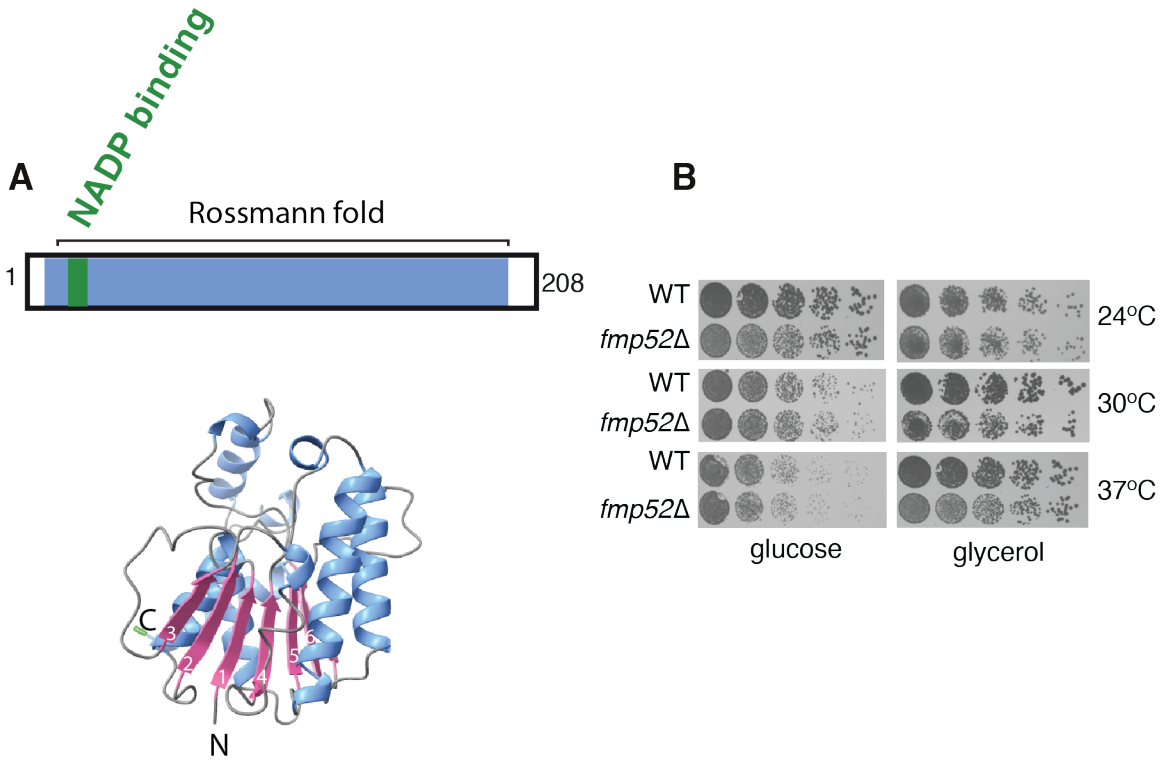

Figure 20. Characterisation of Fmp52. (A) Schematic representation of the Fmp52 protein (above). Model structure of Fmp52 protein as predicted from AlphaFold protein structure database (Jumper et al., 2021) (below) **(B)** Serial dilutions of wild-type (WT) and *fmp52*Δ yeast cells were spotted onto full medium with glucose or glycerol as the carbon source and grown under indicated temperature conditions.

We performed growth assays to assess the effects of Fmp52 deletion in yeast cells. Deletion of *FMP52* did not result in a striking difference in growth in fermentative and respiratory media in comparison with the wild-type (WT) yeast cells at permissive conditions (Figure 20B). However, mild growth defects were observed under respiratory conditions at elevated temperatures further pointing towards a mitochondrial specific function of Fmp52.

To further evaluate the impact of deleting *FMP52* on essential mitochondrial functions, steady-state protein levels of mitochondrial proteins were analyzed by SDS-PAGE followed by immunodetection (Figure 21A). The steady-state protein levels of the TOM subunits, respiratory chain subunits, and mitochondrial quality control factors were unaffected. Most mitochondrial proteins were present in comparable amounts upon deletion of *FMP52* as in the wild-type (WT) mitochondria. We then studied the assembly of the oxidative phosphorylation complexes and the TOM complex by BN-PAGE (Figure 21B). Moreover, the assembly of oxidative phosphorylation complexes III, IV, and V and the TOM complex remained unaltered in the mitochondria of strains lacking Fmp52.

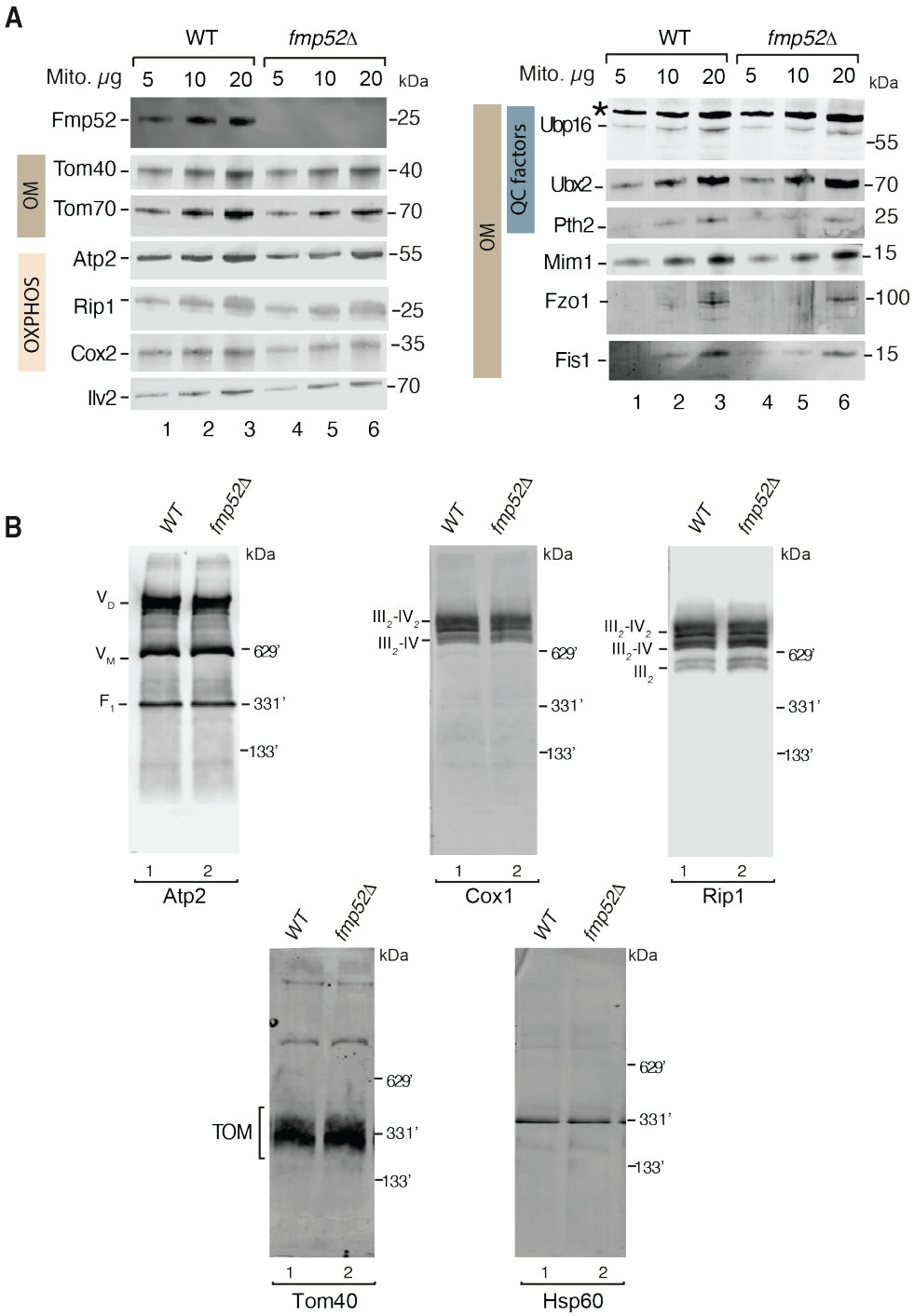

Figure 21. Characterization of Fmp52 deficient mitochondria. (A) Mitochondria isolated from wild-type (WT) and *fmp52*Δ yeast cells were analyzed by SDS-PAGE and immunodetection with the indicated antisera. The asterisk marks an unspecific signal of anti-Ubp16. OXPHOS., oxidative phosphorylation., OM., outer membrane; QC factors., quality control factors. **(B)** Mitochondria isolated from the indicated strains were lysed with digitonin and analyzed by BN-PAGE and immunodetection with the indicated antisera**.** II**,** complex II (succinate dehydrogenase); III, complex III (cytochrome c reductase); IV, complex IV (cytochrome c oxidase); V, complex V (F_1- F_o-ATP synthase) of mitochondrial OXPHOS machinery; V_D, dimer of ATP synthase; V_M, monomer of ATP synthase; F_1, F_1 domain of ATP synthase.

4.3.3 Fmp52 is dually localized to the mitochondrial outer membrane and cytosol

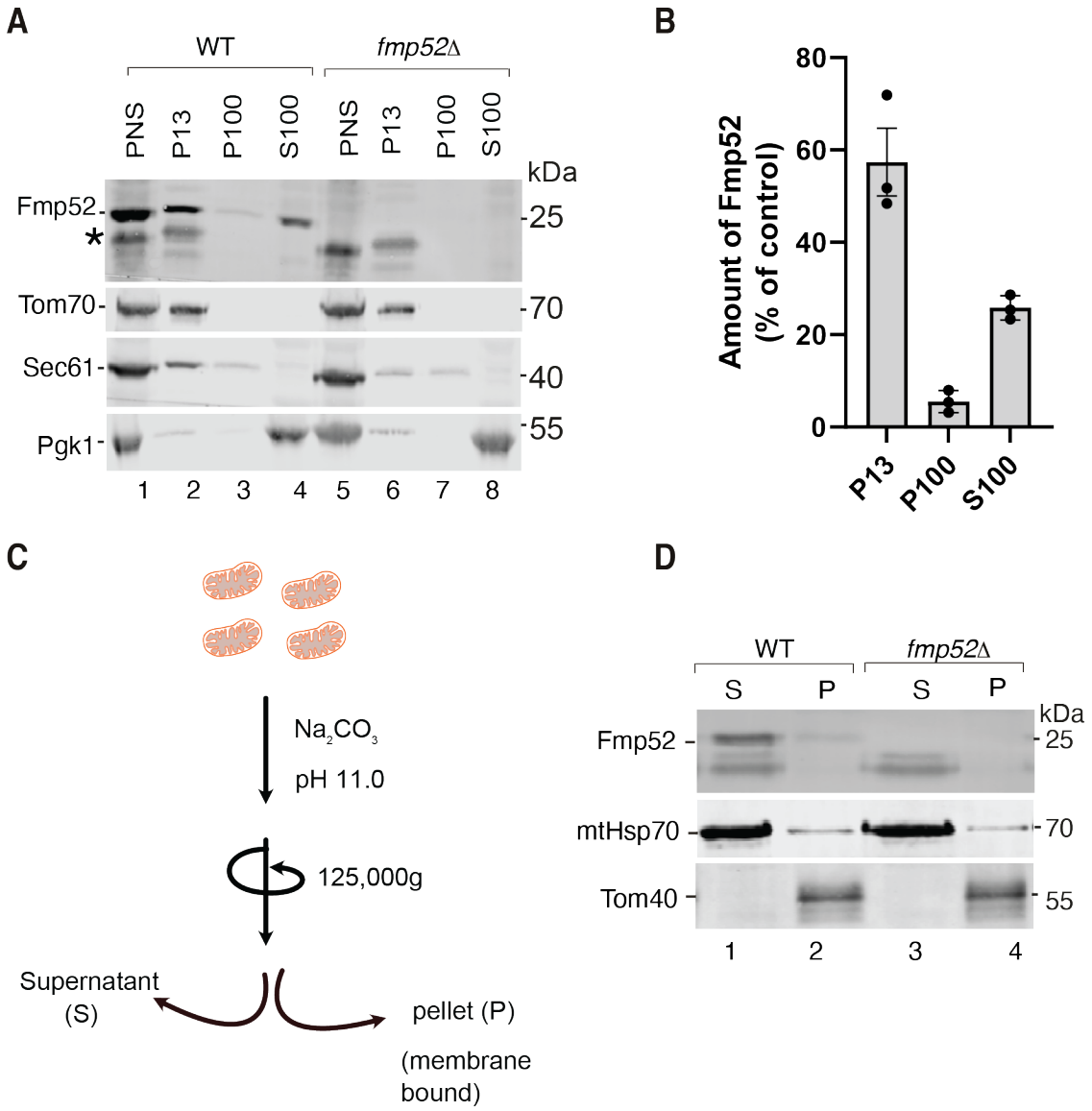

Figure 22. Fmp52 is localized both in mitochondria and cytosol. **(A)** Cellular fractionation samples of wild-type (WT) and *fmp52*Δ yeast cells were analyzed by SDS-PAGE and immunodetection with indicated antisera**.** PNS, Post-nuclear supernatant fraction; P13, mitochondria enriched; S100, cytosolic fraction. The asterisk marks an unspecific signal of anti-Fmp52. **(B)** Quantification of the distribution of Fmp52 in different fractions. The amount of Fmp52 in the PNS sample was set to 100% (control). Mean ± s.e.m (n=3). **(C)** Schematic representation of the experimental set-up used for carbonate extraction. **(D)** Mitochondria isolated from indicated strains were treated with 0.1M sodium carbonate, and subsequently analyzed by SDS-PAGE and immunodetection.

Fmp52 has previously been found to localize in the mitochondrial outer membrane in large-scale proteomic studies (Zahedi et al., 2006; Burkhart et al., 2016; Morgenstern et al., 2017; Vögtle et al., 2017). Cellular fractionation experiments were performed to confirm the localization of Fmp52 (Figure 22A). Surprisingly, Fmp52 was found both in the mitochondria-enriched (P13) and cytosolic fractions (S100). The intriguing observation that Fmp52 was dually localized in the mitochondria and the cytosol raised the possibility of a regulatory role of Fmp52 in coordinating stress responses between the mitochondria and the cytosol.
We wanted to further assess the membrane association of Fmp52 and therefore treated purified mitochondria with sodium carbonate, which separates peripheral membrane proteins from integral membranes (Figure 22D) (Fujiki et al., 1982). We observed that Fmp52 was found in the supernatant fraction (S) upon carbonate treatment as it dissociated from mitochondria during this treatment in contrast to integral membrane protein Tom40 which was found in the pellet fraction (P) and was largely resistant to carbonate treatment. Our data revealed that Fmp52 behaved as a peripheral membrane protein which is associated with but not fully integrated into the lipid bilayer. Indeed, using different prediction programs we could not detect any trans-membrane segment in Fmp52.

4.4 Novel protein Fmp52 is critical for mitochondrial quality control

Previous studies showed that Fmp52 protein levels were increased upon proteotoxic stress triggered by the inactivation of essential mitochondrial processing peptidase (MPP). This increase in the steady-state protein levels of Fmp52 was proposed as a mechanism to counteract the potential import stress resulting from compromised processing by mitochondrial proteases (Burkhart et al., 2016). The physiological relevance of this effect remains yet unknown.

4.4.1 Fmp52 is increased upon proteasomal inhibition

We analyzed the degradation of Fmp52 protein levels upon inhibition of proteasome. The proteasome was blocked by the addition of the proteasome inhibitor MG-132 in yeast cells lacking *PDR5.* To overcome the impermeability of the yeast cell wall that prevents the uptake of proteasomal inhibitors in wild-type cells, a mutant strain *pdr5*Δ was used (Liu et al., 2007). Excitingly, an overall increase in the Fmp52 protein levels was observed upon inhibition of the proteasome (Figure 23A). We further examined the degradation kinetics of Fmp52 upon proteasomal inhibition using cycloheximide to block protein synthesis. On addition of MG-132

followed by a subsequent chase, degradation of Fmp52 was reduced, leading to stabilization of the Fmp52 protein levels (Figure 23B).

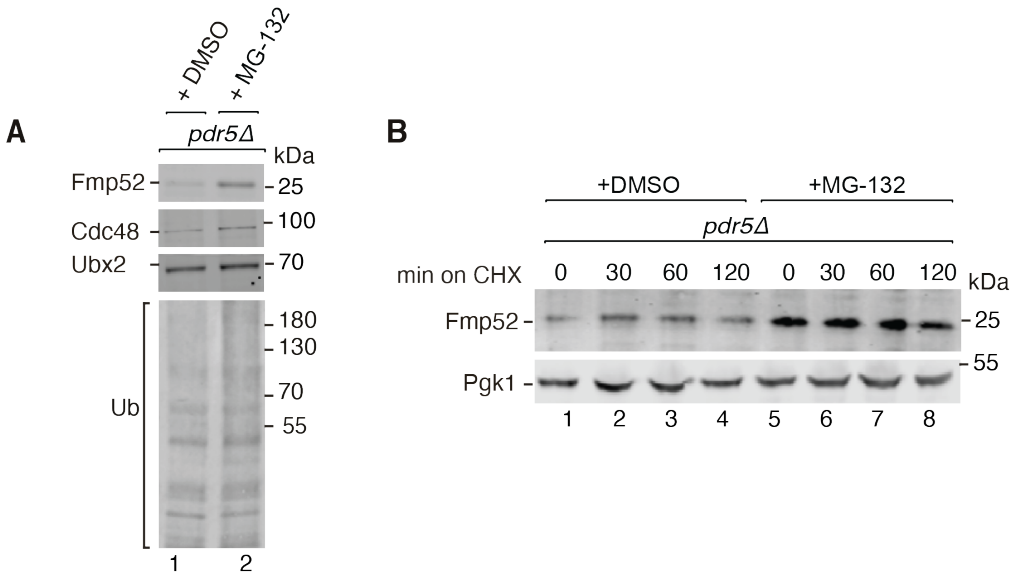

Figure 23. Proteasomal inhibition increases Fmp52 protein levels. **(A)** Impact of proteasomal inhibition on the steady-state protein levels of Fmp52 were analyzed in cell extracts from an otherwise wild-type strain lacking *PDR5* and in the absence or presence of MG-132. Samples were analyzed by SDS-PAGE and immunodetection with indicated antisera. **(B)** The degradation kinetics of Fmp52 levels were analyzed in cell extracts from an otherwise wild-type strain lacking *PDR5* after 1 hour of treatment with MG-132. Samples were analyzed by SDS-PAGE and immunodetection with indicated antisera.

4.4.2 Fmp52 is increased upon clogging

Overexpression of clogging proteins such as cytochrome b_2-DHFR-HB clogs the TOM complex as these constructs are very slowly and poorly imported into mitochondria (see chapter 4.1.4). As a consequence, the cell elucidates a wide range of responses both at the mRNA and protein levels to counteract the potential proteotoxicity caused by the accumulation of precursor proteins (Boos et al., 2019; Boos et al., 2020). Supporting this notion, we analyzed the Fmp52 levels in the transcriptomic and proteomic data obtained from the studies performed by Dr. Felix Boos and colleagues (Boos et al., 2019) (Figure 25A). In line with our assumption, Fmp52 was enriched both at the mRNA and protein levels upon clogger expression. In contrast, the expression of clogger constructs mildly increased in the components of the mitoTAD (mitochondrial translocation-associated degradation) machinery, namely Ubx2, and Cdc48. (Boos et al., 2019).

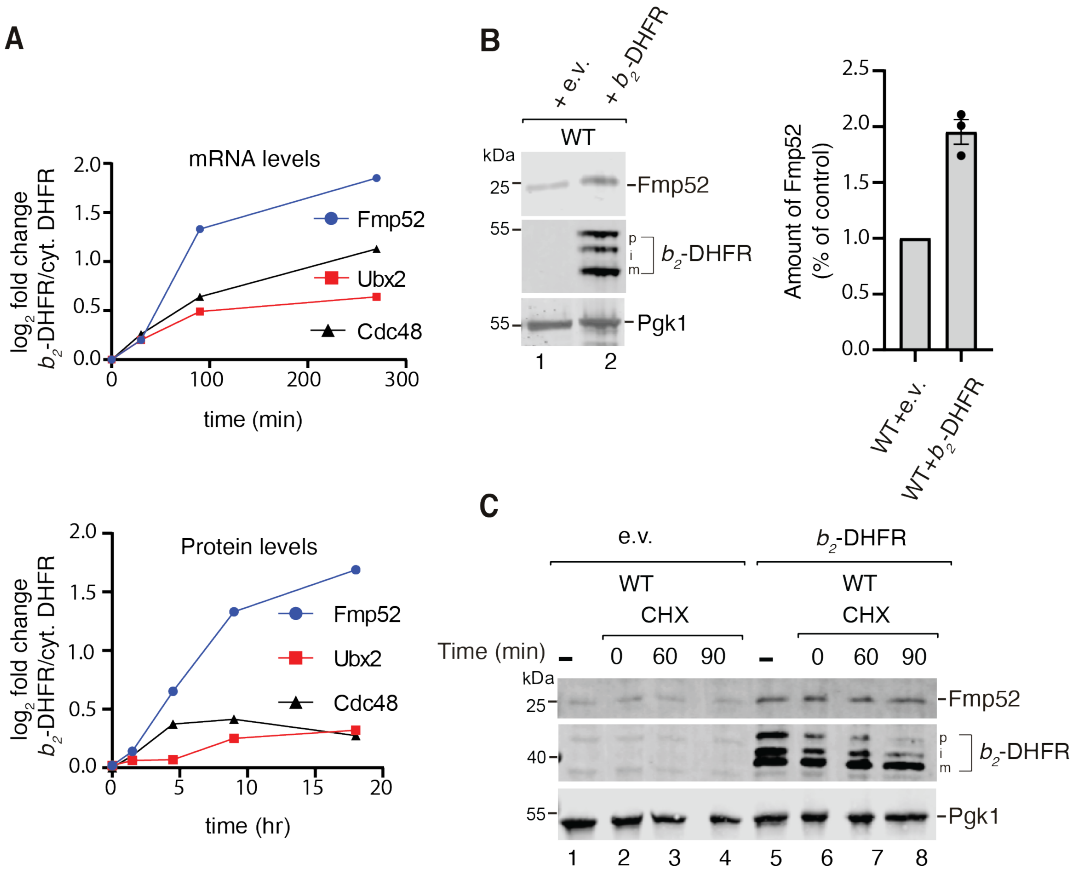

Figure 24. Overexpression of cytochrome b_2-DHFR-HB constructs leads to an increase in steady-state levels of Fmp52. (A) Graphs illustrating transcriptomics (above) and proteomics (below) data of $\log_2$ fold changes of b_2-DHFR normalized to cyt. DHFR for Fmp52, Ubx2, and Cdc48 obtained from Boos et al., 2019. DHFR., dihydrofolate reductase; cyt. DHFR., cytosolic DHFR; b_2-DHFR., DHFR construct that adopts an intermembrane mitochondrial targeting sequence from cytochrome b_2. **(B)** Fmp52 levels in cell extracts of wild-type (WT) cells expressing b_2-DHFR-HB constructs were analyzed by SDS-PAGE and immunodetection with indicated antisera. Quantification of the amount of Fmp52 levels in the indicated strains. The amount of Fmp52 in WT cells + e.v. was set to 1 (control). Mean ± s.e.m (n=3). e.v., empty vector; p., precursor; i., intermediate form; m, mature form of b_2-DHFR-HB precursor. **(C)** The degradation kinetics of Fmp52 levels were analyzed in cell extracts from the indicated mutant strains.

Based on these findings, we expressed cytochrome b_2-DHFR-HB constructs in yeast cells and analyzed Fmp52 steady-state protein levels in cell extracts using SDS-PAGE followed by immunodetection (Figure 24B). Fmp52 levels were increased in response to the presence of clogger protein, b_2-DHFR-HB. We further examined the stability of Fmp52 protein using cycloheximide chase upon the expression of clogger protein (Figure 24C). We did not observe substantial degradation of the Fmp52 protein over two hours of the chase period. Rather, the Fmp52 protein seemed to be stabilized upon clogging of the TOM complex.

4.4.3 Fmp52 facilitates the removal of arrested precursors proteins from the TOM complex

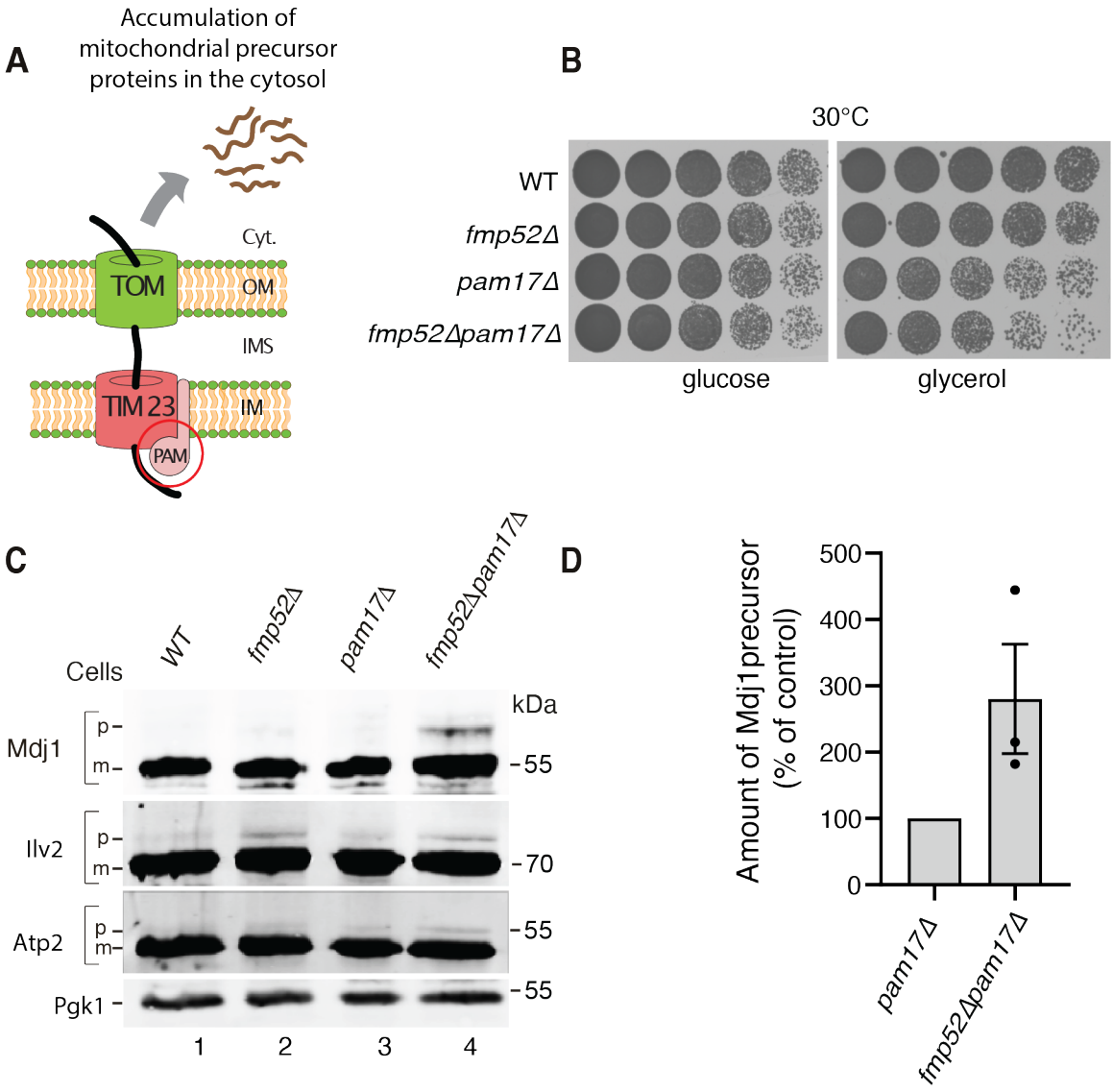

Figure 25. Characterization of the role of Fmp52 upon import stress induced by deletion of Pam17. (A) Model showing the effect of deletion of *PAM17*, a non-essential component of the PAM motor. Deletion of *PAM17* impairs import and subsequently leads to the accumulation of mitochondrial precursor proteins in the cytosol. Cyt., cytosol; OM., outer membrane; IMS, intermembrane space. **(B)** Serial dilutions of wild-type (WT), *fmp52Δ*, *pam17Δ*, and *fmp52Δpam17Δ* yeast cells were spotted on full medium with glucose or glycerol as carbon source and grown at 30°C. **(C)** Cell extracts from indicated strains were analyzed by SDS-PAGE and immunodetection with indicated antisera**.** Pgk1 was used as a control. p, precursor; m, mature form of Mdj1, Ilv2 or Atp2 precursor. **(D)** Quantification of the Mdj1 precursor levels. The amount of Mdj1 in pam17Δ cells was set to 100% (control). Mean ± s.e.m (n=3).

In order to elucidate the function of Fmp52 in proteotoxic stress, we deleted *PAM17* in the *fmp52*Δ background yeast strain. On the deletion of *PAM17*, protein transport into the mitochondrial matrix is impaired, thereby mimicking proteotoxic stress (see chapter 4.1.3). We then conducted a growth assay to analyze the double deletion strain with respect to the single deletions. While the single deletion strains displayed only mild growth defects, growth of the *fmp52*Δ*pam17*Δ double mutant strain was profoundly reduced on a non-fermentable carbon source at permissive temperature conditions (Figure 25B). We were then motivated to analyze the cell extracts from the double mutant strain *fmp52*Δ*pam17*Δ in comparison with respective single deletion strains. Deletion of *PAM17*, led to a mild accumulation of mitochondrial precursor proteins, which was profoundly increased when *FMP52* was deleted in parallel. Interestingly, the accumulation of precursor proteins was observed under permissive non-stressed conditions (Figure 25C).

Studies have shown that the overexpression of both cytochrome b_2-constructs (b_2-DHFR-HB and b_2Δ-DHFR-HB) leads to the accumulation of precursor proteins at the TOM complex (see 4.1.4) (Boos et al., 2019; Mårtensson et al., 2019). We asked the impact of the deletion of Fmp52 on clogger-mediated toxicity. To this end, cell extracts from WT and *fmp52*Δ yeast cells expressing b_2-DHFR-HB and b_2Δ-DHFR-HB constructs were analyzed by SDS-PAGE followed by immunodetection (Figure 26B). Remarkably, an increased amount of accumulation of the precursor form of Mdj1 was observed in cell extracts from *fmp52*Δ cells expressing the clogger constructs (b_2-DHFR-HB or b_2Δ-DHFR-HB) as compared to their corresponding wild-type cells indicating the role of Fmp52 in the removal of non-imported precursor proteins from the TOM complex.

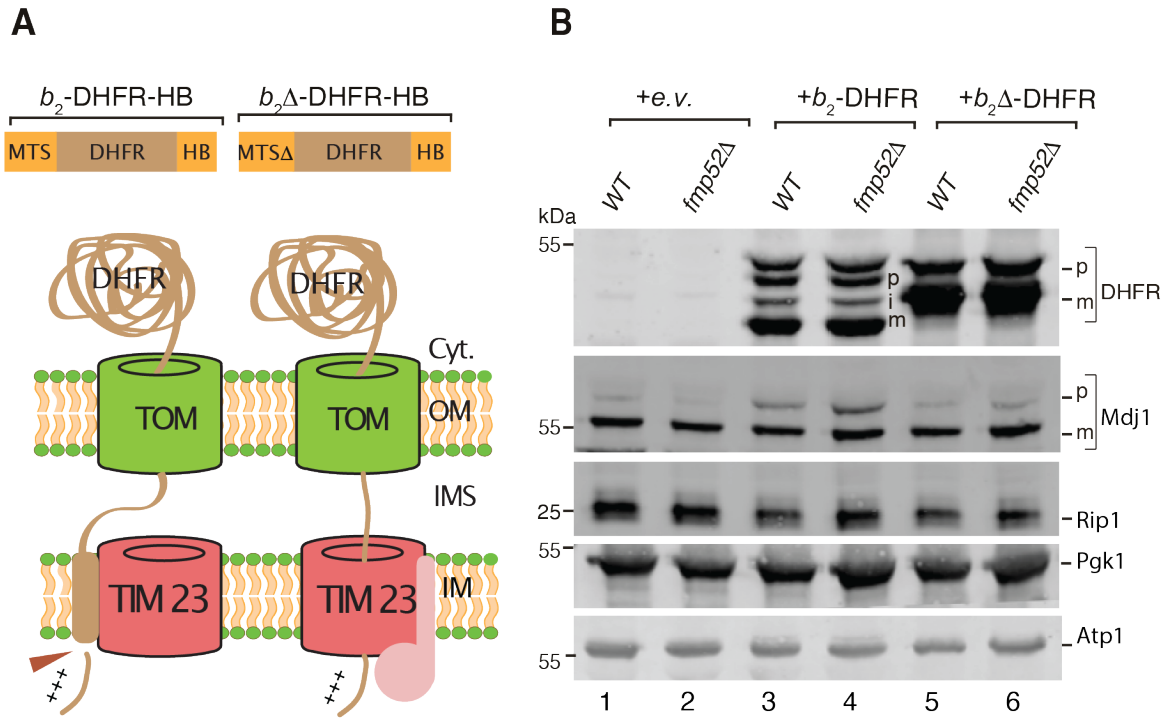

Figure 26. Expression of cytochrome b_2-constructs in Fmp52 deficient cells. (A) Schematic representing the linear structures of cytochrome b_2-DHFR-HB and $b_2\Delta$-DHFR-HB construct that harbors a mitochondrial targeting sequence from cytochrome b_2, a moiety of DHFR, and a heme group. Since the mitochondrial targeting sequence of cytochrome b_2 consists of a sorting signal, the precursor is laterally released into the inner membrane. The mitochondrial processing peptidase (MPP) cleaves the presequence and subsequently, the sorting signal is cleaved. In contrast, $b_2\Delta$-DHFR-HB lacks the sorting signal and is pulled into the matrix by the PAM machinery. The DHFR domain stably folds in the cytosol, thereby delaying the import of precursors, and subsequently clogging the TOM complex. MTS., mitochondrial targeting sequence; DHFR, dihydrofolate reductase; HB, heme-binding domain. Cyt., cytosol; OM., outer membrane; IMS, intermembrane space; IM, intermembrane. Pgk1 was used as a control. p., precursor; i., intermediate form, m., mature form of Mdj1, Ilv2 Atp2, b_2-DHFR or $b_2\Delta$-DHFR. **(B)** Cell extracts of wild-type (WT) and *fmp52*Δ yeast cells expressing b_2-DHFR-HB and $b_2\Delta$-DHFR-HB were analyzed by SDS-PAGE and immunodetection with indicated antisera**.**

4.4.4 Fmp52 genetically interacts with Vms1

We wanted to further investigate the interaction of Fmp52 with other quality control components, including Vms1, Ubp16, and Pth2. To this end, we deleted *FMP52* in the backgrounds of *vms1*Δ, *ubp16*Δ, and *pth2*Δ yeast strains (Figure 27A).

The yeast mutant strain *fmp52*Δ*vms1*Δ showed a strong growth defect at elevated temperatures under both fermentative and respiratory conditions indicating a genetic interaction between the two genes. Parallel deletion of *FMP52* in *pth2*Δ or *ubp16*Δ backgrounds did not have any

noticeable alterations in growth phenotypes to their respective single deletions. Thus, it is possible that Fmp52 functions in collaboration with Vms1 in mitochondrial quality control.

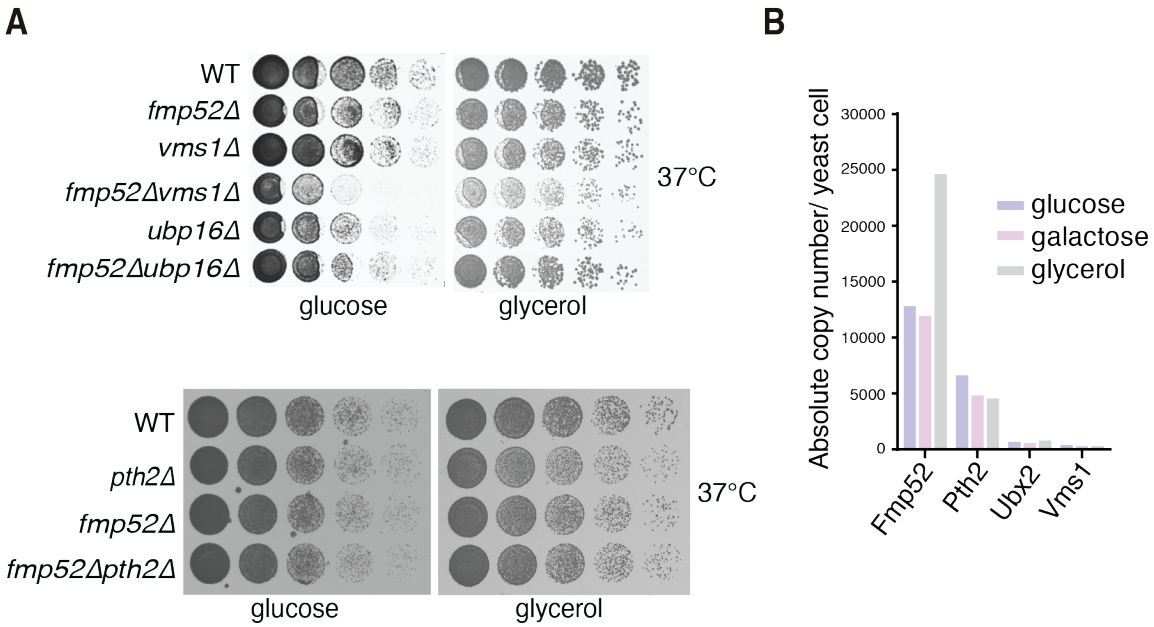

Figure 27. Characterization of Fmp52, Vms1, Pth2 and Ubp16. (A) Serial dilutions of the indicated strains were spotted onto full medium with glucose or glycerol as carbon source and incubated at indicated temperatures. WT., wild-type. **(B)** Absolute copy number per yeast cell of the indicated proteins. Values are based on the quantification of mitochondrial proteins grown on different carbon sources by Morgenstern et al., 2017.

We compared the absolute copy number per yeast cell based on the quantification of mitochondrial proteins grown on different carbon sources by Morgenstern et al., 2017 (Figure 27B). Fmp52 exhibits a higher copy number in comparison with other quality control components, such as Pth2, Ubx2, and Vms1. The abundance of Fmp52 nearly doubled when glycerol was used as a carbon source, thereby indicating a mitochondria specific function of Fmp52.

4.4.5 Fmp52 co-operates with Ubx2 in quality control

Interestingly, simultaneous deletion of *FMP52* and *UBX2* showed strong growth defects under non-stressed conditions under respiratory conditions in comparison to their respective single deletion strains (Figure 28A). To further elucidate the genetic interaction between Fmp52 and

Ubx2, we conducted affinity purification assays with HA-tagged Ubx2. Fmp52 was co-purified with HA-tagged Ubx2 (Figure 28B). In addition, subunits of the TOM complex (Tom22 and Tom40) and MIM machinery (Mim1) were efficiently co-purified with $Ubx2_{HA}$ as previously seen (Mårtensson et al., 2019).

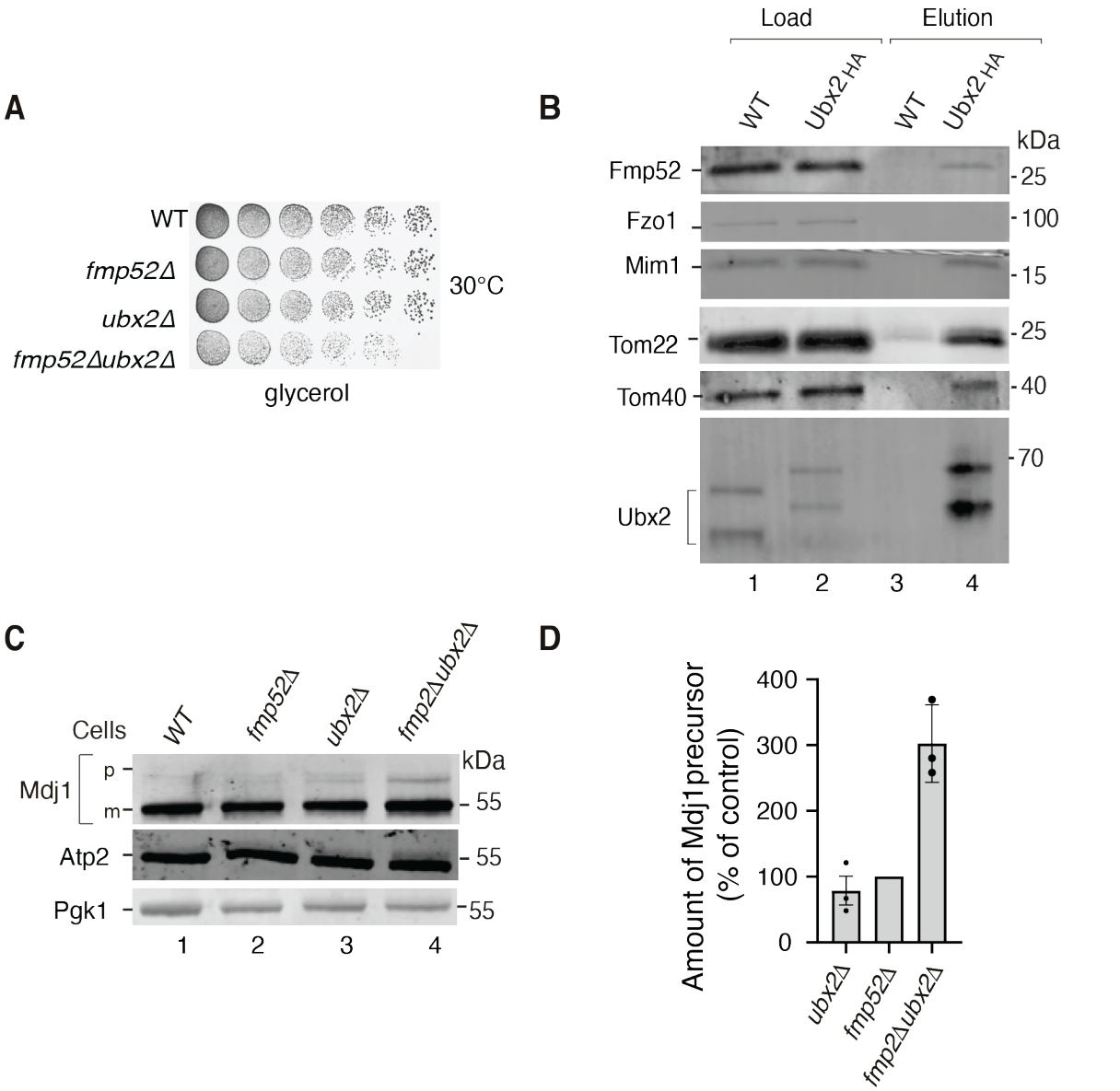

Figure 28. Fmp52 shows a link Ubx2. (A) Serial dilutions of the indicated strains were spotted on full medium with glycerol as carbon source and grown at 30°C. **(B)** Wild-type (WT) and Ubx2-HA yeast mitochondria were solubilized with digitonin and used for affinity purification with anti-HA affinity matrix. After washing steps, samples were eluted with SDS-sample buffer. Samples were analyzed by SDS-PAGE and immunodetection with the indicated antisera. **(C)** Cell extracts of WT, fmp52Δ*, ubx2*Δ, and *fmp52*Δ*ubx2*Δ yeast cells were analyzed by SDS-PAGE and immunodetection with indicated antisera**. (D)** Quantification of the Mdj1 precursor levels. The amount of Mdj1 in WT cells was set to 1 (control). Mean ± s.e.m (n=3).

To investigate the physiological role of this interplay between Fmp52 and Ubx2, we analyzed cell extracts from the double mutant strain *fmp52*Δ*ubx2*Δ in comparison with respective single deletions on SDS-PAGE followed by immunodetection (Figure 28C). A strong accumulation of the precursor form of Mdj1 was seen in the double mutant strain under permissive conditions suggesting that Fmp52 cooperates with Ubx2 in the removal of accumulated precursor proteins from the TOM complex. Our results point towards overlapping functions of Fmp52 and Ubx2 in mitochondrial quality control that results in strong defects upon loss of both systems.

Our results reveal that the deletion of *FMP52* when combined with previously stressed yeast cells such as the absence of *PAM17* or *UBX2*, results in the failure of the removal of accumulated precursor proteins. Moreover, Fmp52 deletion exacerbates the challenges associated with the clearance of precursor proteins. In conclusion, our findings established Fmp52 as a novel and essential quality control component that plays a critical role in the clearance of accumulated precursor proteins from the TOM channel as well as in regulating proteotoxic stress.

5. Discussion

Impaired protein import leads to the accumulation of mitochondrial precursor proteins, which can have severe physiological consequences on the cell. Upon blockage of the TOM complex, various stress response pathways (mPOS, UPRam, and mitoCPR) are activated to counteract the stress caused by protein accumulation (Wrobel et al., 2015; Weidberg and Amon, 2018; Boos et al., 2019). Altogether, these stress responses aim to restore proteostasis by strategies such as increased expression of chaperones, altered protein biosynthesis (mPOS), increased activation and assembly of the proteasome (UPRam). Recent findings suggest that cells deal with perturbations in protein homeostasis by the temporary aggregation of proteins into dedicated granules in the cytosol, termed as MitoStores (Krämer et al., 2023). In addition, the mitochondrial compromised protein import response (mitoCPR) pathway involves the expression of the stress-induced transcription factor *CIS1,* which in turn recruits the outer membrane AAA-ATPase Msp1 to the Tom70 receptor, enabling the removal of non-imported proteins from the mitochondrial surface (Weidberg and Amon, 2018). All these pathways are characterized by responses induced by acute stress such as prolonged blockage of the TOM channel with clogging-prone intermediates, defects in mitochondrial protein import due to mutations in the translocon subunits, or decreased membrane potential (Wang and Chen, 2015; Weidberg and Amon, 2018; Boos et al., 2019; Rolland et al., 2019). Nonetheless, the heavy standard protein load on the TOM channel necessitates the need for quality control mechanisms even under basal non-stressed conditions. While there are studies on cellular stress responses induced by import stress, our knowledge of monitoring mechanisms that prevent the accumulation of precursor proteins under standard growth conditions is limited.

This study culminated in the identification of a novel quality control pathway responsible for the removal of accumulated non-imported precursor proteins from the TOM complex, which was centered around the peptidyl tRNA-hydrolase, Pth2. It was found that Pth2 binds to the TOM complex and serves as a mitochondrial receptor for the cytosolic protein Dsk2, the sole yeast homolog of human ubiquilin (UBQLN) family of proteins (Figure 29). Dsk2 contains a ubiquitin-associated (UBA) domain, ubiquitin-like (UBL) domain, and a methionine-rich M-domain that confers substrate specificity (Ishii et al., 2006; Itakura et al., 2016). We demonstrated that Dsk2 cooperates with Pth2 to bind ubiquitylated proteins at the TOM complex and further mediates the transfer of ubiquitylated substrates to the proteasome for their subsequent degradation. Altogether, our findings reflect that the Pth2-Dsk2 quality control

pathway constitutes an alternative degradation system for the clearance of non-imported accumulated precursor proteins, thereby regenerating the import capacity of the TOM translocon.

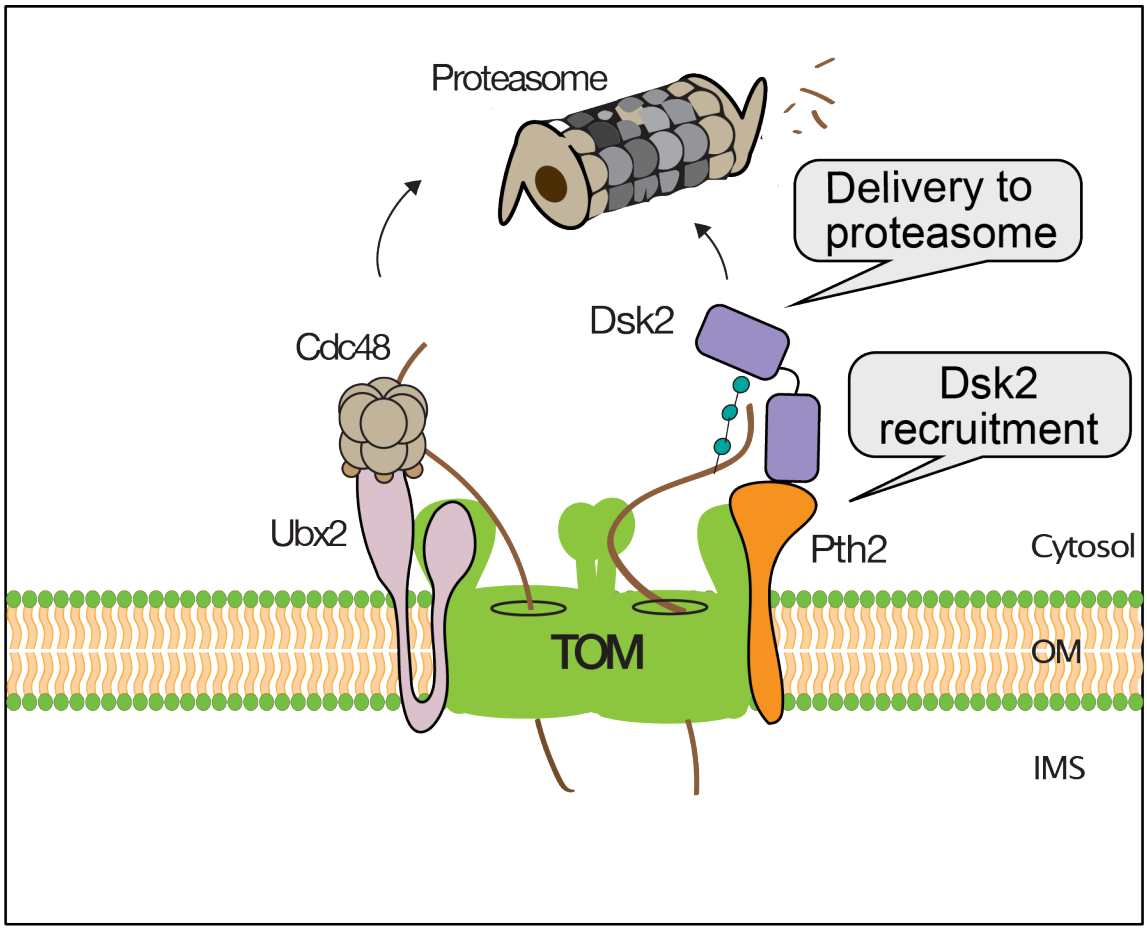

Figure 29. Constitutive quality control at the TOM complex. The proposed model of constitutive quality control for the removal of accumulated precursor proteins from the TOM complex. Ubx2 constantly monitors the TOM complex, and upon clogging of the TOM complex recruits the AAA-ATPase Cdc48 for extraction of stalled precursor proteins from the TOM complex. Pth2 binds to the TOM complex independently of Ubx2. Pth2 serves as the mitochondrial receptor for Dsk2, which in turn binds ubiquitylated proteins and transfers them to the proteasome for degradation. OM., outer membrane; IMS., intermembrane space.

The first concrete study defining a mechanism that continuously safeguards the TOM complex was presented by the mitochondrial protein translocation-associated degradation (mitoTAD) pathway. The mitoTAD pathway provides a system that clears stalled precursors from the TOM channel without activation of import stress responses, representing a first line of import quality

control (Mårtensson et al., 2019). Previously known for its function in the endoplasmic reticulum-associated degradation (ERAD) (Neuber et al., 2005; Schuberth and Buchberger, 2005), Ubx2 recruits Cdc48 to the clogged TOM complex for the extraction of precursor proteins and facilitates proteasomal turnover of proteins clogging the TOM complex (Mårtensson et al., 2019). However, the mechanisms by which the stalled proteins were recognized and ubiquitylated remained still elusive. A recent study by Schulte et al., demonstrated that cytosolic E3-ubiquitin ligase Rsp5 is necessary for ubiquitylating precursor proteins to facilitate their degradation, whereas, the outer membrane deubiquitylating enzyme, Ubp16, modulates the removal of ubiquitin moieties thereby facilitating protein import. It was shown that subsequent ubiquitylation/deubquitylation of precursor proteins at the TOM channel by Rsp5/Ubp16 further fine-tune the mitochondrial quality control (Schulte et al., 2023). However, it remains unclear whether Pth2 interacts with Rsp5/Ubp16 in ensuring mitochondrial quality control.

Our study revealed that the Pth2-TOM interaction does not depend on the mitoTAD key component Ubx2, thereby suggesting that the recruitment of the Pth2-Dsk2 pathway to the TOM complex is independent of the established mitoTAD pathway. Despite the Ubx2-independent interaction of Pth2 with the TOM channel, we observed a strong synthetic growth defect in the double deletion strain lacking both *PTH2* and *UBX2* suggesting partial redundancy in both pathways for the surveillance of the TOM complex under constitutive conditions. By having alternative pathways for degradation, substantial robustness in quality control systems is maintained by the cell.

It has been shown that in mammalian cells, the ubiquilin (UBQLN) family, triages tail-anchored mitochondrial proteins, thereby supporting proper mitochondrial membrane insertion, and if targeting fails they facilitate the turnover of mislocalized membrane proteins (Itakura et al., 2016; Juszkiewicz and Hegde, 2018). Just like Ubx2, Dsk2 plays an active role in the ERAD pathway avoiding the aggregation of misfolded proteins in the cytosol (Medicherla et al., 2004; Kim et al., 2008). In line with the function of UBQLNs in regulating cytosolic protein homeostasis in mammalian cells, it was found in this study that Dsk2 participated in mitochondria-specific quality control in yeast. Moreover, mutations in UBQLN2 have been associated with neurodegenerative diseases in humans and in mice (Deng et al., 2011; Hjerpe et al., 2016; Le et al., 2016).

The mitochondrial ribosome-associated quality control (mitoRQC) pathway mediates the removal of stalled mitochondrial proteins from the ribosomal subunits that escaped ubiquitylation (Izawa et al., 2017; Matsuo et al., 2017; Su et al., 2019). Here, Vms1, a

peptidyl-tRNA hydrolase, functions to protect mitochondria from the toxic effects of CAT-tailed protein aggregation by releasing the nascent chain from the 60S ribosomal subunit (Izawa et al., 2017; Verma et al., 2018; Zurita Rendón et al., 2018). In the present study, we were able to identify two independent functions of Pth2 in quality control. One related to its role in the removal of non-imported precursor proteins during mitochondrial import. The other function of Pth2 is related to its peptidyl-tRNA hydrolase activity in the Vms1-linked pathway. As demonstrated in this study, Pth2 supports Vms1 in clearing ribosome stalled polypeptides This study also re-instates the fact that quality control factors are considerably less abundant than the TOM complex and therefore they interact only transiently with the TOM complex. The absolute copy number of Pth2 as determined by mass spectrometry-based approaches was approximately 2,900 and 4,000 copies per yeast cell under fermentative conditions (Kulak et al., 2014; Morgenstern et al., 2017). In contrast, the cell contains roughly 18,000 Tom40 subunits which assemble into dimeric channels at the TOM complex, resulting in an approximate count of 9,000 TOM complexes per cell (Morgenstern et al., 2017; Araiso et al., 2019). Based on these copy numbers, it seems likely that Pth2 subunits are dynamically distributed among TOM complexes rather than having a one-to-one stoichiometric binding to each individual TOM complex. Such adaptable and flexible nature of the Pth2 binding with the TOM complex provides a means for the cell to efficiently regulate mitochondrial protein import according to cellular requirements. Interestingly, Pth2 exhibits a higher abundance in comparison to other mitochondrial quality control factors (Ubx2, Vms1) thereby reflecting the two functions of Pth2 in quality control.

Recent studies reveal that PTRH2, the mammalian homolog of yeast Pth2, is linked with infantile-onset multisystem disorder causing severe neurological, pancreatic, and endocrine diseases in patients (Hu et al., 2014; Ando et al., 2022). Whether PTRH2 and UBQLNs serve functions equivalent to those of mitochondrial protein quality control in yeast remains yet to be analyzed. Most mechanisms of mitochondrial biogenesis and quality control have remained conserved in evolution from yeast to humans (Anderson and Haynes, 2020; Morgenstern et al., 2021). Understanding these conserved mechanisms can provide valuable insights into human health and diseases related to mitochondrial dysfunction.

The findings presented in the latter part of this study established Fmp52, previously reported to be induced upon DNA damage, as a novel mitochondrial quality control factor at the TOM complex (Dardalhon et al., 2007). Our results suggest that Fmp52 plays a critical role in the clearance of accumulated precursor proteins from the TOM channel as well as in regulating proteotoxic stress. In this study, we were able to assign a quality control function to Fmp52. In

addition, our sub-cellular localization results demonstrated that Fmp52 is dually localized both in mitochondria and in the cytosol. This finding was intriguing as previous studies described Fmp52 to be localized only in mitochondria (Zahedi et al., 2006; Burkhart et al., 2016; Morgenstern et al., 2017). It seems likely that Fmp52 coordinates stress responses between the mitochondria and the cytosol, thereby regulating quality control.

Recent studies revealed that yeast cells lacking Fmp52 showed greater resistance to hydrogen peroxide-induced stress response. Using a multi-omic analysis with machine learning approach, it was suggested that Fmp52 interacts with two proteins, Fmp40 and Aim25, in coordinating the oxidative stress response (Dickinson et al., 2022). In addition, it has been shown that Fmp52 protein levels were increased in yeast cells upon proteotoxic stress triggered by the inactivation of essential mitochondrial processing peptidase (MPP) (Burkhart et al., 2016). It seemed likely that proteotoxic stress caused by overburdening the TOM complex such as the over-expression of slowly-imported precursor proteins could have a similar effect on Fmp52 levels. Indeed, data obtained from quantitative mass spectrometry analysis of cells expressing clogging-prone constructs and thereby under protein import stress, depicted that both transcriptomic and proteomic levels of Fmp52 are upregulated upon clogging of the TOM complex (Boos et al., 2019). Supporting this finding, biochemical results presented in this study corroborate the observation that Fmp52 levels are upregulated upon proteotoxic stress caused by clogging of the TOM complex. In light of these findings, it seems likely that Fmp52 plays a crucial role in regulating the cellular response to proteotoxic stress. However, further mechanistic insights into how Fmp52 regulates stress responses still need to be elucidated. One such possibility could be that Fmp52 cooperates with existing quality control pathways such as the mitoTAD pathway. As a matter of fact, we observed that double deletion of *FMP52* and *UBX2*, resulted in a synthetic growth defect in yeast cells, an effect that was much more pronounced than single protein deletions. Interestingly, *FMP52* also showed a strong genetic interaction with *VMS1*, suggesting molecular cross-talk between the two proteins. Based on the results presented in this study, the following model on the function of Fmp52 at the TOM complex is proposed (Figure 30). First, Fmp52 interacts with the TOM complex for the removal of non-imported precursor proteins arrested at the translocon. Second, Fmp52 co-operates with mitoTAD key component, Ubx2 in ensuring efficient removal of arrested precursors from the TOM complex. Third, Fmp52 levels are increased upon proteotoxic stress such as clogging of the TOM translocon. This increase in Fmp52 levels could serve as a stress response to combat imbalances in mitochondrial import machinery and deal with the accumulation of precursor proteins.

Moreover, Fmp52 exhibits a higher copy number per yeast cell, suggesting the existence of various populations of Fmp52 in cells.

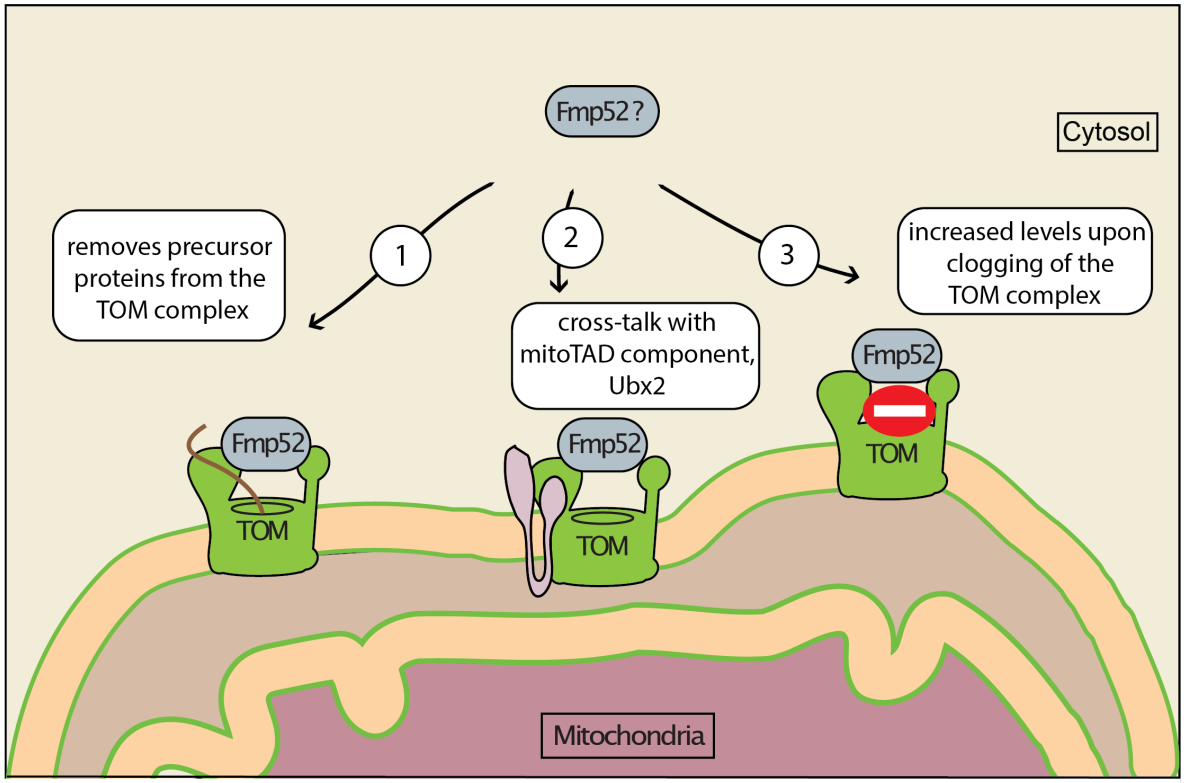

Figure 30. Possible roles of Fmp52 at the TOM complex. Model depicting the possible functions of Fmp52 at the TOM complex**.** The novel protein, Fmp52 binds to the TOM complex under non-stressed conditions. First, it removes accumulated precursors from the TOM complex. Second, it is involved in molecular cross-talk with the mitoTAD pathway. Third, Fmp52 levels are increased upon proteotoxic stress such as clogging of the TOM translocon.

In conclusion, the studies presented in this work provide new insights into the mechanisms of safeguarding protein import at the mitochondrial entry gate. Two novel factors involved in protein quality control at the TOM complex were identified. First, the peptidyl tRNA-hydrolase, Pth2 cooperates with Dsk2 in the removal of accumulated precursor protein from the TOM pore. Second, Fmp52, a novel protein of unknown function, was identified to be involved in mitochondrial quality control at the TOM complex.

6. Experimental Procedures

6.1 Handling of yeast strains

The *Saccharomyces cerevisiae* strains used in this study are listed in Table 1 and derived from the wild-type (WT) strains YPH499 and BY4741. The strains BY4741, *pth2*Δ,, *ubx2*Δ, *vms1*Δ, *fmp52*Δ, *ubp16*Δ were obtained from EUROSCARF. Yeast strains YPH499, $Tom40_{HA}$, $Tom40_{HA}$*ubx2*Δ, *pam17*Δ, *ubx2*Δ*pth2*Δ, $Tom20_{His}$, *dsk2*Δ, *dsk2*Δ*pam17*Δ and $Ubx2_{HA}$ have been described previously (Mårtensson et al., 2019; Schulte et al., 2023). Tagging and deletion of open reading frames (ORF) was performed via homologous recombination using DNA cassettes amplified by PCR by Taq and Vent polymerase (New England BioLabs) (Janke et al., 2004). To generate strains expressing proteins of interest with a His- or HA- at the C-terminus ($Pth2_{His,}$) a DNA cassette encoding the sequence for the affinity tag and a His3MX6 selection marker was amplified by PCR. The generated PCR product was transformed into the corresponding yeast strain. Via homologous recombination, the PCR product was integrated at the C-terminal end of the chosen coding sequence, in front of the stop codon (Knop et al., 1999). Deletion of *FMP52* in *ubx2*Δ, *vms1*Δ, *pth2*Δ, and *ubp16*Δ and *PAM17* in *fmp52*Δ yeast cells was performed using the pFA6a His3MX6 cassette (Longtine et al., 1998). Deletion of *PTH2* in *pam17*Δ and *vms1*Δ yeast cells was performed using the pFA6a KanMX6 cassette (Longtine et al., 1998). Deletion of *PTH2* in *dsk2*Δ*pam17*Δ and *LTN1* in *pth2*Δ yeast cells was performed using the pFA6a hphNT2 cassette (Janke et al., 2004). Primers used for the generation of yeast strains are listed in Table 3. In order to perform *in vivo* rescue experiments with Pth2, the sequence encoding the *PTH2* ORF and its endogenous promoter and terminator was cloned into the pRS416 plasmid using Gibson assembly (primers mentioned in Table 3) (Gibson et al., 2009). The primers were designed such that they contained overlapping sequences with the insert vector pRS416. *PTH2* ORF and its endogenous promoter and terminator were amplified from yeast *Saccharomyces cerevisiae* genomic DNA using Phusion high fidelity DNA polymerase (New England BioLabs). The plasmid was linearized using KpnI and SalI restriction enzymes. Subsequently, the linearized plasmid and the amplified insert were assembled using Gibson Assembly Master Mix (New England BioLabs).

Using the Pth2-pRS416 construct, site-directed mutagenesis was performed to generate D174A point mutant (pRS416 pPTH2 Pth2 D174A) and delete the trans-membrane (TM) region of Pth2 (pRS416 pPTH2 Pth2 ΔTM).

Yeast cells were cultured in a medium containing 1% [w/v] yeast extract and 2% [w/v] bacto-peptone, pH 4.9 adjusted with HCl. As a carbon source either 2% glucose (YPD), 3% glycerol (YPG), 2% sucrose (YPS) or 2% galactose (YPGal) was used. Depending on the strain and experiment, cells were grown at 24°C, 30°C, or 37°C overnight (12-24 hours). Strains containing a plasmid were grown on selective minimal media (0.67% [w/v] yeast nitrogen base without amino acids, 0.2% [w/v] SC amino acid mixture, 3% [w/v] glycerol, 0.1% [w/v] glucose) in order to keep the plasmid. For expressing clogger-prone intermediates, a pYE PD 1/8-10 plasmid encoding for either cytochrome b_2-DHFR-HB or b_2Δ-DHFR-HB was introduced in WT BY471, *pth2*Δ , or *fmp52*Δ yeast strains. To induce overexpression from the *GAL1* promoter, cells were induced by the addition of galactose (final 2% [w/v]) at the early logarithmic phase.

Table 2. Yeast strains used in this study

Strain	**Genetic background**	**Source**	**identifier**
YPH499 (WT)	MATa, ura3-52, lys2-801_amber, ade2-101_ochre, trp1-Δ63, his3-Δ200, leu2Δ1	(Sikorski and Hieter, 1989)	TB1
BY4741 (WT)	MATa, his3Δ1, leu2Δ0, met15Δ0, ura3Δ0	EUROSCARF	TB2
$Pth2_{His}$	YPH499 pth2::PTH2-10His::HIS3MX6	(Schulte et al., 2023)	TB3
$Tom40_{HA}$	BY4741 tom40::TOM40-3HA-HIS3MX6	(Schulte et al., 2023)	TB4
$Tom40_{HA}$*ubx2*Δ	BY4741 ubx2::kanMX4, tom40::TOM40-3HA-HIS3MX6	(Schulte et al., 2023)	TB6
*pth2*Δ*pam17*Δ	BY4741 pth2::KanMX4 pam17Δ:: hphNT1	(Schulte et al., 2023)	TB7
*pth2*Δ	BY4741 pth2::KanMX4	EUROSCARF	TB8
*pam17*Δ	BY4741 pam17::hphNT1	(Mårtensson et al., 2019)	TB9
*ubx2*Δ	BY4741 ubx2::KanMX4	EUROSCARF	TB22
*ubx2*Δ*pth2*Δ	BY4741 ubx2::KanMX4 pth2::HIS3MX6	(Schulte et al., 2023)	TB27
*pth2*Δ*vms1*Δ	BY4741 pth2::kanMX4 vms1::HIS3MX6	(Schulte et al., 2023)	TB35
*pth2*Δ*pam17*Δ + pRS416	BY4741 pth2::KanMX4 pam17Δ:: hphNT1 + pRS416	(Schulte et al., 2023)	TB166
*pth2*Δ*pam17*Δ + pPth2	BY4741 pth2::KanMX4 pam17Δ:: hphNT1 + pRS416 pPTH2 Pth2	(Schulte et al., 2023)	TB167

*pth2*Δ*pam17*Δ + pPth2D174A	BY4741 pth2::KanMX4 pam17Δ:: hphNT1 + pRS416 pPTH2 Pth2 D174A	(Schulte et al., 2023)	TB168
*pth2*Δ*pam17*Δ + pPth2ΔTM	BY4741 pth2::KanMX4 pam17Δ:: hphNT1 + pRS416 pPTH2 Pth2 ΔTM (Δ aa12-32)	(Schulte et al., 2023)	TB169
*pth2*Δ*vms1*Δ + pRS416	BY4741 pth2::kanMX4 vms1::HIS3MX6 + pRS416	(Schulte et al., 2023)	TB171
*pth2*Δ*vms1*Δ + pPth2	BY4741 pth2::kanMX4 vms1::HIS3MX6 + pRS416 pPTH2 Pth2	(Schulte et al., 2023)	TB172
*pth2*Δ*vms1*Δ + pPth2D174A	BY4741 pth2::kanMX4 vms1::HIS3MX6 + pRS416 pPTH2 Pth2 D174A	(Schulte et al., 2023)	TB173
*pth2*Δ*vms1*Δ + pPth2ΔTM	BY4741 pth2::kanMX4 vms1::HIS3MX6 + pRS416 pPTH2 Pth2 ΔTM (Δ aa12-32)	(Schulte et al., 2023)	TB174
$Ubx2_{HA}$	BY4741 ubx2:: *UBX2-3HA::HIS3MX6*	(Mårtensson et al., 2019)	TB45
$Tom20_{His}$	YPH499 tom20::Tom20-10His::HIS3MX6	(Schulte et al., 2023)	TB331
*ltn1*Δ*vms1*Δ	BY4741 vms1::KanMX4 ltn1Δ:: HIS3MX6	this study	TB333
*pth2*Δ*ltn1*Δ	BY4741 pth2::KanMX4 ltn1Δ::NatNT2	this study	TB54
*dsk2*Δ	BY4741 dsk2::KanMX4	(Schulte et al., 2023)	TB102
*dsk2*Δ*pam17*Δ	BY4741 dsk2::KanMX4 pam17Δ::hphNT1	(Schulte et al., 2023)	TB100
*pth2*Δ*dsk2*Δ*pam17*Δ	BY4741 dsk2::KanMX4 pam17Δ::hphNT1 pth2::NatNT2	this study	TB137
*fmp52*Δ	BY4741 fmp52::KanMX4	EUROSCARF	TB332
*fmp52*Δ*ubx2*Δ	BY4741 fmp52:: HIS3MX6 ubx2:: KanMX4	this study	TB339
*fmp52*Δ*vms1*Δ	BY4741 fmp52:: HIS3MX6 vms1:: KanMX4	this study	TB318
*vms1*Δ	BY4741 vms1:: KanMX4	EUROSCARF	TB23
*fmp52*Δ*pth2*Δ	BY4741 fmp52:: HIS3MX6 pth2:: KanMX4	this study	TB316
*fmp52*Δ*ubp16*Δ	BY4741 fmp52:: HIS3MX6 ubp16:: KanMX4	this study	TB320
*ubp16*Δ	BY4741 ubp16:: KanMX4	EUROSCARF	TB21
*fmp52*Δ*pam17*Δ	BY4741 fmp52::KanMX4 pam17:: HIS3MX6	this study	TB352
*pdr5*Δ	BY4741 pdr5::NatNT2	(den Brave et al., 2020)	TB336
WT + pFL39	YPH499 + pFL39	this study	ASG279
WT + pFL39-Tom40-HA	YPH499 + pFL39-Tom40-HA	this study	ASG280
*tom20*Δ + pFL39-Tom40-HA	YPH499 tom20:: Ura3-52 + pFL39-Tom40-HA	this study	ASG281
*tom70*Δ + pFL39-Tom40-HA	YPH499 tom70:: Ura3-52 + pFL39-Tom40-HA	this study	ASG282

WT + pYEp352	BY4741 + pYEp352	this study	ASG293
WT + pCYB2-DHFR-HB	BY4741 + pDP-CYB2 (1-84)-DHFR-HB (81-181)	this study	ASG295
WT + pCYB2Δ-DHFR-HB	BY4741 + pDP-CYB2 (1-84)Δ-DHFR-HB (81-181)	this study	ASG297
*fmp52*Δ+ pYEp352	BY4741 fmp52::KanMX4 + pYEp352	this study	ASG294
*fmp52*Δ + pCYB2-DHFR-HB	BY4741 fmp52::KanMX4 + pDP-CYB2 (1-84)-DHFR-HB (81-181)	this study	ASG296
*fmp52*Δ + pCYB2Δ-DHFR-HB	BY4741 fmp52::KanMX4 + pDP-CYB2 (1-84)Δ-DHFR-HB (81-181)	this study	ASG298

Table 3. Plasmids used in this study

Plasmid	Source	Identifier
pRS416	(Schulte et al., 2023)	pTB94
pRS416 pPTH2 Pth2	(Schulte et al., 2023)	pTB91
pRS416 pPTH2 Pth2 D174A	(Schulte et al., 2023)	pTB92
pRS416 pPTH2 Pth2 ΔTM (Δaa12-32)	(Schulte et al., 2023)	pTB93
pFA6a His3MX6	(Longtine et al., 1998)	pTB2
pFA6a hphNT1	(Janke et al., 2004)	pTB6
pFA6a hphNT2	(Longtine et al., 1998)	pTB5
pFA6a KanMX6	(Longtine et al., 1998)	pTB1
pFA6a 3HA-His3MX6	(Knop et al., 1999)	pTB12
pYEp352	(Schulte et al., 2023)	pTB51
pDP-CYB2 (1-84)-DHFR-HB(81-181)	(Bömer et al., 1997)	pTB7
pDP-CYB2 (1-84)-Δ(46-66)-DHFR-HB(81-181)	(Bömer et al., 1997)	pTB8
pRS415	(Schulte et al., 2023)	pTB103
pADH His-Ubiquitin	(Cohen et al., 2008)	pTB3
pFL39	(Becker et al., 2011)	pTB22
pFL39-Tom40-HA	(Becker et al., 2011)	PTB174

Table 4. Primers used for the generation of yeast cells

Primer	Sequence (5'-3')	Identifier
Pth2-S1	TTTCTTGCTATATTACTTGTTGACAGCGGAGTAACATGATAACGTCTTTTTAATGC GTACGCTGCAGGTCGAC	**TB(P5)**
Pth2 -S2	TTAATATATAAATGCACGTATATCTATACCCGTAGTATATATCATTTGTACCTCAAT CGATGAATTCGAGCTCG	**TB(P6)**
Pth2-colony	GTCTTCTTGGCCTTCTTCGT	**TB(P7)**
Ubx2-S1	GCAGCAGGTATTACGATAGAAGTATGTAATAGCTTTCATAGTGTAATCGAAGAT GCGTACGCTGCAGGTCGAC	**TB(P11)**
Ubx2-S2	ACTCCAGAAACTCTTTGTACGCGTTTGTCGTTTTTAACGATATGCTATTTTATCAAT CGATGAATTCGAGCTCG	**TB(P12)**
Ubx2-colony	GAATATTCCCCCAAAGGAGC	**TB(P139**
Vms1-S1	AGAAAAAGGATTTTCAAAAGATCTGCACGCCTGTTGACAAGCTTCCAATAGCATG CGTACGCTGCAGGTCGAC	**TB(P14)**
Vms1-S2	AATATATGCAAATGCTAAGAAAAATCCTAAAAATTTGAATATGAGATATTCCTCA ATCGATGAATTCGAGCTCG	**TB(P15)**
Vms1-colony	GCCACAGAATTGGTTCGAAG	**TB(P16)**
Ubp16-S1	TCCTTCTGCCCAAACAGTATATGCAAGGTACAGCAGTTACTACAAGCACAATATG CGTACGCTGCAGGTCGAC	**TB(P8)**
Ubp16-S2	GGATATGGATGCGTAACTTACTATTATTATAATATACCTATGTACAGGGCGGTTA ATCGATGAATTCGAGCTCG	**TB(P99**
Ubp16-colony	TTGCTTACTATATTGGCCCC	**TB(P10)**
Ltn1-S1	AGTTCAAATCTGCTAAGCCATCAAAAAAAGTTCAAGCAATAGTTGGTTCTTAATG CGTACGCTGCAGGTCGAC	**TB(P47)**
Ltn1-S2	GAACTTTGTTTAAAAAATGTAGTACATTTATATGAAATTTATATGCGATAGTCTAA TCGATGAATTCGAGCTCG	**TB(P48)**
Ltn1-colony	GATTCCGGACTCGTCCAAAT	**TB(P49)**
Dsk2-S1	GACGAGAGGCAAATAAGACGGATCAAAGACACCGAATCATTCTAGCACGATAAT GCGTACGCTGCAGGTCGAC	**TB(P33)**
Dsk2-S2	ATGCCGATAGAGTAGGGTAAAAGTATATAGGTTGCGGCATCTAGACGTTTATTTA ATCGATGAATTCGAGCTCG	**TB(P34)**
Fmp52-S1	CTCCTACTGATGAGAAAGATAGGATGGATTATATAGAAGAGCACAAGCAACGAT GCGTACGCTGCAGGTCGAC	**TB(P193)**
Fmp52-S2	GTACGTCACAGTAAAATACAACTGTAGCTGCGAGAAGAAGCCGTTGGTTGATTT AATCGATGAATTCGAGCTCG	**TBP(194)**
Fmp52-colony	CGTAAATCGCGGCGAAAAAG	**TBP(195)**
Pam17-S1	ATGTTCAAAGAAGTGTTAAAAACATTCAGAAAACATTGTCCGCCTCTTCAAAATG CGTACGCTGCAGGTCGAC	**TB(P2)**
Pam17-S2	CATATATGTATATATACAGAGTCTGAGAAGAAGGAAAAGATCACACGTTCAATCA ATCGATGAATTCGAGCTCG	**TB(P3)**
Pam17-colony	CTGTTGGAGAACGGTATCAC	**TBP4**
Colony-rev	GACTGTCAAGGAGGGTATTCTG	**TB(P1)**
Pth2-pRS416-fw	CTATAGGGCGAATTGGGTACCATTCAAATTGTGACAAATG	**ASG(P35)**
Pth2-pRS416-rev	CAAGCTTATCGATACCGTCGACTATAAAAAATTAGATGAG	**ASG(P36)**
D174A-Pth2-pRS416-fw	CTTGGGGTGAATGCAGCAGTTATTCATGCTGCTGGTAGAA	**ASG(P48)**

D174A-Pth2-pRS416-rev	TTCCCGCAGCAATCTGTGTTCTACCAGCAGCATGAATAAC	**ASG(P49)**
TMdel-Pth2-pRS416-fw	GACAGTTTCTTCGAATTACACCAACGCATCATCAACTAAG	**ASG(P52)**
TMdel-Pth2-pRS416-rev	TAAAGTAGCTGAGGATTTCTTAGTTGATGATGCGTTGGTG	**ASG(P53)**

6.2 Yeast growth assays

Yeast cells were grown overnight in respective growth medium at 30°C until an early logarithmic phase. Cells with an optical density of 1 at 600nm (OD600) were harvested by centrifugation at (3,000 x g, 4 min). The cell pellet was resuspended in 1 mL of sterile distilled water. From these ten-fold serial dilutions (1:10, 1:100, 1:1000, and so on) were prepared and spotted on a solid medium containing 3% [w/v] agar and incubated at 24°C, 30°C, and 37°C.

6.3 Isolation of mitochondria

Yeast cells were cultured in the respective medium until the early logarithmic growth phase and the cells were collected with centrifugation (3,000 x g, 8 min, 20°C). Cells were washed once with dH_2O and then incubated in DTT buffer under constant shaking at 130 rpm (0.1 M Tris/H_2SO4 pH 9.4, 10 mM DTT) for 20 min at 30°C. The cells were collected again by centrifugation (3,000 x g, 5 min) and washed once with zymolase buffer (20 mM KPi pH 7.4, 1.2 M sorbitol) without zymolase. The cells were collected by centrifugation (2,500 x g, 5 min) followed by resuspension in zymolase buffer containing 4 mg/g of cells zymolyase (Nacalai Tesque) and incubated for 45 min at 30°C under constant shaking at 130 rpm for cell wall removal. The resulting spheroblasts were collected with centrifugation (1,500 x g, 5 min), washed once with zymolase buffer and resuspended in 6.5 ml/g cells homogenization buffer with zymolase buffer. The spheroblasts were resuspended in ice-cold homogenization buffer (10 mM Tris HCl pH 7.4, 0.6 M sorbitol, 1 mM EDTA, 0.2% [w/v] BSA). Spheroblasts were opened by mechanical disruption on ice using a glass potter grinder. The lysate was cleared from cell and nuclear debris with two consecutive centrifugation steps followed by isolation of mitochondria from the cell lysate (17,000 x g, 10min, 4°C). Finally, mitochondria were resuspended in SEM buffer, centrifuged (2,500 x g, 5 min, 4°C) and the resulting supernatant was collected. Mitochondria were re-collected (17,000 x g, 15 min, 4°C) and resuspended in a

small volume of SEM buffer. Total protein concentration of the mitochondrial proteins were determined using ROTI-Quant reagent (Roth). Mitochondria were aliquoted, flash frozen in liquid nitrogen and kept at -80°C until further use.

6.4 Preparation of cell extracts

Yeast cells were grown in YPG or YPD medium at 24°C or 30°C until early logarithmic phase. Cells with an optical density of 2.5 at 600nm (OD600) were harvested by centrifugation at (3,000 x g, 4 min). Cell pellets were resuspended in 0.1 M NaOH and incubated for 5 min at room temperature. After centrifugation (16,000 x g, 1 min) cell pellets were resuspended in sample buffer (8 M urea, 5% [w/v] SDS, 1 mM EDTA, 1.5 % [w/v] DTT, 0.025% [w/v] bromophenol blue, 200mM Tris HCl pH 6.8) and denatured for 10 min at 65°C shaking at 14,000 rpm.
Yeast cells for large scale affinity purifications were grown in respective conditions until early logarithmic phase. Cells with an optical density of 200-400 at 600nm (OD600) were harvested by centrifugation at (3,000 x g, 4 min). Cells were washed once with dH_20 and the cell pellets with desired ODs were flash frozen in liquid nitrogen until further use.

6.5 Affinity purification of His-tagged proteins

To investigate the interaction partners of His-tagged proteins, affinity purification assays with Ni^{2+}-NTA Agarose (Qiagen) were performed. Isolated mitochondria from yeast cells expressing His-tagged proteins were solubilized in lysis buffer (20 mM Tris/HCl pH 7.4, 0.1 mM EDTA, 50 mM NaCl, 10% [v/v] glycerol) containing 0.8-1.0 % [w/v] digitonin and 10 mM imidazole at a concentration of 1 mg mitochondrial protein/ml. The samples were incubated for 15 min on ice and the unsolubilized materials were removed by centrifugation (10 min; 17,000 x g; 4°C).
For pulldowns with cell extracts, cells with a desired optical density were solubilized in lysis buffer and resuspended in lysis buffer (0.1 M EDTA; 50 mM NaCl; 10% [v/v] glycerol; 20 mM Tris/HCl pH 7.4) with protease inhibitors (1 mM PMSF, 1xHALT protease inhibitor cocktail (Thermofisher) and 10 mM imidazole). Cells were then ruptured with silica beads for 5 times for 3 min with 3 min break in between at 4°C on a cell disruptor (Retsch MM400 mill). Cell extracts were cleared by centrifugation (2,000 x g, 4 min, 4°C). The cells were solubilized with

1% digitonin [w/v] and the cells were incubated for 30 min on ice. The solubilized samples were cleared by centrifugation (10 min; 17,000 x g; 4°C).

For both mitochondria and cells extracts, a part of the supernatant (0.2% - 1%) was retained for the load fraction. The rest of the supernatant was incubated with Ni-NTA agarose beads (Qiagen) that were pre-equilibrated in lysis buffer with 0.1% [w/v] digitonin and 10 mM imidazole. After 1h incubation at 4°C under constant rotation for mitochondria samples and 1.5 h incubation for cell extracts, unbound proteins were removed and the affinity matrix was washed with an excess amount of lysis buffer containing 0.1% [w/v] digitonin and 40 mM imidazole. Bound proteins were eluted with lysis buffer containing 0.1% [w/v] digitonin and 250 mM imidazole. All centrifugation steps during washing steps were performed at 100 x g for 1 min at 4°C. The samples were denatured for 5 min at 95°C with addition of SDS sample buffer and analyzed by SDS-PAGE.

6.6 Affinity purification of HA-tagged proteins

To investigate the interaction partners of HA-tagged proteins, affinity purification assays with HA-tagged beads (Roche) were performed. Isolated mitochondria from yeast cells expressing HA-tagged proteins were solubilized in lysis (0.1 M EDTA; 50 mM NaCl; 10% [v/v] glycerol; 20 mM Tris/HCl pH 7.4) buffer containing 1% [w/v] of digitonin. The samples were incubated for 15 min on ice and the solubilized samples were cleared by centrifugation (10 min; 17,000 x g; 4°C).

For pulldowns with cell extracts, cells with a desired optical density were solubilized in lysis buffer with resuspended in lysis with protease inhibitors (1 mM PMSF, 1xHALT protease inhibitor cocktail). Cells were then ruptured with silica beads for 5 times for 3 min with 3 min break in between at 4°C on a cell disruptor (Retsch MM400 mill). Cell extracts were cleared by centrifugation (2,000 x g, 4 min, 4°C). The cells were solubilized with 1% digitonin [w/v] and the cells were incubated for 30 min on ice. The solubilized samples were cleared by centrifugation (10 min; 17,000 x g; 4°C).

For both mitochondria and cells extracts, a part of the supernatant (0.2% - 1%) was retained for the load fraction. The rest of the supernatant was incubated with anti HA-tagged matrix (30-60µL) that were pre-equilibrated in lysis buffer with 0.1% [w/v] digitonin. After 1 h incubation at 4°C under constant rotation for mitochondria samples and 1.5 h incubation for cell extracts, unbound proteins were removed and the affinity matrix was washed with excess amount of lysis

buffer containing 0.1% [w/v] digitonin. Bound proteins were eluted with 60µL of SDS sample buffer. All centrifugation steps during washing steps were performed at 100 x g for 1 min at 4°C. The samples were denatured for 5 min at 95°C.

6.7 Denaturing Ni^{2+}-NTA pulldowns

Proteins conjugated to His-tagged ubiquitin were purified via affinity purification assays with Ni^{2+}-NTA agarose beads (Qiagen) under denaturing conditions as previously described (Psakhye and Jentsch, 2016; Schulte et al., 2023). Cells expressing His-tagged ubiquitin were grown to logarithmic phase in selective media after which cells corresponding to an optical density of 200 at 600nm (OD600) were harvested by centrifugation at (3,000 x g, 4 min) and washed with distilled H_2O. The cells were resuspended in 1 mL of denaturing buffer A to inactivate proteases (6 M guanidinium hydrochloride; 100 mM NaH_2PO_4; 10 mM Tris-HCl, pH 8.0), followed by subsequent addition of silica beads and cell disruption using a cell disruptor for 5 min (Vortex Disruptor, Genie). Cellular lysates were cleared by centrifugation (500 x g, 4 min, 4°C) to remove residual beads. Subsequently, the samples were diluted 1:2 with the addition of 1 mL of buffer A with 0.1% [v/v] Tween-20 and 40 mM imidazole followed by 30 min incubation under constant rotation at 4°C. The solubilized samples were cleared by centrifugation (10 min; 17,000 x g; 4°C) and the remaining supernatants were incubated with Ni-NTA agarose beads for 1.5 h under constant rotation at 4°C. After the removal of unbound proteins, the beads were washed twice with buffer A containing 0.05% [v/v] Tween-20 and 20 mM imidazole, followed by four wash steps with buffer C (8 M urea; 100 mM NaH_2PO_4; 10 mM Tris-HCl, pH 6.3; 0.05% Tween 20; 20 mM imidazole). Bound proteins containing His-conjugated were eluted with HU-buffer (8 M urea; 5% [w/v] SDS; 1 mM EDTA; 1.5% [w/v] DTT, 0.025% [w/v] bromophenol blue; 200 mM Tris-HCl pH 6.8) for 10 min at 65°C.

6.8 Sodium-dodecyl Sulphate polyacrylamide gel electrophoresis

Proteins were separated and analyzed by sodium-dodecyl sulphate-polyacrylamide gel electrophoresis (SDS-PAGE) using 10% MOPS gels (8.25% [w/v] Acrylamide, 1M MOPS, 1M ris-base, 2% SDS, 20mM EDTA). Samples were resuspended in sample buffer and boiled for 10 min at 95°C. The running of the gel was performed in MOPS running buffer (1M Bis-

Tris, pH 6.4). PageRuler Prestained Protein Ladder (Thermo Fisher Scientific) was used as a molecular weight marker for size reference.

6.9 Blue native polyacrylamide gel electrophoresis

Blue native polyacrylamide gel electrophoresis (BN-PAGE) was used for the separation of native mitochondrial proteins and was performed as previously described (Schägger and von Jagow, 1991; Wittig and Schägger, 2005). For analysis via BN-PAGE, isolated mitochondria were solubilized in lysis buffer (0.1 M EDTA; 50 mM NaCl; 10% [v/v] glycerol; 20 mM Tris/HCl pH 7.4) containing 1% [w/v] digitonin for 15 min on ice. Insoluble material was removed (17,000 x g, 10 min, 4°C) and the supernatant was supplemented with BN sample buffer (0.5% [w/v] Coomassie Brilliant Blue G-250, 10 mM Bis-Tris pH 7.0 and 50 mM 6-aminocaproic acid) to achieve a 1x final concentration. Typically, BN gels with a gradient of 4-13% (4-13% [w/v] Acrylamide, 0.12-0.40% [w/v] Bis-Acrylamide, 67 mM ε-amino n-caproic acid, 50 mM Bis-Tris/HCl pH 7.0) were used. A BN protein marker consisting of blue native protein mix (Cytiva) dissolved in lysis buffer and BN sample buffer was used for estimation of the molecular weight of protein complexes. Sample separation was performed in the presence of BN cathode (0.02% [w/v] Coomassie G, 50 mM Tricine, 15 mM Bis-Tris/HCl pH 7.0) and BN anode buffer (50 mM Bis-Tris/HCl pH 7.0) at 15 mA for 2 h. After approximately 20 min of separation, BN cathode buffer was replaced with clear cathode buffer (50 mM Tricine, 15 mM Bis-Tris/HCl pH 7.0) without Coomassie G.

6.10 Western blotting and immunodetection

Proteins separated on polyacrylamide gels were transferred by semi-dry western blot transfer system (model:700-1220, VWR) to PVDF membranes (Immobilon®-P, Merck Millipore). The sandwich for transfer was constructed in the following manner from anode to cathode; filter paper, PVDF membrane, the polyacrylamide gel and then filter paper. All components were immersed in transfer buffer (20% [v/v] ethanol; 150 mM Glycine, 0.02% [w/v] SDS; 20 mM Tris Base) and the PVDF membrane was activated in 100% [w/v] ethanol. The transfer was carried out for 2 h at 250 mA. After blotting, membranes were washed briefly with TBS-T (12.5 mM NaCl; 20 mM Tris/HCl; pH 7.4; 0.1% [v/v] Tween 20) and blocked with blocking buffer (5% [w/v] skimmed milk powder in TBS-T or RotiBlock (Roth)) for 1 h.

Membranes were incubated with primary antibody in blocking buffer (Table. 4) for 1-2 h at room temperature or overnight at 4°C. Subsequently, membranes were washed three times over 30 min with excess TBS-T buffer, incubated with secondary antibody for 1h at room temperature, and washed again three times with TBS-T buffer to remove unbound antibodies.

Table 5. Antibodies used in this study.

Antigen	**Dilution**	**Company and number**	**Source**
Rabbit polyclonal anti-Ubx2	1:500 roti block in TBS-T	GR1484	(Mårtensson et al., 2019)
Rabbit polyclonal anti-Pth2	1:500 roti block in TBS-T	GR 797-3	(Schulte et al., 2023)
Rabbit polyclonal anti-Tom70	1:500 roti block in TBS-T	GR657-3	(Schulte et al., 2023)
Rabbit polyclonal anti-Ubp16	1:250 milk in TBS-T	GR5040-4	(Schulte et al., 2023)
Rabbit polyclonal anti-Tom22	1:1000 roti block in TBS-T	GR3227-2	(Schulte et al., 2023)
Rabbit polyclonal anti-Tom20	1:1000 roti block in TBS-T	GR3225-7	(Schulte et al., 2023)
Rabbit polyclonal anti-Tom40	1:1000 roti block in TBS-T	GR168-5	(Schulte et al., 2023)
Rabbit polyclonal anti-Mim1	1:1000 roti block in TBS-T	GR544-2	(Doan et al., 2020)
Rabbit polyclonal anti-Om45	1:1000 roti block in TBS-T	GR1311	(Schulte et al., 2023)
Rabbit polyclonal anti-Por1	1:1000 roti block in TBS-T	GR3621	(Schulte et al., 2023)
Rabbit polyclonal anti-Om14	1:1000 roti block in TBS-T	GR3041	(Mårtensson et al., 2019)
Rabbit polyclonal anti-Rip1	1:5000 roti block in TBS-T	GR542-4	(Böttinger et al., 2013)
Rabbit polyclonal anti-Mdj1	1:500 milk in TBS-T	121-7	(Schulte et al., 2023)
Rabbit polyclonal anti-Ilv2	1:500 milk in TBS-T	GR1010	(Schulte et al., 2023)
Rabbit polyclonal anti-Rsp5	1:250 milk in TBS-T	GR5064	(Schulte et al., 2023)
Rabbit polyclonal anti-Fis1	1:500 milk in TBS-T	GR310	(Schulte et al., 2023)
Rabbit polyclonal anti-Msp1	1:500 milk in TBS-T	GR1469	(Schulte et al., 2023)
Rabbit polyclonal anti-Hsp60	1:500 milk in TBS-T	GR170	(Schulte et al., 2023)
Rabbit polyclonal anti-mtHsp70	1:500 milk in TBS-T	GR1830-2	(Mårtensson et al., 2019)
Rabbit polyclonal anti-Cdc48	1:500 milk in TBS-T	GR 5015	(Schulte et al., 2023)
Rabbit polyclonal anti-Fmp52	1:500 roti block in TBS-T	GR1498	(Morgenstern et al., 2017)
Rabbit polyclonal anti-Atp2	1:1000 roti block in TBS-T	GR861	(Böttinger et al., 2013)
Rabbit polyclonal anti-Sec61	1:500 milk in TBS-T	GR759-5	(Mårtensson et al., 2019)
Rabbit polyclonal anti-Sod2	1:500 milk in TBS-T	GR1051-4	(Mårtensson et al., 2019)
Rabbit polyclonal anti-Tim44	1:500 milk in TBS-T	GR1835-4	(Böttinger et al., 2013)
Rabbit polyclonal anti-Tim23	1:250 milk in TBS-T	GR3878-4	(Böttinger et al., 2013)
Rabbit polyclonal anti-Mdh1	1:500 milk in TBS-T	GR1088-6	(Priesnitz et al., 2022)
Rabbit polyclonal anti-Cox1	1:500 milk in TBS-T	GR1539-4	(Böttinger et al., 2013)
Rabbit polyclonal anti-Cox4	1:500 milk in TBS-T	GR578-5	(Böttinger et al., 2013)
Rabbit polyclonal anti-Cox12	1:500 milk in TBS-T	GR1937-4	(Böttinger et al., 2013)

mouse-monoclonal anti-DHFR	Santa Cruz	sc-377091	(Schulte et al., 2023)
mouse-monoclonal anti-Pgk1	Invitrogen	459250	(Schulte et al., 2023)
mouse-monoclonal anti-ubiquitin	Santa Cruz	sc-8017	(Schulte et al., 2023)

Different types of secondary antibodies were used. Secondary antibody against rabbit or mouse coupled to fluorescent labels (IRDye 800CW, anti-mouse; IRDye 800CW, anti-rabbit; IRDye 680RD, anti-mouse) were used at 1:10,000 dilution in blocking buffer for detection of signals with the Licor system. Fluorescent secondary antibody signals were detected on Odyssey CLx Infrared Imaging System (Li-Cor) and analyzed using Image Studio software (v.5.2.5; Li-Cor). Incase of detection of signals for secondary antibody against rabbit or mouse coupled to horseradish peroxidase, an image analyzer or X-ray films were used. Secondary antibody (Jackson ImmunoResearch) was used at 1:10,000 dilution in blocking buffer for detection of signal with chemiluminescence. An enhanced chemiluminescence (ECL)-solution (Haan and Behrmann, 2007) was added to the membrane and the resulting chemiluminescence signal was analyzed by either a LAS 3000 imager reader (Fujifilm) or with Amersham Imager 680 (Cytiva).

6.11 Cellular fractionation

Yeast cells were cultured in YPG medium at 30°C until early logarithmic growth phase. Cells with an optical density of 100 at 600nm (OD600) were harvested by centrifugation (3,000 x g, 5 min). Cells were washed once with dH2O and then incubated in DTT buffer under constant shaking (0.1 M Tris/H_2SO4 pH 9.4, 10 mM DTT) for 20 min at 30°C. The cells were pelleted (3,000 x g, 5 min) followed by resuspension in zymolase buffer (20 mM KPi pH 7.4, 1.2 M sorbitol) containing 8 mg zymolyase (Nacalai Tesque) and incubated for 45 min at 30°C under constant shaking for cell wall removal. Resulting spheroblasts were collected with centrifugation (1,500 x g, 5 min) and washed once with zymolase buffer. The spheroblasts were resuspended in ice-cold homogenization buffer (10 mM Tris HCl pH 7.4, 0.6 M sorbitol, 1 mM ethylenediaminetetraacetic acid (EDTA)) and subjected to mechanical disruption on ice using a glass potter grinder. Cell and nucleur debris were removed with centrifugation (1,500 x g, 5 min) and a clear lysate was obtained. One half of the lysate was retained as the post-nuclear supernatant (PNS) and the other half was centrifuged (17,000 x g, 10min, 4°C) to obtain the enriched mitochondrial fraction P13. The resulting supernatant was subjected to ultra-

centrifugation to (100,000 x g, 1h, 4°C) to separate the mircrosomal fraction P100 pellet from the cytosolic supernatant P100. Proteins from S100 and PNS fractions were precipitated with 10% trichloroacetic acid. All samples were dissolved in SDS buffer containing and analyzed on MOPS gel.

6.12 Cycloheximide treatment

Cycloheximide (Thermo Fisher Scientific) treatment was performed to study the stability of proteins. Yeast cells were grown on YPD at 30°C until the early logarithmic growth phase. Cells were supplemented with Cycloheximide (final concentration 50μg/mL). Cells with an optical density of 2.5 at 600nm (OD600) were harvested by centrifugation before and after treatment at defined time points. Harvested cells were flash-frozen with liquid nitrogen and total cell extracts were prepared as described above.

6.13 Carbonate extraction

Carbonate Extraction was performed to study whether mitochondrial proteins are soluble, membrane-associated or membrane-integrated (Fujiki et al., 1982). Purified mitochondria samples were treated with 0.1M Na_2CO_3 pH 10.8 or 11.5 for 30 min, at 4°C. After treatment with Na_2CO_3, the samples were subjected to ultra-centrifugation (136,000 x g, 30 min, 4°C). The resulting supernatant was collected and the membrane pellet was resuspended in SEM buffer. Supernatant and membrane fractions were precipitated with trichloroacetic acid and analyzed by SDS-PAGE and immunodetection.

6.14 In-gel activity staining

The activity of complex IV of the respiratory chain was determined by in-gel activity staining after analyzing the purified mitochondria samples on a blue native gel (Schuler et al., 2016). In order to detect the activity of complex IV, the gel was stained for 30 min with staining solution (1 mg/ml cytochrome C from equine heart (Sigma Aldrich), 1.4 mM 3,3’ -diaminobenzidine tetrahydrochloride hydrate, 2mg/ml catalase, 220 mM sucrose and 40 mM NaP_i buffer pH 7.2). The reaction was stopped by the transfer of the gel in distilled H_20

6.15 Aggregation assay

Yeast cells were cultured in YPGal medium at 37°C until the early logarithmic growth phase. Cells with an optical density of 15 at 600nm (OD600) were harvested by centrifugation (3,000 x g, 5 min) and washed with dH2O. The cells were resuspended in 300 µL of ice cold lysis buffer (100 mM HEPES pH 7.5, 1 % Triton X-100, 300mM NaCl) with protease inhibitors (1 mM PMSF, 1xHALT protease inhibitor cocktail). Cells were then ruptured with silica beads for 5 times for 30 seconds with 1 min break in between at 4°C using a cell disruptor (Vortex Disruptor, Genie). Cell extracts were cleared by centrifugation (2,000 x g, 5 min, 4°C) and the resulting total cell extracts (T fraction) were fractioned by a second centrifugation step (10 min; 17,000 x g; 4°C) to yield soluble (S) and insoluble pellet (P) fractions. 20 µL of each, the total and soluble fractions were mixed with 30 µL HU buffer (8 M urea; 5% [w/v] SDS; 1 mM EDTA; 1.5% [w/v] DTT, 0.025% [w/v] bromophenol blue; 200 mM Tris-HCl pH 6.8) and denatured for 10 min at 65°C. The pellet was washed twice with 200 µL ice cold lysis buffer and resolubilized in 50 µL HU sample buffer and denatured for 10 min at 65°C.
Isolated mitochondria were solubilized in 180 µL of lysis buffer (0.1 M EDTA; 50 mM NaCl; 10% [v/v] glycerol; 20 mM Tris/HCl pH 7.4) containing 1% [w/v] of digitonin. The samples were incubated for 30 min at 4°C with end-to-end shaking. Protein aggregates were collected by centrifugation (10 min; 17,000 x g; 4°C). The resulting supernatant (S) was mixed with SDS sample buffer. The pellet (P) was washed once with lysis buffer and resolubilized in with SDS sample buffer. Both supernatant (S) and pellet (P) fractions were denatured for 10 min at 95°C and analyzed by SDS-PAGE.

.

7. References

Abe, Y., Shodai, T., Muto, T., Mihara, K., Torii, H., Nishikawa, S., Endo, T., and Kohda, D. (2000). Structural basis of presequence recognition by the mitochondrial protein import receptor Tom20. Cell *100*, 551-560.

Ahting, U., Thieffry, M., Engelhardt, H., Hegerl, R., Neupert, W., and Nussberger, S. (2001). Tom40, the pore-forming component of the protein-conducting TOM channel in the outer membrane of mitochondria. J Cell Biol *153*, 1151-1160.

Anderson, N.S., and Haynes, C.M. (2020). Folding the Mitochondrial UPR into the Integrated Stress Response. Trends Cell Biol *30*, 428-439.

Ando, M., Higuchi, Y., Takeuchi, M., Hashiguchi, A., and Takashima, H. (2022). The first case of infantile-onset multisystem neurologic, endocrine, and pancreatic disease caused by novel PTRH2 mutation in Japan. Neurol Sci *43*, 2133-2136.

Araiso, Y., and Endo, T. (2022). Structural overview of the translocase of the mitochondrial outer membrane complex. Biophys Physicobiol *19*, e190022.

Araiso, Y., Tsutsumi, A., Qiu, J., Imai, K., Shiota, T., Song, J., Lindau, C., Wenz, L.S., Sakaue, H., Yunoki, K.*, et al.* (2019). Structure of the mitochondrial import gate reveals distinct preprotein paths. Nature *575*, 395-401.

Archibald, J.M. (2015). Endosymbiosis and Eukaryotic Cell Evolution. Curr Biol *25*, R911-921.

Backes, S., Bykov, Y.S., Flohr, T., Raschle, M., Zhou, J., Lenhard, S., Kramer, L., Muhlhaus, T., Bibi, C., Jann, C.*, et al.* (2021). The chaperone-binding activity of the mitochondrial surface receptor Tom70 protects the cytosol against mitoprotein-induced stress. Cell Rep *35*, 108936.

Backes, S., Hess, S., Boos, F., Woellhaf, M.W., Godel, S., Jung, M., Muhlhaus, T., and Herrmann, J.M. (2018). Tom70 enhances mitochondrial preprotein import efficiency by binding to internal targeting sequences. J Cell Biol *217*, 1369-1382.

Basch, M., Wagner, M., Rolland, S., Carbonell, A., Zeng, R., Khosravi, S., Schmidt, A., Aftab, W., Imhof, A., Wagener, J.*, et al.* (2020). Msp1 cooperates with the proteasome for extraction of arrested mitochondrial import intermediates. Mol Biol Cell *31*, 753-767.

Bausewein, T., Mills, D.J., Langer, J.D., Nitschke, B., Nussberger, S., and Kuhlbrandt, W. (2017). Cryo-EM Structure of the TOM Core Complex from Neurospora crassa. Cell *170*, 693-700 e697.

Becker, L., Bannwarth, M., Meisinger, C., Hill, K., Model, K., Krimmer, T., Casadio, R., Truscott, K.N., Schulz, G.E., Pfanner, N.*, et al.* (2005). Preprotein translocase of the outer mitochondrial membrane: reconstituted Tom40 forms a characteristic TOM pore. J Mol Biol *353*, 1011-1020.

Becker, T., Pfannschmidt, S., Guiard, B., Stojanovski, D., Milenkovic, D., Kutik, S., Pfanner, N., Meisinger, C., and Wiedemann, N. (2008). Biogenesis of the mitochondrial TOM complex: Mim1 promotes insertion and assembly of signal-anchored receptors. J Biol Chem *283*, 120-127.

Becker, T., Song, J., and Pfanner, N. (2019). Versatility of Preprotein Transfer from the Cytosol to Mitochondria. Trends Cell Biol *29*, 534-548.

Becker, T., Wenz, L.S., Kruger, V., Lehmann, W., Müller, J.M., Goroncy, L., Zufall, N., Lithgow, T., Guiard, B., Chacinska, A.*, et al.* (2011). The mitochondrial import protein Mim1 promotes biogenesis of multispanning outer membrane proteins. J Cell Biol *194*, 387-395.

Bengtson, M.H., and Joazeiro, C.A. (2010). Role of a ribosome-associated E3 ubiquitin ligase in protein quality control. Nature *467*, 470-473.

Bömer, U., Meijer, M., Guiard, B., Dietmeier, K., Pfanner, N., and Rassow, J. (1997). The sorting route of cytochrome b2 branches from the general mitochondrial import pathway at the preprotein translocase of the inner membrane. J Biol Chem *272*, 30439-30446.

Boos, F., Krämer, L., Groh, C., Jung, F., Haberkant, P., Stein, F., Wollweber, F., Gackstatter, A., Zöller, E., van der Laan, M.*, et al.* (2019). Mitochondrial protein-induced stress triggers a global adaptive transcriptional programme. Nat Cell Biol *21*, 442-451.

Boos, F., Labbadia, J., and Herrmann, J.M. (2020). How the Mitoprotein-Induced Stress Response Safeguards the Cytosol: A Unified View. Trends Cell Biol *30*, 241-254.

Böttinger, L., Guiard, B., Oeljeklaus, S., Kulawiak, B., Zufall, N., Wiedemann, N., Warscheid, B., van der Laan, M., and Becker, T. (2013). A complex of Cox4 and mitochondrial Hsp70 plays an important role in the assembly of the cytochrome c oxidase. Mol Biol Cell *24*, 2609-2619.

Bragoszewski, P., Gornicka, A., Sztolsztener, M.E., and Chacinska, A. (2013). The ubiquitin-proteasome system regulates mitochondrial intermembrane space proteins. Mol Cell Biol *33*, 2136-2148.

Brandman, O., and Hegde, R.S. (2016). Ribosome-associated protein quality control. Nat Struct Mol Biol *23*, 7-15.

Brandman, O., Stewart-Ornstein, J., Wong, D., Larson, A., Williams, C.C., Li, G.W., Zhou, S., King, D., Shen, P.S., Weibezahn, J.*, et al.* (2012). A ribosome-bound quality control complex triggers degradation of nascent peptides and signals translation stress. Cell *151*, 1042-1054.

Brix, J., Dietmeier, K., and Pfanner, N. (1997). Differential recognition of preproteins by the purified cytosolic domains of the mitochondrial import receptors Tom20, Tom22, and Tom70. J Biol Chem *272*, 20730-20735.

Burkhart, J.M., Taskin, A.A., Zahedi, R.P., and Vögtle, F.N. (2016). Correction to "Quantitative Profiling for Substrates of the Mitochondrial Presequence Processing Protease Reveals a Set of Nonsubstrate Proteins Increased upon Proteotoxic Stress". J Proteome Res *15*, 1386.

Bykov, Y.S., Rapaport, D., Herrmann, J.M., and Schuldiner, M. (2020). Cytosolic Events in the Biogenesis of Mitochondrial Proteins. Trends Biochem Sci *45*, 650-667.

Chacinska, A., Koehler, C.M., Milenkovic, D., Lithgow, T., and Pfanner, N. (2009). Importing mitochondrial proteins: machineries and mechanisms. Cell *138*, 628-644.

Chacinska, A., Lind, M., Frazier, A.E., Dudek, J., Meisinger, C., Geissler, A., Sickmann, A., Meyer, H.E., Truscott, K.N., Guiard, B*., et al.* (2005). Mitochondrial presequence translocase: switching between TOM tethering and motor recruitment involves Tim21 and Tim17. Cell *120*, 817-829.

Chacinska, A., Rehling, P., Guiard, B., Frazier, A.E., Schulze-Specking, A., Pfanner, N., Voos, W., and Meisinger, C. (2003). Mitochondrial translocation contact sites: separation of dynamic and stabilizing elements in formation of a TOM-TIM-preprotein supercomplex. EMBO J *22*, 5370-5381.

Chen, H., Feng, J., Kweon, O., Xu, H., and Cerniglia, C.E. (2010). Identification and molecular characterization of a novel flavin-free NADPH preferred azoreductase encoded by azoB in Pigmentiphaga kullae K24. BMC Biochem *11*, 13.

Chen, L., and Madura, K. (2002). Rad23 promotes the targeting of proteolytic substrates to the proteasome. Mol Cell Biol *22*, 4902-4913.

Chuang, K.H., Liang, F., Higgins, R., and Wang, Y. (2016). Ubiquilin/Dsk2 promotes inclusion body formation and vacuole (lysosome)-mediated disposal of mutated huntingtin. Mol Biol Cell *27*, 2025-2036.

Cohen, M.M., Leboucher, G.P., Livnat-Levanon, N., Glickman, M.H., and Weissman, A.M. (2008). Ubiquitin-proteasome-dependent degradation of a mitofusin, a critical regulator of mitochondrial fusion. Mol Biol Cell *19*, 2457-2464.

Dardalhon, M., Lin, W., Nicolas, A., and Averbeck, D. (2007). Specific transcriptional responses induced by 8-methoxypsoralen and UVA in yeast. FEMS Yeast Res *7*, 866-878.

Das, G., and Varshney, U. (2006). Peptidyl-tRNA hydrolase and its critical role in protein biosynthesis. Microbiology (Reading) *152*, 2191-2195.

De Los Rios, P., Ben-Zvi, A., Slutsky, O., Azem, A., and Goloubinoff, P. (2006). Hsp70 chaperones accelerate protein translocation and the unfolding of stable protein aggregates by entropic pulling. Proc Natl Acad Sci U S A *103*, 6166-6171.

De Pereda, J.M., Waas, W.F., Jan, Y., Ruoslahti, E., Schimmel, P., and Pascual, J. (2004). Crystal structure of a human peptidyl-tRNA hydrolase reveals a new fold and suggests basis for a bifunctional activity. J Biol Chem *279*, 8111-8115.

Demine, S., Reddy, N., Renard, P., Raes, M., and Arnould, T. (2014). Unraveling biochemical pathways affected by mitochondrial dysfunctions using metabolomic approaches. Metabolites *4*, 831-878.

den Brave, F., Engelke, J., and Becker, T. (2021). Quality control of protein import into mitochondria. Biochem J *478*, 3125-3143.

den Brave, F., Cairo, L.V., Jagadeesan, C., Ruger-Herreros, C., Mogk, A., Bukau, B., and Jentsch, S. (2020). Chaperone-mediated protein disaggregation triggers proteolytic clearance of intra-nucleur protein inclusions. *Cell Rep.*

Deng, H.X., Chen, W., Hong, S.T., Boycott, K.M., Gorrie, G.H., Siddique, N., Yang, Y., Fecto, F., Shi, Y., Zhai, H.*, et al.* (2011). Mutations in UBQLN2 cause dominant X-linked juvenile and adult-onset ALS and ALS/dementia. Nature *477*, 211-215.

Deshaies, R.J., Koch, B.D., Werner-Washburne, M., Craig, E.A., and Schekman, R. (1988). A subfamily of stress proteins facilitates translocation of secretory and mitochondrial precursor polypeptides. Nature *332*, 800-805.

Dickinson, Q., Aufschnaiter, A., Ott, M., and Meyer, J.G. (2022). Multi-omic integration by machine learning (MIMaL). Bioinformatics *38*, 4908-4918.

Diederichs, K.A., Ni, X., Rollauer, S.E., Botos, I., Tan, X., King, M.S., Kunji, E.R.S., Jiang, J., and Buchanan, S.K. (2020). Structural insight into mitochondrial beta-barrel outer membrane protein biogenesis. Nat Commun *11*, 3290.

Doan, K.N., Grevel, A., Mårtensson, C.U., Ellenrieder, L., Thornton, N., Wenz, L.S., Opalinski, L., Guiard, B., Pfanner, N., and Becker, T. (2020). The Mitochondrial Import Complex MIM Functions as Main Translocase for alpha-Helical Outer Membrane Proteins. Cell Rep *31*, 107567.

Drwesh, L., Heim, B., Graf, M., Kehr, L., Hansen-Palmus, L., Franz-Wachtel, M., Macek, B., Kalbacher, H., Buchner, J., and Rapaport, D. (2022). A network of cytosolic (co)chaperones promotes the biogenesis of mitochondrial signal-anchored outer membrane proteins. eLife *11*.

Eliyahu, E., Pnueli, L., Melamed, D., Scherrer, T., Gerber, A.P., Pines, O., Rapaport, D., and Arava, Y. (2010). Tom20 mediates localization of mRNAs to mitochondria in a translation-dependent manner. Mol Cell Biol *30*, 284-294.

Ellenrieder, L., Dieterle, M.P., Doan, K.N., Mårtensson, C.U., Floerchinger, A., Campo, M.L., Pfanner, N., and Becker, T. (2019). Dual Role of Mitochondrial Porin in Metabolite Transport across the Outer Membrane and Protein Transfer to the Inner Membrane. Mol Cell *73*, 1056-1065 e1057.

Endo, T., and Yamano, K. (2009). Multiple pathways for mitochondrial protein traffic. Biol Chem *390*, 723-730.

Eppinger, B., Kray, J., Mock, B., and Mecklinger, A. (2008). Better or worse than expected? Aging, learning, and the ERN. Neuropsychologia *46*, 521-539.

Fernandez-Vizarra, E., and Zeviani, M. (2018). Mitochondrial complex III Rieske Fe-S protein processing and assembly. Cell Cycle *17*, 681-687.

Fujiki, Y., Hubbard, A.L., Fowler, S., and Lazarow, P.B. (1982). Isolation of intracellular membranes by means of sodium carbonate treatment: application to endoplasmic reticulum. J Cell Biol *93*, 97-102.

Funfschilling, U., and Rospert, S. (1999). Nascent polypeptide-associated complex stimulates protein import into yeast mitochondria. Mol Biol Cell *10*, 3289-3299.

Gadir, N., Haim-Vilmovsky, L., Kraut-Cohen, J., and Gerst, J.E. (2011). Localization of mRNAs coding for mitochondrial proteins in the yeast Saccharomyces cerevisiae. RNA *17*, 1551-1565.

Galluzzi, L., Kepp, O., and Kroemer, G. (2012). Mitochondria: master regulators of danger signalling. Nat Rev Mol Cell Biol *13*, 780-788.

Gärtner, F., Bömer, U., Guiard, B., and Pfanner, N. (1995). The sorting signal of cytochrome b2 promotes early divergence from the general mitochondrial import pathway and restricts the unfoldase activity of matrix Hsp70. EMBO J *14*, 6043-6057.

George, R., Beddoe, T., Landl, K., and Lithgow, T. (1998). The yeast nascent polypeptide-associated complex initiates protein targeting to mitochondria in vivo. Proc Natl Acad Sci U S A *95*, 2296-2301.

Gold, V.A., Chroscicki, P., Bragoszewski, P., and Chacinska, A. (2017). Visualization of cytosolic ribosomes on the surface of mitochondria by electron cryo-tomography. EMBO Rep *18*, 1786-1800.

Gold, V.A., Ieva, R., Walter, A., Pfanner, N., van der Laan, M., and Kuhlbrandt, W. (2014). Visualizing active membrane protein complexes by electron cryotomography. Nat Commun *5*, 4129.

Gomkale, R., Linden, A., Neumann, P., Schendzielorz, A.B., Stoldt, S., Dybkov, O., Kilisch, M., Schulz, C., Cruz-Zaragoza, L.D., Schwappach, B*., et al.* (2021). Mapping protein interactions in the active TOM-TIM23 supercomplex. Nat Commun *12*, 5715.

Gray, M.W., Burger, G., and Lang, B.F. (1999). Mitochondrial evolution. Science *283*, 1476-1481.

Gregersen, N., Bross, P., Vang, S., and Christensen, J.H. (2006). Protein misfolding and human disease. Annu Rev Genomics Hum Genet *7*, 103-124.

Grevel, A., and Becker, T. (2020). Porins as helpers in mitochondrial protein translocation. Biol Chem *401*, 699-708.

Grousl, T., Ungelenk, S., Miller, S., Ho, C.T., Khokhrina, M., Mayer, M.P., Bukau, B., and Mogk, A. (2018). A prion-like domain in Hsp42 drives chaperone-facilitated aggregation of misfolded proteins. J Cell Biol *217*, 1269-1285.

Guan, Z., Yan, L., Wang, Q., Qi, L., Hong, S., Gong, Z., Yan, C., and Yin, P. (2021). Structural insights into assembly of human mitochondrial translocase TOM complex. Cell Discov *7*, 22.

Gupta, A., and Becker, T. (2021). Mechanisms and pathways of mitochondrial outer membrane protein biogenesis. Biochim Biophys Acta Bioenerg *1862*, 148323.

Gibson, D. G., Young, L., Chuang, R. Y., Venter, J. C., Hutchison, C. A., 3rd, & Smith, H. O. (2009). Enzymatic assembly of DNA molecules up to several hundred kilobases. Nat Methods, 6(5), 343-345.

Haan, C., and Behrmann, I. (2007). A cost effective non-commercial ECL-solution for Western blot detections yielding strong signals and low background. J Immunol Methods *318*, 11-19.

Hahn, J.S., Neef, D.W., and Thiele, D.J. (2006). A stress regulatory network for co-ordinated activation of proteasome expression mediated by yeast heat shock transcription factor. Mol Microbiol *60*, 240-251.

Hällberg, B.M., and Larsson, N.G. (2014). Making proteins in the powerhouse. Cell Metab *20*, 226-240.

Hansen, K.G., and Herrmann, J.M. (2019). Transport of Proteins into Mitochondria. Protein J *38*, 330-342.

Harbauer, A.B., Zahedi, R.P., Sickmann, A., Pfanner, N., and Meisinger, C. (2014). The protein import machinery of mitochondria-a regulatory hub in metabolism, stress, and disease. Cell Metab *19*, 357-372.

Hartl, F.U., Schmidt, B., Wachter, E., Weiss, H., and Neupert, W. (1986). Transport into mitochondria and intramitochondrial sorting of the Fe/S protein of ubiquinol-cytochrome c reductase. Cell *47*, 939-951.

Hell, K., Neupert, W., and Stuart, R.A. (2001). Oxa1p acts as a general membrane insertion machinery for proteins encoded by mitochondrial DNA. EMBO J *20*, 1281-1288.

Heo, J.M., Nielson, J.R., Dephoure, N., Gygi, S.P., and Rutter, J. (2013). Intramolecular interactions control Vms1 translocation to damaged mitochondria. Mol Biol Cell *24*, 1263-1273.

Hernandez-Sanchez, J., Valadez, J.G., Herrera, J.V., Ontiveros, C., and Guarneros, G. (1998). lambda bar minigene-mediated inhibition of protein synthesis involves accumulation of peptidyl-tRNA and starvation for tRNA. EMBO J *17*, 3758-3765.

Hill, K., Model, K., Ryan, M.T., Dietmeier, K., Martin, F., Wagner, R., and Pfanner, N. (1998). Tom40 forms the hydrophilic channel of the mitochondrial import pore for preproteins [see comment]. Nature *395*, 516-521.

Hjerpe, R., Bett, J.S., Keuss, M.J., Solovyova, A., McWilliams, T.G., Johnson, C., Sahu, I., Varghese, J., Wood, N., Wightman, M.*, et al.* (2016). UBQLN2 Mediates Autophagy-Independent Protein Aggregate Clearance by the Proteasome. Cell *166*, 935-949.

Horten, P., Colina-Tenorio, L., and Rampelt, H. (2020). Biogenesis of Mitochondrial Metabolite Carriers. Biomolecules *10*.

Hu, H., Matter, M.L., Issa-Jahns, L., Jijiwa, M., Kraemer, N., Musante, L., de la Vega, M., Ninnemann, O., Schindler, D., Damatova, N.*, et al.* (2014). Mutations in PTRH2 cause novel infantile-onset multisystem disease with intellectual disability, microcephaly, progressive ataxia, and muscle weakness. Ann Clin Transl Neurol *1*, 1024-1035.

Ishii, T., Funakoshi, M., and Kobayashi, H. (2006). Yeast Pth2 is a UBL domain-binding protein that participates in the ubiquitin-proteasome pathway. EMBO J *25*, 5492-5503.

Itakura, E., Zavodszky, E., Shao, S., Wohlever, M.L., Keenan, R.J., and Hegde, R.S. (2016). Ubiquilins Chaperone and Triage Mitochondrial Membrane Proteins for Degradation. Mol Cell *63*, 21-33.

Izawa, T., Park, S.H., Zhao, L., Hartl, F.U., and Neupert, W. (2017). Cytosolic Protein Vms1 Links Ribosome Quality Control to Mitochondrial and Cellular Homeostasis. Cell *171*, 890-903 e818.

Janke, C., Magiera, M.M., Rathfelder, N., Taxis, C., Reber, S., Maekawa, H., Moreno-Borchart, A., Doenges, G., Schwob, E., Schiebel, E.*, et al.* (2004). A versatile toolbox for PCR-based tagging of yeast genes: new fluorescent proteins, more markers and promoter substitution cassettes. Yeast *21*, 947-962.

Joazeiro, C.A.P. (2019). Mechanisms and functions of ribosome-associated protein quality control. Nat Rev Mol Cell Biol *20*, 368-383.

Jores, T., Lawatscheck, J., Beke, V., Franz-Wachtel, M., Yunoki, K., Fitzgerald, J.C., Macek, B., Endo, T., Kalbacher, H., Buchner, J.*, et al.* (2018). Cytosolic Hsp70 and Hsp40 chaperones enable the biogenesis of mitochondrial beta-barrel proteins. J Cell Biol *217*, 3091-3108.

Joza, N., Susin, S.A., Daugas, E., Stanford, W.L., Cho, S.K., Li, C.Y., Sasaki, T., Elia, A.J., Cheng, H.Y., Ravagnan, L.*, et al.* (2001). Essential role of the mitochondrial apoptosis-inducing factor in programmed cell death. Nature *410*, 549-554.

Jumper, J., Evans, R., Pritzel, A., Green, T., Figurnov, M., Ronneberger, O., Tunyasuvunakool, K., Bates, R., Zidek, A., Potapenko, A.*, et al.* (2021). Highly accurate protein structure prediction with AlphaFold. Nature *596*, 583-589.

Juszkiewicz, S., and Hegde, R.S. (2018). Quality Control of Orphaned Proteins. Mol Cell *71*, 443-457.

Kamiński, K., Ludwiczak, J., Jasiński, M., Bukala, A., Madaj, R., Szczepaniak, K., & Dunin-Horkawicz, S. (2022). Rossmann-toolbox: a deep learning-based protocol for the prediction and design of cofactor specificity in Rossmann fold proteins. *Briefings in bioinformatics*, *23*(1), bbab371.

Kampinga, H.H., and Craig, E.A. (2010). The HSP70 chaperone machinery: J proteins as drivers of functional specificity. Nat Rev Mol Cell Biol *11*, 579-592.

Kater, L., Wagener, N., Berninghausen, O., Becker, T., Neupert, W., and Beckmann, R. (2020). Structure of the Bcs1 AAA-ATPase suggests an airlock-like translocation mechanism for folded proteins. Nat Struct Mol Biol *27*, 142-149.

Kim, T.Y., Kim, E., Yoon, S.K., and Yoon, J.B. (2008). Herp enhances ER-associated protein degradation by recruiting ubiquilins. Biochem Biophys Res Commun *369*, 741-746.

Klein, A., Israel, L., Lackey, S.W., Nargang, F.E., Imhof, A., Baumeister, W., Neupert, W., and Thomas, D.R. (2012). Characterization of the insertase for beta-barrel proteins of the outer mitochondrial membrane. J Cell Biol *199*, 599-611.

Knop, M., Siegers, K., Pereira, G., Zachariae, W., Winsor, B., Nasmyth, K., and Schiebel, E. (1999). Epitope tagging of yeast genes using a PCR-based strategy: more tags and improved practical routines. Yeast *15*, 963-972.

Kowalski, L., Bragoszewski, P., Khmelinskii, A., Glow, E., Knop, M., and Chacinska, A. (2018). Determinants of the cytosolic turnover of mitochondrial intermembrane space proteins. BMC Biol *16*, 66.

Kozjak, V., Wiedemann, N., Milenkovic, D., Lohaus, C., Meyer, H.E., Guiard, B., Meisinger, C., and Pfanner, N. (2003). An essential role of Sam50 in the protein sorting and assembly machinery of the mitochondrial outer membrane. J Biol Chem *278*, 48520-48523.

Krakowiak, J., Zheng, X., Patel, N., Feder, Z.A., Anandhakumar, J., Valerius, K., Gross, D.S., Khalil, A.S., and Pincus, D. (2018). Hsf1 and Hsp70 constitute a two-component feedback loop that regulates the yeast heat shock response. eLife *7*.

Krämer, L., Dalheimer, N., Raschle, M., Storchova, Z., Pielage, J., Boos, F., and Herrmann, J.M. (2023). MitoStores: chaperone-controlled protein granules store mitochondrial precursors in the cytosol. EMBO J, e112309.

Krämer, L., Groh, C., and Herrmann, J.M. (2021). The proteasome: friend and foe of mitochondrial biogenesis. FEBS Lett *595*, 1223-1238.

Kulak, N.A., Pichler, G., Paron, I., Nagaraj, N., and Mann, M. (2014). Minimal, encapsulated proteomic-sample processing applied to copy-number estimation in eukaryotic cells. Nat Methods *11*, 319-324.

Lang, B.F., Gray, M.W., and Burger, G. (1999). Mitochondrial genome evolution and the origin of eukaryotes. Annu Rev Genet *33*, 351-397.

Lapointe, C.P., Stefely, J.A., Jochem, A., Hutchins, P.D., Wilson, G.M., Kwiecien, N.W., Coon, J.J., Wickens, M., and Pagliarini, D.J. (2018). Multi-omics Reveal Specific Targets of the RNA-Binding Protein Puf3p and Its Orchestration of Mitochondrial Biogenesis. Cell Syst *6*, 125-135 e126.

Laurino, P., Tóth-Petróczy, Á., Meana-Pañeda, R., Lin, W., Truhlar, D. G., & Tawfik, D. S. (2016). An ancient fingerprint indicates the common ancestry of Rossmann-fold enzymes utilizing different ribose-based cofactors. *PLoS biology*, *14*(3), e1002396.

Le, N.T., Chang, L., Kovlyagina, I., Georgiou, P., Safren, N., Braunstein, K.E., Kvarta, M.D., Van Dyke, A.M., LeGates, T.A., Philips, T.*, et al.* (2016). Motor neuron disease, TDP-43 pathology, and memory deficits in mice expressing ALS-FTD-linked UBQLN2 mutations. Proc Natl Acad Sci U S A *113*, E7580-E7589.

Lesnik, C., Cohen, Y., Atir-Lande, A., Schuldiner, M., and Arava, Y. (2014). OM14 is a mitochondrial receptor for cytosolic ribosomes that supports co-translational import into mitochondria. Nat Commun *5*, 5711.

Lill, R., and Freibert, S.A. (2020). Mechanisms of Mitochondrial Iron-Sulfur Protein Biogenesis. Annu Rev Biochem *89*, 471-499.

Liu, C., Apodaca, J., Davis, L.E., and Rao, H. (2007). Proteasome inhibition in wild-type yeast Saccharomyces cerevisiae cells. Biotechniques *42*, 158, 160, 162.

Longtine, M.S., Fares, H., and Pringle, J.R. (1998). Role of the yeast Gin4p protein kinase in septin assembly and the relationship between septin assembly and septin function. J Cell Biol *143*, 719-736.

Marcero, J.R., Piel Iii, R.B., Burch, J.S., and Dailey, H.A. (2016). Rapid and sensitive quantitation of heme in hemoglobinized cells. Biotechniques *61*, 83-91.

Mårtensson, C.U., Priesnitz, C., Song, J., Ellenrieder, L., Doan, K.N., Boos, F., Floerchinger, A., Zufall, N., Oeljeklaus, S., Warscheid, B.*, et al.* (2019). Mitochondrial protein translocation-associated degradation. Nature *569*, 679-683.

Martinez-Reyes, I., Diebold, L.P., Kong, H., Schieber, M., Huang, H., Hensley, C.T., Mehta, M.M., Wang, T., Santos, J.H., Woychik, R.*, et al.* (2016). TCA Cycle and Mitochondrial Membrane Potential Are Necessary for Diverse Biological Functions. Mol Cell *61*, 199-209.

Masser, A.E., Kang, W., Roy, J., Mohanakrishnan Kaimal, J., Quintana-Cordero, J., Friedlander, M.R., and Andreasson, C. (2019). Cytoplasmic protein misfolding titrates Hsp70 to activate nuclear Hsf1. eLife *8*.

Matilainen, O., Sleiman, M.S.B., Quiros, P.M., Garcia, S., and Auwerx, J. (2017). The chromatin remodeling factor ISW-1 integrates organismal responses against nuclear and mitochondrial stress. Nat Commun *8*, 1818.

Matsuo, Y., Ikeuchi, K., Saeki, Y., Iwasaki, S., Schmidt, C., Udagawa, T., Sato, F., Tsuchiya, H., Becker, T., Tanaka, K.*, et al.* (2017). Ubiquitination of stalled ribosome triggers ribosome-associated quality control. Nat Commun *8*, 159.

McBride, H.M., Neuspiel, M., and Wasiak, S. (2006). Mitochondria: more than just a powerhouse. Curr Biol *16*, R551-560.

Medicherla, B., Kostova, Z., Schaefer, A., and Wolf, D.H. (2004). A genomic screen identifies Dsk2p and Rad23p as essential components of ER-associated degradation. EMBO Rep *5*, 692-697.

Michalska, K., Zhang, K., March, Z.M., Hatzos-Skintges, C., Pintilie, G., Bigelow, L., Castellano, L.M., Miles, L.J., Jackrel, M.E., Chuang, E.*, et al.* (2019). Structure of Calcarisporiella thermophila Hsp104 Disaggregase that Antagonizes Diverse Proteotoxic Misfolding Events. Structure *27*, 449-463 e447.

Miller, S.B., Mogk, A., and Bukau, B. (2015). Spatially organized aggregation of misfolded proteins as cellular stress defense strategy. J Mol Biol *427*, 1564-1574.

Mogk, A., and Bukau, B. (2017). Role of sHsps in organizing cytosolic protein aggregation and disaggregation. Cell Stress Chaperones *22*, 493-502.

Mohanraj, K., Wasilewski, M., Beninca, C., Cysewski, D., Poznanski, J., Sakowska, P., Bugajska, Z., Deckers, M., Dennerlein, S., Fernandez-Vizarra, E.*, et al.* (2019). Inhibition of proteasome rescues a pathogenic variant of respiratory chain assembly factor COA7. EMBO Mol Med *11.*

Morgenstern, M., Peikert, C.D., Lubbert, P., Suppanz, I., Klemm, C., Alka, O., Steiert, C., Naumenko, N., Schendzielorz, A., Melchionda, L.*, et al.* (2021). Quantitative high-confidence human mitochondrial proteome and its dynamics in cellular context. Cell Metab *33*, 2464-2483 e2418.

Morgenstern, M., Stiller, S.B., Lubbert, P., Peikert, C.D., Dannenmaier, S., Drepper, F., Weill, U., Hoss, P., Feuerstein, R., Gebert, M.*, et al.* (2017). Definition of a High-Confidence Mitochondrial Proteome at Quantitative Scale. Cell Rep *19*, 2836-2852.

Neuber, O., Jarosch, E., Volkwein, C., Walter, J., and Sommer, T. (2005). Ubx2 links the Cdc48 complex to ER-associated protein degradation. Nat Cell Biol *7*, 993-998.

Neupert, W., and Herrmann, J.M. (2007). Translocation of proteins into mitochondria. Annu Rev Biochem *76*, 723-749.

Nowicka, U., Chroscicki, P., Stroobants, K., Sladowska, M., Turek, M., Uszczynska-Ratajczak, B., Kundra, R., Goral, T., Perni, M., Dobson, C.M.*, et al.* (2021). Cytosolic aggregation of mitochondrial proteins disrupts cellular homeostasis by stimulating the aggregation of other proteins. eLife *10*.

Nunnari, J., and Suomalainen, A. (2012). Mitochondria: in sickness and in health. Cell *148*, 1145-1159.

Opaliński, Ł., Song, J., Priesnitz, C., Wenz, L.S., Oeljeklaus, S., Warscheid, B., Pfanner, N., and Becker, T. (2018). Recruitment of Cytosolic J-Proteins by TOM Receptors Promotes Mitochondrial Protein Biogenesis. Cell Rep *25*, 2036-2043 e2035.

Ordureau, A., Paulo, J.A., Zhang, J., An, H., Swatek, K.N., Cannon, J.R., Wan, Q., Komander, D., and Harper, J.W. (2020). Global Landscape and Dynamics of Parkin and USP30-Dependent Ubiquitylomes in iNeurons during Mitophagic Signaling. Mol Cell *77*, 1124-1142 e1110.

Ott, M., Amunts, A., and Brown, A. (2016). Organization and Regulation of Mitochondrial Protein Synthesis. Annu Rev Biochem *85*, 77-101.

Pagliarini, D.J., Calvo, S.E., Chang, B., Sheth, S.A., Vafai, S.B., Ong, S.E., Walford, G.A., Sugiana, C., Boneh, A., Chen, W.K.*, et al.* (2008). A mitochondrial protein compendium elucidates complex I disease biology. Cell *134*, 112-123.

Pfanner, N., Warscheid, B., and Wiedemann, N. (2019). Mitochondrial proteins: from biogenesis to functional networks. Nat Rev Mol Cell Biol *20*, 267-284.

Phu, L., Rose, C.M., Tea, J.S., Wall, C.E., Verschueren, E., Cheung, T.K., Kirkpatrick, D.S., and Bingol, B. (2020). Dynamic Regulation of Mitochondrial Import by the Ubiquitin System. Mol Cell *77*, 1107-1123 e1110.

Picard, M., Wallace, D.C., and Burelle, Y. (2016). The rise of mitochondria in medicine. Mitochondrion *30*, 105-116.

Ponce-Rojas, J.C., Avendano-Monsalve, M.C., Yanez-Falcon, A.R., Jaimes-Miranda, F., Garay, E., Torres-Quiroz, F., DeLuna, A., and Funes, S. (2017). alphabeta'-NAC cooperates with Sam37 to mediate early stages of mitochondrial protein import. FEBS J *284*, 814-830.

Priesnitz, C., Bottinger, L., Zufall, N., Gebert, M., Guiard, B., van der Laan, M., and Becker, T. (2022). Coupling to Pam16 differentially controls the dual role of Pam18 in protein import and respiratory chain formation. Cell Rep *39*, 110619.

Psakhye, I., and Jentsch, S. (2016). Identification of Substrates of Protein-Group SUMOylation. Methods Mol Biol *1475*, 219-231.

Qin, W., Myers, S.A., Carey, D.K., Carr, S.A., and Ting, A.Y. (2021). Spatiotemporally-resolved mapping of RNA binding proteins via functional proximity labeling reveals a mitochondrial mRNA anchor promoting stress recovery. Nat Commun *12*, 4980.

Qiu, J., Wenz, L.S., Zerbes, R.M., Oeljeklaus, S., Bohnert, M., Stroud, D.A., Wirth, C., Ellenrieder, L., Thornton, N., Kutik, S.*, et al.* (2013). Coupling of mitochondrial import and export translocases by receptor-mediated supercomplex formation. Cell *154*, 596-608.

Quenault, T., Lithgow, T., and Traven, A. (2011). PUF proteins: repression, activation and mRNA localization. Trends Cell Biol *21*, 104-112.

Raasi, S., and Pickart, C.M. (2003). Rad23 ubiquitin-associated domains (UBA) inhibit 26 S proteasome-catalyzed proteolysis by sequestering lysine 48-linked polyubiquitin chains. J Biol Chem *278*, 8951-8959.

Rajakumar, S., Vijayakumar, R., Abhishek, A., Selvam, G.S., and Nachiappan, V. (2020). Loss of ERAD bridging factor UBX2 modulates lipid metabolism and leads to ER stress-associated apoptosis during cadmium toxicity in Saccharomyces cerevisiae. Curr Genet *66*, 1003-1017.

Rao, H., and Sastry, A. (2002). Recognition of specific ubiquitin conjugates is important for the proteolytic functions of the ubiquitin-associated domain proteins Dsk2 and Rad23. J Biol Chem *277*, 11691-11695.

Rath, S., Sharma, R., Gupta, R., Ast, T., Chan, C., Durham, T.J., Goodman, R.P., Grabarek, Z., Haas, M.E., Hung, W.H.W.*, et al.* (2021). MitoCarta3.0: an updated mitochondrial proteome now with sub-organelle localization and pathway annotations. Nucleic Acids Res *49*, D1541-D1547.

Rehling, P., Model, K., Brandner, K., Kovermann, P., Sickmann, A., Meyer, H.E., Kuhlbrandt, W., Wagner, R., Truscott, K.N., and Pfanner, N. (2003). Protein insertion into the mitochondrial inner membrane by a twin-pore translocase. Science *299*, 1747-1751.

Rolland, S.G., Schneid, S., Schwarz, M., Rackles, E., Fischer, C., Haeussler, S., Regmi, S.G., Yeroslaviz, A., Habermann, B., Mokranjac, D.*, et al.* (2019). Compromised Mitochondrial Protein Import Acts as a Signal for UPR(mt). Cell Rep *28*, 1659-1669 e1655.

Rosenzweig, R., Nillegoda, N.B., Mayer, M.P., and Bukau, B. (2019). The Hsp70 chaperone network. Nat Rev Mol Cell Biol *20*, 665-680.

Sahi, C., Kominek, J., Ziegelhoffer, T., Yu, H.Y., Baranowski, M., Marszalek, J., and Craig, E.A. (2013). Sequential duplications of an ancient member of the DnaJ-family expanded the functional chaperone network in the eukaryotic cytosol. Mol Biol Evol *30*, 985-998.

Schägger, H., and von Jagow, G. (1991). Blue native electrophoresis for isolation of membrane protein complexes in enzymatically active form. Anal Biochem *199*, 223-231.

Schlagowski, A.M., Knoringer, K., Morlot, S., Sanchez Vicente, A., Flohr, T., Kramer, L., Boos, F., Khalid, N., Ahmed, S., Schramm, J.*, et al.* (2021). Increased levels of mitochondrial import factor Mia40 prevent the aggregation of polyQ proteins in the cytosol. EMBO J *40*, e107913.

Schuberth, C., and Buchberger, A. (2005). Membrane-bound Ubx2 recruits Cdc48 to ubiquitin ligases and their substrates to ensure efficient ER-associated protein degradation. Nat Cell Biol *7*, 999-1006.

Schuler, M.H., Di Bartolomeo, F., Mårtensson, C.U., Daum, G., and Becker, T. (2016). Phosphatidylcholine Affects Inner Membrane Protein Translocases of Mitochondria. J Biol Chem *291*, 18718-18729.

Schulte, U., den Brave, F., Haupt, A., Gupta, A., Song, J., Müller, C.S., Engelke, J., Mishra, S., Mårtensson, C., Ellenrieder, L.*, et al.* (2023). Mitochondrial complexome reveals quality-control pathways of protein import. Nature *614*, 153-159.

Shakya, V.P., Barbeau, W.A., Xiao, T., Knutson, C.S., Schuler, M.H., and Hughes, A.L. (2021). A nuclear-based quality control pathway for non-imported mitochondrial proteins. eLife *10*.

Sheffield, W.P., Shore, G.C., and Randall, S.K. (1990). Mitochondrial precursor protein. Effects of 70-kilodalton heat shock protein on polypeptide folding, aggregation, and import competence. J Biol Chem *265*, 11069-11076.

Shen, P.S., Park, J., Qin, Y., Li, X., Parsawar, K., Larson, M.H., Cox, J., Cheng, Y., Lambowitz, A.M., Weissman, J.S.*, et al.* (2015). Protein synthesis. Rqc2p and 60S ribosomal subunits mediate mRNA-independent elongation of nascent chains. Science *347*, 75-78.

Shiota, T., Imai, K., Qiu, J., Hewitt, V.L., Tan, K., Shen, H.H., Sakiyama, N., Fukasawa, Y., Hayat, S., Kamiya, M.*, et al.* (2015). Molecular architecture of the active mitochondrial protein gate. Science *349*, 1544-1548.

Shorter, J., and Southworth, D.R. (2019). Spiraling in Control: Structures and Mechanisms of the Hsp104 Disaggregase. Cold Spring Harb Perspect Biol *11*.

Sickmann, A., Reinders, J., Wagner, Y., Joppich, C., Zahedi, R., Meyer, H.E., Schönfisch, B., Perschil, I., Chacinska, A., Guiard, B.*, et al.* (2003). The proteome of Saccharomyces cerevisiae mitochondria. Proc Natl Acad Sci U S A *100*, 13207-13212.

Sikorski, R.S., and Hieter, P. (1989). A system of shuttle vectors and yeast host strains designed for efficient manipulation of DNA in Saccharomyces cerevisiae. Genetics *122*, 19-27.

Song, J., Herrmann, J.M., and Becker, T. (2021). Quality control of the mitochondrial proteome. Nat Rev Mol Cell Biol *22*, 54-70.

Sonntag, K.C., Ryu, W.I., Amirault, K.M., Healy, R.A., Siegel, A.J., McPhie, D.L., Forester, B., and Cohen, B.M. (2017). Late-onset Alzheimer's disease is associated with inherent changes in bioenergetics profiles. Sci Rep *7*, 14038.

Specht, S., Miller, S.B., Mogk, A., and Bukau, B. (2011). Hsp42 is required for sequestration of protein aggregates into deposition sites in Saccharomyces cerevisiae. J Cell Biol *195*, 617-629.

Stojanovski, D., Milenkovic, D., Müller, J.M., Gabriel, K., Schulze-Specking, A., Baker, M.J., Ryan, M.T., Guiard, B., Pfanner, N., and Chacinska, A. (2008). Mitochondrial protein import: precursor oxidation in a ternary complex with disulfide carrier and sulfhydryl oxidase. J Cell Biol *183*, 195-202.

Su, J., Liu, D., Yang, F., Zuo, M.Q., Li, C., Dong, M.Q., Sun, S., and Sui, S.F. (2022). Structural basis of Tom20 and Tom22 cytosolic domains as the human TOM complex receptors. Proc Natl Acad Sci U S A *119*, e2200158119.

Su, T., Izawa, T., Thoms, M., Yamashita, Y., Cheng, J., Berninghausen, O., Hartl, F.U., Inada, T., Neupert, W., and Beckmann, R. (2019). Structure and function of Vms1 and Arb1 in RQC and mitochondrial proteome homeostasis. Nature *570*, 538-542.

Sutandy, F.X.R., Gossner, I., Tascher, G., and Munch, C. (2023). A cytosolic surveillance mechanism activates the mitochondrial UPR. Nature *618*, 849-854.

Takeda, H., Tsutsumi, A., Nishizawa, T., Lindau, C., Busto, J.V., Wenz, L.S., Ellenrieder, L., Imai, K., Straub, S.P., Mossmann, W*., et al.* (2021). Mitochondrial sorting and assembly machinery operates by beta-barrel switching. Nature *590*, 163-169.

Taylor, A.B., Smith, B.S., Kitada, S., Kojima, K., Miyaura, H., Otwinowski, Z., Ito, A., and Deisenhofer, J. (2001). Crystal structures of mitochondrial processing peptidase reveal the mode for specific cleavage of import signal sequences. Structure *9*, 615-625.

Tucker, K., and Park, E. (2019). Cryo-EM structure of the mitochondrial protein-import channel TOM complex at near-atomic resolution. Nat Struct Mol Biol *26*, 1158-1166.

Uszczynska-Ratajczak, B., Sugunan, S., Kwiatkowska, M., Migdal, M., Carbonell-Sala, S., Sokol, A., Winata, C.L., and Chacinska, A. (2023). Profiling subcellular localization of nuclear-encoded mitochondrial gene products in zebrafish. Life Sci Alliance *6*.

van der Laan, M., Chacinska, A., Lind, M., Perschil, I., Sickmann, A., Meyer, H.E., Guiard, B., Meisinger, C., Pfanner, N., and Rehling, P. (2005). Pam17 is required for architecture and translocation activity of the mitochondrial protein import motor. Mol Cell Biol *25*, 7449-7458.

van der Laan, M., Hutu, D.P., and Rehling, P. (2010). On the mechanism of preprotein import by the mitochondrial presequence translocase. Biochim Biophys Acta *1803*, 732-739.

Verma, R., Reichermeier, K.M., Burroughs, A.M., Oania, R.S., Reitsma, J.M., Aravind, L., and Deshaies, R.J. (2018). Vms1 and ANKZF1 peptidyl-tRNA hydrolases release nascent chains from stalled ribosomes. Nature *557*, 446-451.

Vogel, F., Bornhövd, C., Neupert, W., and Reichert, A.S. (2006). Dynamic subcompartmentalization of the mitochondrial inner membrane. J Cell Biol *175*, 237-247.

Vögtle, F.N., Burkhart, J.M., Gonczarowska-Jorge, H., Kucukkose, C., Taskin, A.A., Kopczynski, D., Ahrends, R., Mossmann, D., Sickmann, A., Zahedi, R.P.*, et al.* (2017). Landscape of submitochondrial protein distribution. Nat Commun *8*, 290.

Vögtle, F.N., Wortelkamp, S., Zahedi, R.P., Becker, D., Leidhold, C., Gevaert, K., Kellermann, J., Voos, W., Sickmann, A., Pfanner, N.*, et al.* (2009). Global analysis of the mitochondrial N-proteome identifies a processing peptidase critical for protein stability. Cell *139*, 428-439.

Wallace, D.C. (2018). Mitochondrial genetic medicine. Nat Genet *50*, 1642-1649.

Wang, C.W., and Lee, S.C. (2012). The ubiquitin-like (UBX)-domain-containing protein Ubx2/Ubxd8 regulates lipid droplet homeostasis. J Cell Sci *125*, 2930-2939.

Wang, W., Chen, X., Zhang, L., Yi, J., Ma, Q., Yin, J., Zhuo, W., Gu, J., and Yang, M. (2020). Atomic structure of human TOM core complex. Cell Discov *6*, 67.

Wang, X., and Chen, X.J. (2015). A cytosolic network suppressing mitochondria-mediated proteostatic stress and cell death. Nature *524*, 481-484.

Weidberg, H., and Amon, A. (2018). MitoCPR-A surveillance pathway that protects mitochondria in response to protein import stress. Science *360*.

Wiedemann, N., Kozjak, V., Chacinska, A., Schönfisch, B., Rospert, S., Ryan, M.T., Pfanner, N., and Meisinger, C. (2003). Machinery for protein sorting and assembly in the mitochondrial outer membrane. Nature *424*, 565-571.

Wiedemann, N., and Pfanner, N. (2017). Mitochondrial Machineries for Protein Import and Assembly. Annu Rev Biochem *86*, 685-714.

Wiedemann, N., Pfanner, N., and Ryan, M.T. (2001). The three modules of ADP/ATP carrier cooperate in receptor recruitment and translocation into mitochondria. EMBO J *20*, 951-960.

Wittig, I., and Schägger, H. (2005). Advantages and limitations of clear-native PAGE. Proteomics *5*, 4338-4346.

Wrobel, L., Topf, U., Bragoszewski, P., Wiese, S., Sztolsztener, M.E., Oeljeklaus, S., Varabyova, A., Lirski, M., Chroscicki, P., Mroczek, S.*, et al.* (2015). Mistargeted mitochondrial proteins activate a proteostatic response in the cytosol. Nature *524*, 485-488.

Xiao, T., Shakya, V.P., and Hughes, A.L. (2021). ER targeting of non-imported mitochondrial carrier proteins is dependent on the GET pathway. Life Sci Alliance *4*.

Yamamoto, H., Fukui, K., Takahashi, H., Kitamura, S., Shiota, T., Terao, K., Uchida, M., Esaki, M., Nishikawa, S., Yoshihisa, T.*, et al.* (2009). Roles of Tom70 in import of presequence-containing mitochondrial proteins. J Biol Chem *284*, 31635-31646.

Yamano, K., Yatsukawa, Y., Esaki, M., Hobbs, A.E., Jensen, R.E., and Endo, T. (2008). Tom20 and Tom22 share the common signal recognition pathway in mitochondrial protein import. J Biol Chem *283*, 3799-3807.

Young, J.C., Hoogenraad, N.J., and Hartl, F.U. (2003). Molecular chaperones Hsp90 and Hsp70 deliver preproteins to the mitochondrial import receptor Tom70. Cell *112*, 41-50.

Zachar, I., and Boza, G. (2020). Endosymbiosis before eukaryotes: mitochondrial establishment in protoeukaryotes. Cell Mol Life Sci *77*, 3503-3523.

Zahedi, R.P., Sickmann, A., Boehm, A.M., Winkler, C., Zufall, N., Schönfisch, B., Guiard, B., Pfanner, N., and Meisinger, C. (2006). Proteomic analysis of the yeast mitochondrial outer membrane reveals accumulation of a subclass of preproteins. Mol Biol Cell *17*, 1436-1450.

Zick, M., Rabl, R., and Reichert, A.S. (2009). Cristae formation-linking ultrastructure and function of mitochondria. Biochim Biophys Acta *1793*, 5-19.

Zurita Rendón, O., Fredrickson, E.K., Howard, C.J., Van Vranken, J., Fogarty, S., Tolley, N.D., Kalia, R., Osuna, B.A., Shen, P.S., Hill, C.P.*, et al.* (2018). Vms1p is a release factor for the ribosome-associated quality control complex. Nat Commun *9*, 2197.

8. Acknowledgment

I would like to express my sincere gratitude to everyone who has contributed to the completion of my Ph.D. thesis. I would like to start by thanking Thomas, for his unwavering guidance, expertise, and mentorship throughout my PhD journey. His insightful feedback and constant encouragement have been instrumental in shaping my research and academic career. He has always motivated me to become a better scientist and researcher. We faced two big challenges together- a move from Freiburg to Bonn and the COVID pandemic. He has been a big pillar of support during both of these challenges. I also want to thank Fabian, who has always been there whenever I needed advice or support with my experiments.

I extend my heartfelt thanks to the members of my thesis committee, Prof. Jörg Höhfeld, Prof. Oliver Gruß, and Prof. Wolfgang Voos for reviewing this work. I extend my thanks to the CRC1218 graduate program for its engaging scientific retreats, workshops, seminars and a vibrant atmosphere fostering my intellectual growth.

I am grateful to my colleagues and fellow researchers both at the University of Bonn and Freiburg, who have provided a great lab environment and always motivated me to believe in my results. Heartfelt thanks to Christoph, Chantal and Nicole for teaching me the laboratory work during my initial days. My PhD journey wouldn't have been possible without the support of Swadha, Julianne, Alex, Jeannine, Sandra, Isabel, and Ritwika. They made the transition from Freiburg to Bonn comfortable, and made lab a second home. Special thanks to Lion and Vitasta for their constructive feedback on my PhD thesis. I am grateful to the wonderful team of technicians at our institute, Ralph, Jacqueline, Hannah, Jutta, Ivon, Julia, Ali, and Nobert for always lending a helping hand during my experiments. I would like to thank all employees of the institute, administration, IT, and most importantly colleagues at IBMB. I also want to thank Padma and Adi who have been the most supportive friends during my PhD. I am forever grateful to Abhay for listening to my grievances and the dinner dates to take my mind off PhD.

Last but not least, to my family and my dogs- thanks for being there always for me. It would not have been possible to be the person I am today without you.

9. Publication list

1. Schulte, U*., den Brave, F*., Haupt, A. *, **Gupta, A.** *, Song, J., Muller, C.S., Engelke, J., Mishra, S., Mårtensson, C., Ellenrieder, L., *et al.* (2023). Mitochondrial complexome reveals quality-control pathways of protein import. Nature *614*, 153-159
(*shared first co-authorship)
DOI: 10.1038/s41586-022-05641-w

2. den Brave, F., **Gupta, A.** and Becker, T. (2021) Protein quality control at the mitochondrial surface. Front. Cell Dev. 9
DOI: 10.3389/fcell.2021.795685

3. **Gupta, A.** and Becker, T. (2021) Mechanisms and pathways of mitochondrial outer membrane protein biogenesis. Biochim. Biophys. Acta 1862
DOI: 10.1016/j.bbabio.2020.148323